NASA CR-135392

An Analytical and Experimental Study of Sound Propagation and Attenuation in Variable-Area Ducts

A. H. Nayfeh, J. E. Kaiser,
R. L. Marshall, and C. J. Hurst

Virginia Polytechnic Institute and State University

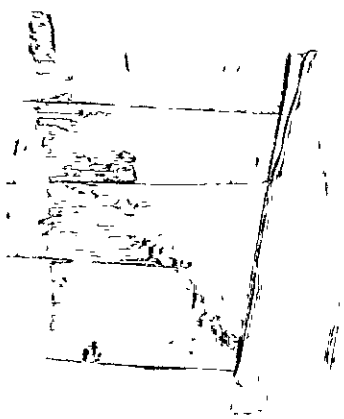

Prepared for
National Aeronautics and Space Administration

NASA Lewis Research Center

NAS 3-18553

1 Report No.	2. Government Accession No.	3 Recipient's Catalog No.
NASA CR-135372		

4. Title and Subtitle	5. Report Date
AN ANALYTICAL AND EXPERIMENTAL STUDY OF SOUND PROPAGATION AND ATTENUATION IN VARIABLE-AREA DUCTS	October 1978
	6 Performing Organization Code
7. Author(s)	8. Performing Organization Report No.
A. H. Nayfeh, J. E. Kaiser, R. L. Marshall, C. J. Hurst	
	10. Work Unit No
9 Performing Organization Name and Address	11. Contract or Grant No.
Virginia Polytechnic Institute and State University Blacksburg, Virginia	NAS 3-18553
	13. Type of Report and Period Covered
12. Sponsoring Agency Name and Address	Contract Report
National Aeronautics and Space Administration Washington, D. C. 20546	14. Sponsoring Agency Code

15 Supplementary Notes

Project Manager, Kenneth J. Baumeister, NASA Lewis Research Center, Cleveland, Ohio

16 Abstract

An experimental and analytical program has been carried out to evaluate the performance of sound suppression techniques in ducts that produce refraction effects due to axial velocity gradients. The analytical program employs a computer code based on the method of multiple scales to calculate the influence of axial variations due to slow changes in the cross-sectional area as well as transverse gradients due to the wall boundary layers. The overall objectives of the study were the verification of the analytical model through direct comparison of experimental and computational results and the analytical determination of the influence of axial gradients on "optimum" liner properties. However, a weak non-uniformity in the standard parallel-duct theory at the "optimum" liner conditions creates a singularity in the higher-order perturbation results (that is, the non-parallel effects); thus the analytical studies have been unable to examine the influence of non-parallel ducts on the optimum liner conditions. However, for liner properties not close to optimum, detailed comparison between the analytical predictions and the experimental measurements have been made. The circumferential variations of pressure amplitudes and phases at several axial positions have been examined in straight and variable-area ducts, hard-wall and lined sections with and without a mean flow. Reasonable agreement between the theoretical and experimental results has been obtained.

17. Key Words (Suggested by Author(s))	18. Distribution Statement
noise acoustics ducts liners	Unclassified - unlimited

19. Security Classif. (of this report)	20. Security Classif. (of this page)	21. No. of Pages	22 Price*
Unclassified	Unclassified	123	

* For sale by the National Technical Information Service, Springfield, Virginia 22161

AN ANALYTICAL AND EXPERIMENTAL STUDY OF SOUND PROPAGATION AND ATTENUATION IN VARIABLE-AREA DUCTS

A. H. Nayfeh, J. E. Kaiser, R. L. Marshall, and C. J. Hurst

Virginia Polytechnic Institute and State University

Final Report

Contract NAS 3-18553

Abstract

An experimental and analytical program has been carried out to evaluate the performance of sound suppression techniques in ducts that produce refraction effects due to axial velocity gradients. The analytical program employs a computer code based on the method of multiple scales to calculate the influence of axial variations due to slow changes in the cross-sectional area as well as transverse gradients due to the wall boundary layers. The overall objectives of the study were the verification of the analytical model through direct comparison of experimental and computational results and the analytical determination of the influence of axial gradients on "optimum" liner properties. However, a weak non-uniformity in the standard parallel-duct theory at the "optimum" liner conditions creates a singularity in the higher-order perturbation results (that is, the non-parallel effects); thus the analytical studies have been unable to examine the influence of non-parallel ducts on the optimum liner conditions. However, for liner properties not close to optimum, detailed comparison between the analytical predictions and the experimental measurements have been made. The circumferential variations of pressure amplitudes and phases at several axial positions have been examined in straight and variable-area ducts, hard-wall and lined sections with and without a mean flow. Reasonable agreement between the theoretical and experimental results has been obtained.

Table of Contents

Table of Contents Con't

List of Figures

List of Tables

I. Introduction and Background

The prediction of noise emission from aircraft engine-duct systems is a problem whose analysis is complicated by the nature of the mean flow within the ducts. Such ducts carry a high-speed mean flow that possesses streamwise gradients due to variations in the duct geometry in addition to strong transverse gradients due to the wall boundary layers. Although these gradients have been shown to have a significant effect on the sound propagation, techniques that are capable of predicting their effect in realistic duct configurations have not been available until recently, primarily due to the difficulty of calculating the effects of the streamwise gradients. The reward for the successful development of such a technique--that is, the ability to identify those duct configurations which possess the most favorable sound attenuation characteristics--has prompted numerous investigations into the effects of area variations; see the review articles of Nayfeh, Kaiser, and Telionis[1] and Nayfeh[2].

Early studies of wave propagation through variable-area ducts restricted their scope to the case of no mean flow. Webster's equation[3] for the propagation of a plane wave is well-known, and numerous investigations have verified or expanded this theory. Isakovitch[4], Salant[5] and Nayfeh[6,7] and Nayfeh and Kandil[8] obtained perturbation solutions for wave propagation in ducts whose walls vary sinusoidally. Several authors (Alfredson[9], Lansing and Zorumski[10] and

Zorumski[11]) used a discretization technique based on the solution for a single duct discontinuity. Nayfeh and Telionis[12] applied the method of multiple scales to obtain a uniformly-valid perturbation solution for a duct of slowly-varying cross section. Beckemeyer and Eversman[13] used the Ritz minimization of fuctionals with the governing equations as stationary conditions in order to waive the restriction of slow variation with axial distance; however, it is not known whether their analysis will converge when the duct variations are large. Recent studies of the no-mean-flow case have been carried out using the method of weighted residuals (Eversman, Cook, and Beckemeyer[14]), integral equations (Quinn[15]) variation of parameters (Kaiser and Nayfeh[16]), finite differences (Quinn[17], Baumeister and Rice[18], and Baumeister[19]), and finite elements (Watson[20] and Eversman and Astley[21]).

The inclusion of the effects of a mean flow to provide a more realistic model makes the problem considerably more difficult, and most studies have employed one or more simplifying assumptions. The most commonly-used assumption is that of quasi-one-dimensional flow, which eliminates the effect of sound refraction through the boundary layer. Powell[22] studied the propagation of sound discontinuities, while Eisenberg and Kao[23], Davis and Johnson[24], Myers and Callegari[25], Callegari and Myers[26], and Nayfeh, Shaker, and Kaiser[27] considered the propagation of the lowest acoustic mode through ducts with variable cross sections. Huerre and

Karamcheti[28] and Grimm[29] and King and Karamcheti[30] investigated the propagation of the lowest acoustic mode using the short wave approximation (ray acoustics) and the method of characteristics. Hogge and Ritzi[31] assumed that the duct can be broken down into cylindrical and conical sections, and they solved the wave equation for a uniform mean flow by application of the method of finite elements. However, the restrictions to one-dimensional flow and/or propagation of the fundamental mode limits the usefulness of such analyses for realistic situations in which the sound is a combination of numerous modes which propagate through a mean flow that possesses both axial and transverse velocity gradients.

Perhaps the only simplifying factor of the problem is the fact that, in many practical situations, for example in the bypass ducts of high-bypass-ratio jet engines, the duct cross-sectional area depends only mildly on the distance along the axis of the duct. Moreover, the growth of the mean boundary layer at high Reynolds numbers is a slow function of the axial distance, except perhaps at the leading edge of the duct inlet. The above factors indicate that a perturbation method should be appropriate. Such a method could determine the correction due to weak nonuniformities of the duct shape, a mean flow with a small normal velocity component, slow variations of the duct liner properties, and a growing boundary-layer thickness, in addition to including the effects of large transverse velocity gradients.

By using the Born approximation, Tam[32] investigated the transmission and scattering of spinning acoustic-wave modes through a duct nonuniformity. Nayfeh, Telionis, and Lekoudis[33] used the method of multiple scales in order to study the propagation of all acoustic modes in a two-dimensional duct with a slowly-varying cross section carrying a sheared incompressible mean flow. Nayfeh, Kaiser, and Telionis[34] extended the analysis to the more practical annular-duct configuration, and Nayfeh and Kaiser[35] applied the technique to propagation through a two-dimensional compressible flow. These multiple-scales analyses include the effects of streamwise variations of the mean velocity, of the liner properties and of the boundary-layer thickness, and the effect of the mean normal velocity and transverse velocity gradient. Thus, acoustic propagation through realistic mean flows can be examined with the multiple-scale analyses.

For ducts with larger axial variations, coupling between modes will occur. Eversman[36] has developed a procedure based on the method of weighted residuals to determine the reflection effects and modal coupling in transmission. Nayfeh, Shaker, and Kaiser[37] have developed a wave-envelope method based on the method of variation of parameters that avoids the necessity of having to integrate through each axial wave length and is thus more efficient than the standard weighted-residual approach. Sigman, Majjigi, and Zinn[38] and Abramson[39] developed finite-element models of sound propagation in nonuniform ducts carrying compressible flows.

In contrast to the considerable efforts that have gone into the development of analytical and numerical methods to predict acoustic propagation in variable-area ducts, few experimental studies have been made to test these analytical models. Although good agreement between theory and experiment has been obtained in lined, straight ducts (for example, by Plumblee[40] and Plumblee, Dean, Wynne and Burrin[41]), no attempt has been made to test the analytical models for variable-area ducts in which the approximations and assumptions of the models are critical. For this reason, a program was undertaken in which a primary objective was direct comparison of experimental results with analytical predictions. The best analytical model available at the start of the program was that based on the method of multiple scales and thus this model was chosen for comparison. A second objective of the analytical program was the determination of the influence of axial gradients on the "optimum" liner properties. As discussed in Section 5.2, under some conditions, in a variable-area duct the non-parallel results exhibit a singularity whose origin has been found to be a non-uniformity in the standard parallel-duct theory whenever two or more modes have equal eigenvalues. Consequently, the perturbation analysis for the variable-area effects are not applicable to cases near multiple roots of the parallel-duct eigenvalue equation.

The experimental facility, the instrumentation and the design parameters for the experimental study are described in Section 2. In Section 3, an analytical formulation for annular, hard-wall ducts with axial variations in the cross-sectional area but no mean flow is developed; preliminary experimental studies to define conditions for comparison of experimental and theoretical results are reported; and the detailed comparison of theoretical and experimental results is given. The analytical development for the lined test section without a mean flow is described in Section 4; in addition, the liner properties are determined from the experimental data for the constant-area duct, and the analytical predictions for the variable-area test section are compared with appropriate experimental data. Cases in which the duct carries a mean flow are considered in Section 5; the analytical basis of the computer code for this case is reviewed; computational studies of the effects of axial variations on wave propagation in ducts with "optimum" liners are described; and the experimental data in variable-area, lined annular ducts are compared with theoretical predictions. Section 6 summarizes the investigation.

2. Experimental Facility and Instrumentation

2.1 General Approach

2.1.1 The Measurement Problem

The basic objective of the experimental investigation was to characterize the modal content of an acoustical traveling wave propagating through an annular duct. Changes in the acoustic propagation were to be related to changes in the geometry of the duct boundaries, the acoustic impedance of the duct walls, and the flow of the transmitting fluid through the annular passage.

To allow comparison with theoretical predictions, it was necessary to measure both the amplitude and relative phase of an acoustical signal at known axial locations at the outer wall of the test passage.

2.1.2 Basic requirements for the experimental system

The measurement program undertaken necessitated the design and construction of a test facility which would allow accurate and repeatable acoustic measurements in the presence of an appreciable flow. In addition, the test apparatus had to allow for the change of several basic parameters with relative ease. The general design constraints imposed on the test-section geometry, air flow, and acoustic-propagation parameters will be discussed in turn.

The foremost geometric requirement on the test section was that it be annular in shape and that it have a varying cross-sectional flow area. In addition, it was required that at least one of the annular walls be acoustically soft.

These geometric requirements were met by using a variable diameter, acoustically-hard center-body running through an outer cylinder of constant inside diameter. The outer wall of one of the annular test sections was made acoustically soft. An acoustically-hard outer wall and a constant area (uniform) center-body were also constructed.

Measurements in the presence of flow required the establishment of a controlled, constant air flow having a flow profile that was reasonably uniform. Extraneous noise was removed from the flow ahead of the test section so that an acoustic signal of known frequency could be detected with a good signal-to-noise ratio. The tests for this study were limited to Mach numbers less than 0.3 in the variable-area test section in order to facilitate comparison with the theoretical results which were based on an incompressible mean-flow model. However, a capability of handling large air flows was desired to allow experimental measurement in flow regimes up to a Mach number of 0.6. The air flow requirements were met by using the compressors and storage tanks of a nearby supersonic wind tunnel. The air was throttled, muffled, and expanded in a settling chamber before passing through a flow straightener and converging section on its way to the test passage.

The acoustic requirements dictated that the test section be free from standing waves in the axial direction and that provision be made for inserting a pure-tone acoustic signal. Furthermore, it was necessary to be able to excite various mode shapes at the inlet of the test section. The minimization of standing waves was accomplished by muffling and by the use of horns on both the downstream end of the test section and the upstream end of the acoustic signal insertion location. Mode shape generation was provided by using multiple acoustic sources. Each source was controllable in both amplitude and phase, consequently allowing some control of the relative modal amplitudes in the propagation wave.

The various aspects of the test apparatus are considered in more detail in the following section.

2.2 Experimental Apparatus

2.2.1 System description

The test apparatus is arranged as shown in Fig. 1. Air from a high-pressure storage system is regulated to a desirable working pressure by a high-capacity regulating valve [1]*. This commercially available 4-inch pressure-regulating valve is designed to reduce an inlet supply pressure of 75 PSI gage to an exit pressure ranging from 1-30 PSI gage, as desired. Under these conditions the valve can deliver approximately 10,000 standard CFM of air. These experiments were run with a pressure downstream of the regulating valve of approximately 25 PSIG. A 4-inch gate valve [2] is used to stop and start the air flow. Final adjustment of the fluid velocity is made with a globe valve [3].

Two mufflers in series serve to eliminate the flow noise and to provide a flow capacitance. American Air Filter (AAF) Pulsco Model LM18-4 line mute [4] is the first muffler in line. This provides some flow resistance and removes the bulk of the throttling noise that results from the regulating valves. The flow is turned and enters an Industrial Acoustics Company (IAC) model 18-PA-2 silencer [5]. This muffler is basically an 18-inch diameter acoustically lined plenum. The diameter was selected to be large enough that the flow velocities in this plenum are quite small. It thus serves as a settling chamber ahead of the test section.

*Numbers in brackets refer to items indicated on Fig. 1.

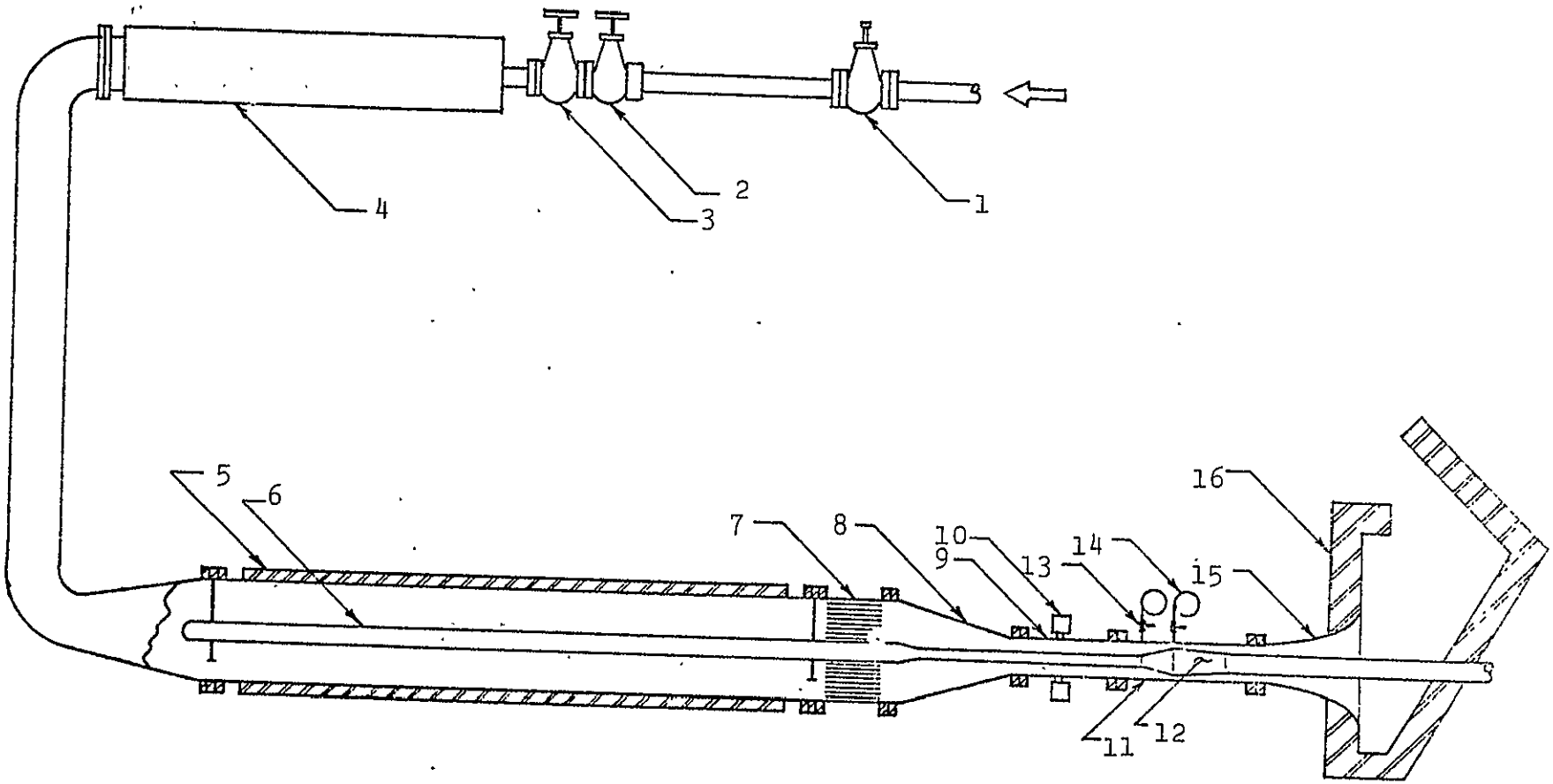

Figure 1. A schematic of test apparatus.

The centerbody [6] begins at the upstream end of this muffler. It continues at a constant 3-inch diameter through the muffler, the contraction section and the test section. By this means, flow disturbances, which would have resulted from the introduction of the centerbody in the established flow field near the test section, are avoided.

After leaving the muffler, the flow passes through a straightening device [7] constructed from 8-inch thick honeycomb having 1/8 inch cells. This device reduces the turbulence of the airstream and acts as an additional flow resistance to help stabilize the air flow. A contraction section [8] then reduces the flow diameter from about 18 inches to 6.100 inches. The contraction section is basically conical in shape, but the downstream end is faired into the upstream end of the signal-insertion section [9] by using a long-radius circular arc.

The signal-insertion section [9] consists of a 6.100 inch inside-diameter honed pipe equipped with four loud-speaker driver units. These units are equally spaced (90°) around the circumference of the outer wall at the same axial location. A thin piece of rayon material covers the driver hole opening on the inner wall of the acoustical-source section. The driver units are individually controlled with regard to amplitude and phase. The loud-speaker driver units are Atlas Sound Model PD-60, rated at 42 watts rms with a useful frequency range from 70-12K Hz [10]. The air temperature and the flow velocity are measured in the

signal-insertion section, which is immediately upstream of the test section.

Two test sections [11] were constructed. These are discussed in more detail in Sections 2.2.2 and 2.2.3.

Two centerbodies [12] were constructed. The straight centerbody was constructed from a 3-inch aluminum tubing having a 1/4 inch thick wall. A conically-shaped centerbody was constructed to provide for the variable-flow area. The details of the construction of this centerbody are given in Section 2.2.4.

A reference microphone probe [13] located at the entrance of the test section is used to maintain the sound pressure level (SPL) constant at the reference point. The signal from this probe also serves as a reference for determining the phase of the signal from the measuring probes.

The measuring probes [14], which are flush mounted, provide the acoustic pressure at the outer wall of the test section. Six axial probe positions are located in each test section. Sufficient circumferential positions are available at the entrance of the test section to define the modal content up to the third circumferential mode. The details of the probe locations are explained in Section 2.2.2, which defines the geometry and construction of the test sections.

The test section is terminated with a horn [15] which was fabricated from the outer section of a large outdoor speaker and, therefore, is not ideally exponential. The horn does have a high efficiency at the desired test

frequencies so that no standing waves were detected in the test section (see Section 3.2).

The system exhausts into an anechoic chamber [16]. The anechoic chamber is of plywood construction and is lined with a 4-inch reticulated foam. Provision is made to exhaust the air through the top of the chamber. All lines of sight into the nozzle exit are blocked. The system is anechoic to 125 Hz. Experiments indicated that the addition of the anechoic termination greatly reduced upstream sound propagation into the test section from external sources.

2.2.2 Hard-walled test section

An acoustically-hard test section was fabricated from a standard 6-inch schedule 40 pipe. The pipe was bored to the required 6.100-inch inside diameter. In addition, the test section was carefully honed to insure that the required diameter is constant around the circumference and along the axial length.

The geometry of the variable-area centerbody dictates the axial positions for the microphone probe placements. Determination of the modal content of the propagating wave dictates the circumferential probe placements. Six axial probe stations are provided, as shown in Fig. 2. The number of circumferential probe locations vary, depending on the axial location.

Station 1 (at the upstream end of the test section) serves as the reference station. It has eight circumferen-

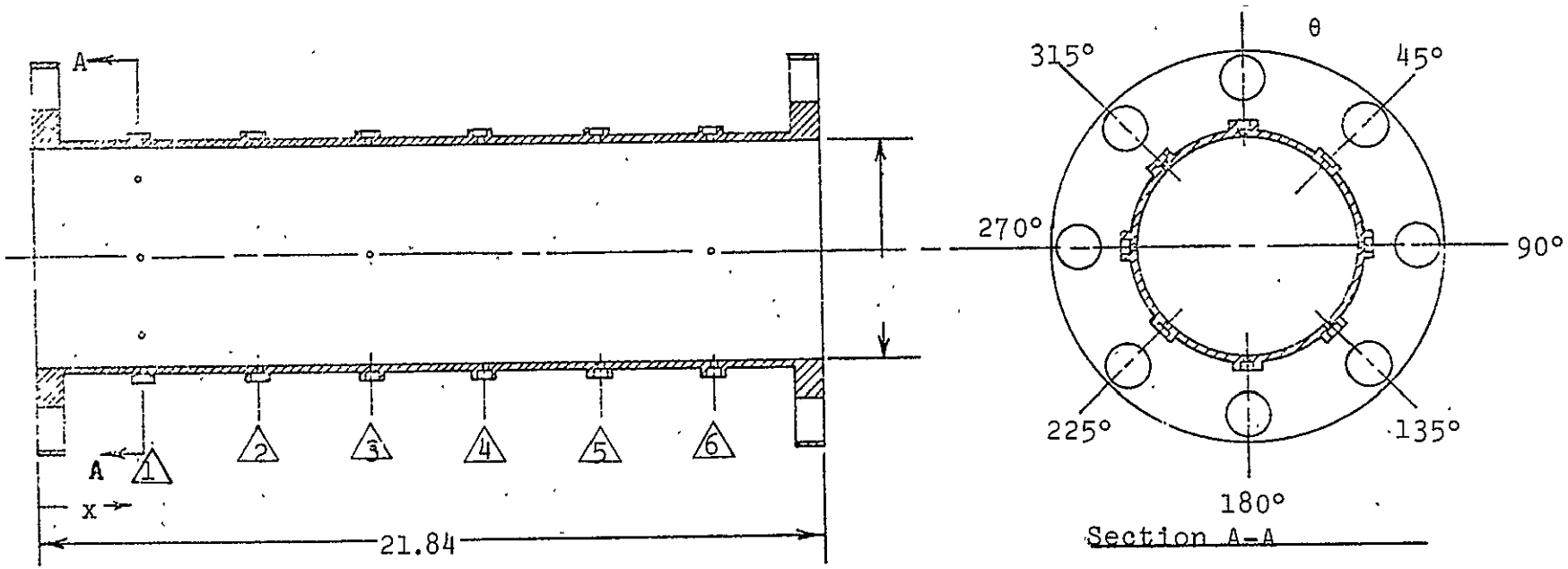

PROBE	x	θ
1	3.00	0,45,90,135,180,225,270,315
2	6.20	0,180
3	9.40	0,90,180,270
4	12.60	0,180
5	15.80	0,180
6	19.00	0,90,180,225

Figure 2. Hard-walled test section.

tial probe positons. When a variable-area centerbody is used, it is positioned so that station 1 is just upstream of the increasing-diameter portion of the centerbody. Station 2 has two diametrically-opposed circumferential probe positions and is axially located approximately midway between the minimum and maximum diameter locations on the variable-area centerbody. Station 3 has four equally-spaced circumferential probe positions. Its axial location corresponds to a position just prior to the location of the maximum diameter of the variable-area centerbody.

All probe holes in the hard-wall section were machined such that one probe assembly could be moved from location to location and the probe tip would be flush with the inner wall to within an acceptable tolerance.

2.2.3 Soft-walled test section

The computer code described in Section 5.1 was used to examine the effects of several liner constructions on the acoustic propagation as a preliminary step in the design[42]. The influence of the liner was investigated for both straight and variable-area centerbodies with and without a mean flow. The liner design was tuned to approximately 3000 Hz, but the peak attenuation was not made so large as to reduce the input signal below the flow noise in the test section. The selected soft-walled test section consists of a hard outer

shell fabricated from an 8-inch diameter steel tube and a 0.625-inch thick "Flex-Core" honeycomb which separates the facing sheet from the outer shell (see Fig. 3). The porous facing sheet is made from "Feltmetal", a material supplied by the Brunswick Corporation. The material selected has a nominal resistance of 40 CGS Rayls. However, visual inspection indicated some obvious variations in porosity across the surface of this sheet. This variation of the facing-sheet resistance is a major difficulty in obtaining agreement between the results of the experimental testing program and the analytical predictions for the soft-walled test cases.

One of the major construction difficulties faced in this project was that of bonding the Feltmetal to the honeycomb without destroying the porosity of the Feltmetal. The construction technique finally worked out to preserve the porosity of the sheet is as follows. A sheet of thermal adhesive is placed on the flex-core. Then a small hole is punched in the sheet adhesive over each flex-core cell. The adhesive is next heated by a heat lamp, which causes the adhesive to contract on the lip of each cell. The test section is then assembled and cured under pressure. Examination of the final assembly has shown that at least 95% of the lips of individual cells are bonded to the Feltmetal by this technique without appreciably destroying the porosity of the Feltmetal.

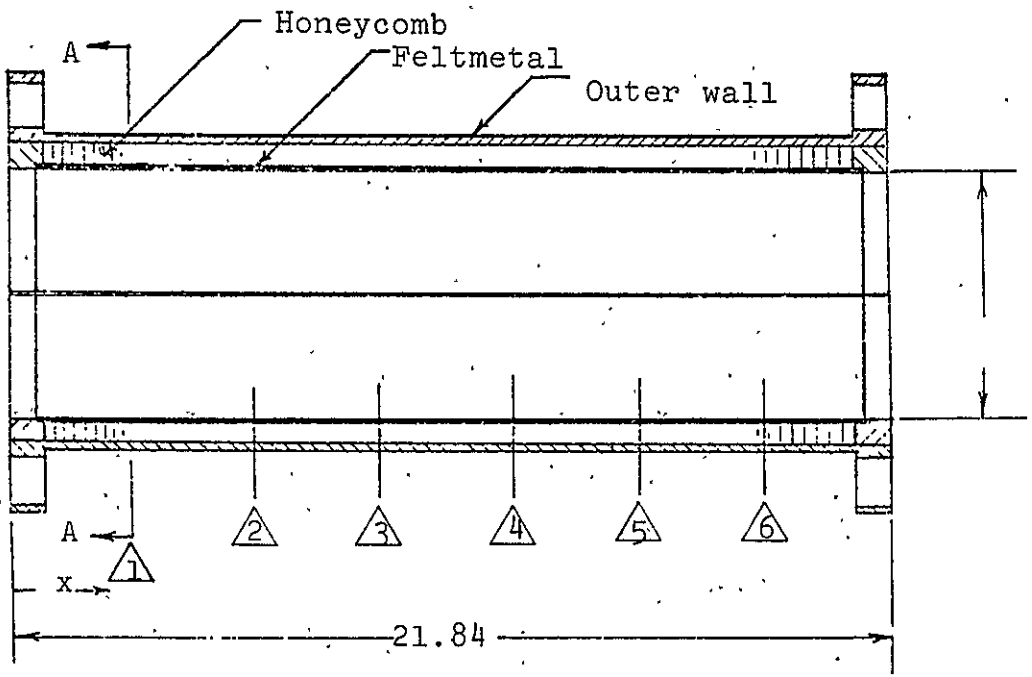

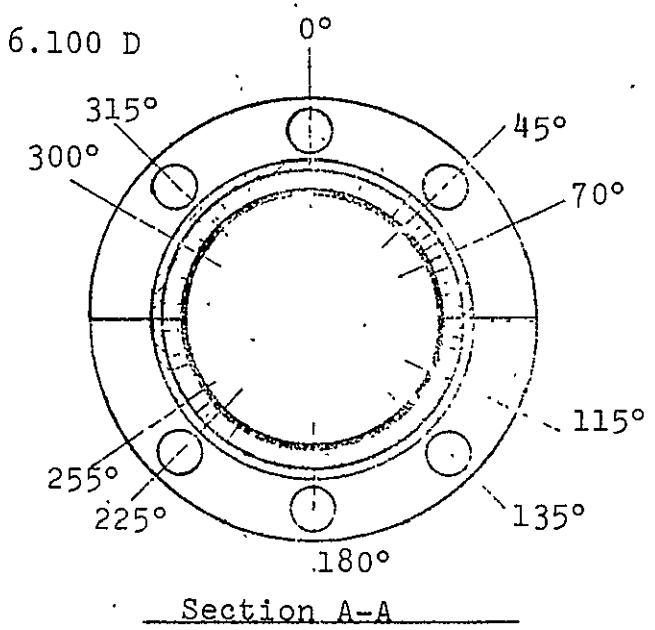

PROBE	x	θ LOCATIONS
1	3.00	0,45,70,115,135,180,225,255,300,315
2	6.20	0,180
3	9.40	0,45,70,115,135,180,225,255,300,315
4	12.60	0,180
5	15.80	0,180
6	19.00	0,45,135,180,225,315

Figure 3. Soft-walled test section.

The axial placement of probes is dictated by the variable-area centerbody and is identical to that employed in the hard-walled test section as discussed above. However, early tests with the hard-walled test section indicated that more circumferential probe positions at stations one, three and six would be desirable. Further, these probe positions should not be equally spaced around the circumference. Consequently axial stations one and three of the soft-walled test section have ten (10) probe positions as specified in Fig. 3.

In order to assure proper alignment of the probe tips flush with the Feltmetal liner surface in the soft-walled experiments, separate probe tips are permanently left in each probe location, and the microphone and probe block are moved from tip to tip during the course of the experiment. Great care has been taken to insure that the probe tips are identical in size and have similar acoustical characteristics. Each probe tip was calibrated with respect to both amplitude and relative phase prior to installation into the soft-walled test section. Section 2.3.2 and Figure 6 provide more detail about the probe assembly.

2.2.4 Variable-area centerbody

The variable-area centerbody was designed to produce a significant velocity gradient along its axial length. The computer code described in Section 5.1 was used to examine

the effects of the axial gradients on the acoustic propagation through the test section. The area variation was selected large enough to produce a measurable non-parallel effect on the acoustic disturbance but not so large as to invalidate the theoretical results with which experimental data were to be compared. The essential dimensions of the variable-area centerbody that was selected are shown in Fig. 4. The approach diameter is two inches, and the diameter increases to a 4.296-inch maximum. The variable-area centerbody tapers to the 3-inch exit diameter at approximately half the approach rate. The various mating surfaces have been blended, and the entire surface is polished to minimize acoustic or flow perturbations that might result from surface imperfections.

For the soft-walled tests, the variable-area centerbody was positioned so that the start of the incline was just downstream from the test-section probe reference station (station 1). The maximum centerbody diameter was then slightly downstream from the third axial probe station (station 3), so that measurements were made prior to the throat.

The exact centerbody geometry was carefully measured with a dial indicator, and the results are shown in Fig. 4.

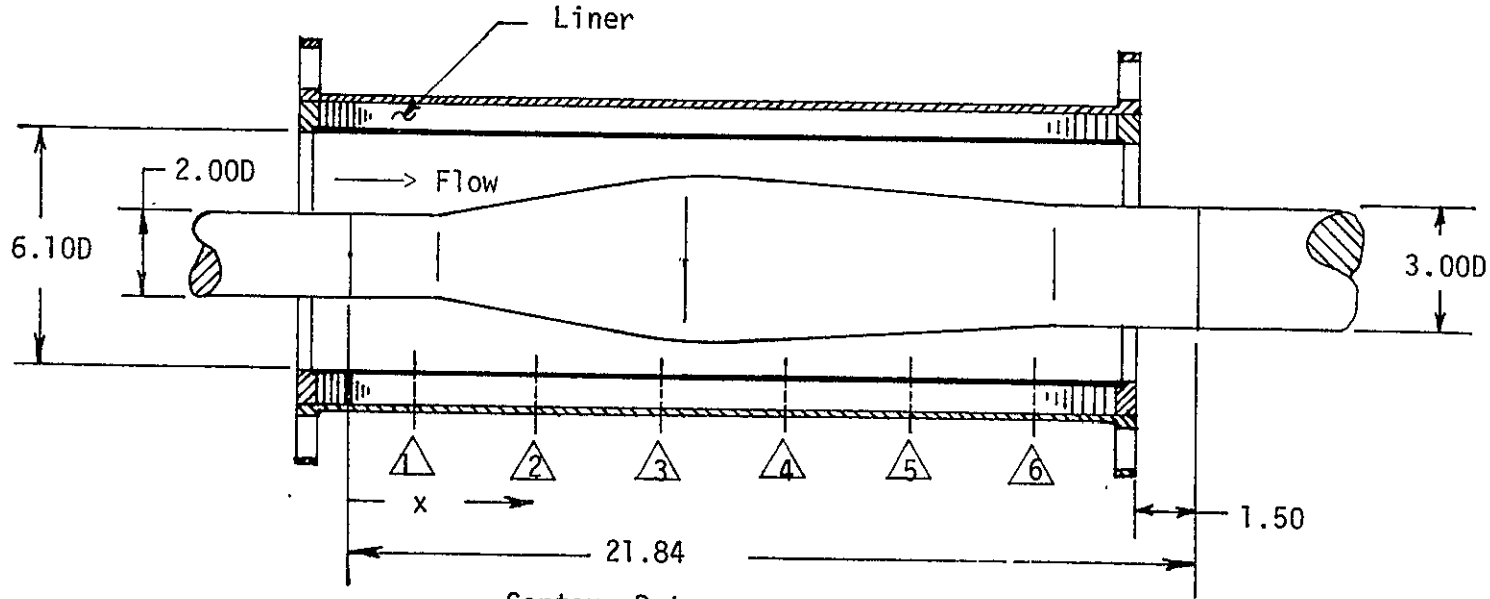

- Contour Data -

x	Diameter	x	Diameter	x	Diameter	x	Diameter
2.250	2.000	7.878	4.241	8.678	4.296	17.250	3.077
2.270	2.005	7.928	4.248	8.778	4.294	17.350	3.0695
2.290	2.010	7.978	4.256	8.878	4.290	17.450	3.062
2.295	2.012	8.028	4.263	9.028	4.282	17.750	3.0370
2.310	2.015	8.078	4.270	9.078	4.279	17.950	3.021
2.340	2.021	8.128	4.276	9.278	4.268	18.250	3.000
2.390	2.031	8.228	4.281	9.478	4.258		
2.470	2.111	8.278	4.285	9.678	4.247		
		8.378	4.291				
		8.478	4.295				
		8.528	4.295				
		8.578	4.296				

All dimensions are in inches

Δ Axial Probe Locations

Figure 4. Variable-area centerbody

2.3 Instrumentation

The instrumentation associated with the experimental facility consists of three parts: source instrumentation, servo-control instrumentation and probe instrumentation. Each of the three parts is explained in detail. A schematic of the complete electronic system is shown in Fig. 5. Since much of the instrumentation has evolved from the Spectral Dynamics vibrational control system, this system is explained in detail prior to explaining each of the separate instrumentation sections.

2.3.1 Basic control system

The basic instrumentation system has been built around a system of Spectral Dynamics instruments that are designed to control vibrational shakers. The four instruments are an SD 104A-5 sweep oscillator, an SD 105-A amplitude servo/monitor, an SD 122 dual channel tracking filter, and an SD 127 MZ/TFA control. A brief explanation of the function of each of the instruments and their interconnection follows.

The SD 104A-5 sweep oscillator provides a constant amplitude sinusoidal voltage. This voltage is used as a source for the SD 105-A amplitude servo/monitor and as a reference frequency by the SD 122 tracking filter.

The SD 105-A amplitude servo/monitor is a servo-control device designed to maintain either acceleration, velocity or displacement constant in shaker application. No instrument

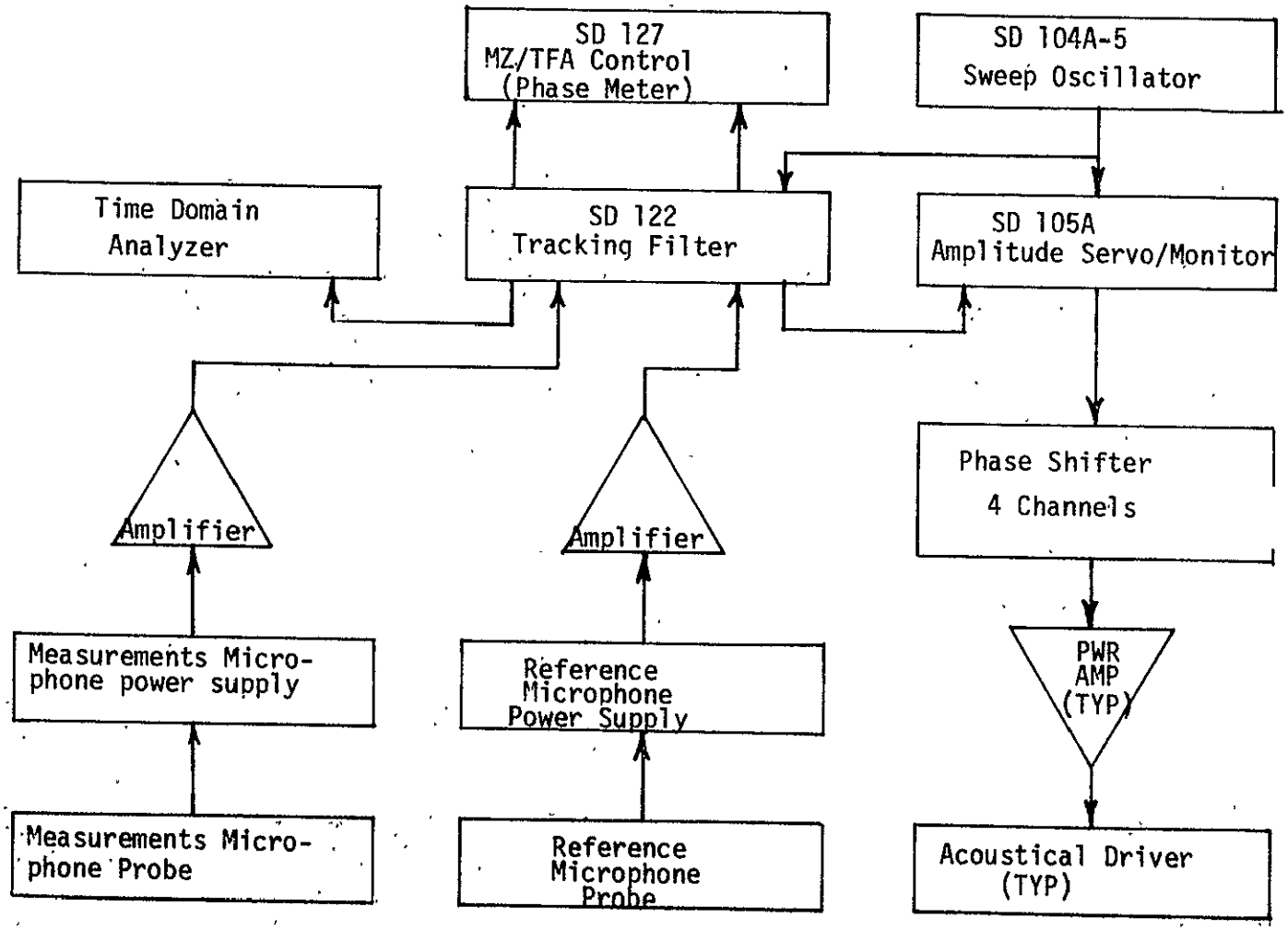

Figure 5. A schematic of acoustic research facility electronics

modification is required for use in these acoustical experiments. In these experiments the SD 105-A is used to keep the sound pressure level constant at the 12:00 o'clock position of axial station 1. A "cross-over" feature is also utilized to insure that the power rating of the acoustical drivers is not exceeded.

The SD 122 tracking filter is a dual channel tunable filter. The unit uses the constant amplitude output of the SD 104A-5 sweep oscillator as a reference frequency. Bandwidths of 2, 5, 10, 20, 50, and 100 Hz are available. In these experiments, one channel of the tracking filter is used in the serro control circuit (10 Hz bandwidth), and the other channel is used in the probe measurement circuit (2 Hz bandwidth) to separate the imput frequency from the flow noise.

The SD 127 MZ/TFA control is basically an integrator used to obtain impedance plots in vibration applications. The SD 127 is interconnected with the SD 122 tracking filter and serves as a phase meter in the experiments.

2.3.2 Microphone Probe Assembly

One of the crucial parts of the measurement system is the microphone probe assembly. A schematic of the assembly is shown in Fig. 6. The four basic components of the probe assembly are a 1/2-inch B&K type 4133 microphone, a probe block, a termination coil, and a probe tip. The basic

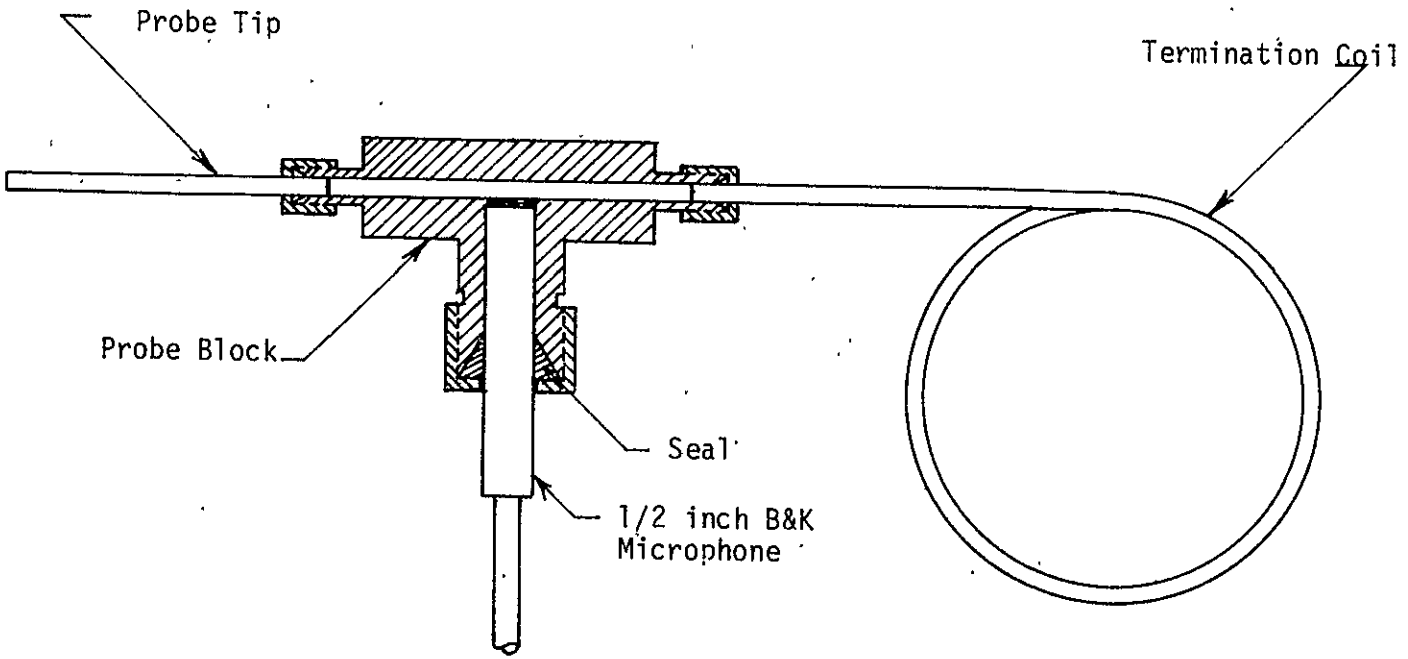

Figure 6. Microphone probe assembly

diameter of the probe tip is 1/8-inch. The design is based on a similar probe utilized by General Electric in jet engine studies[43].

Although the purpose of the termination coil in this design was to eliminate resonances in the microphone assembly, resonances similar to those observed with the standard B & K microphone probe assembly[44] were present. The response of such a probe may be improved over a narrow frequency band by suitable damping. However, since only three discrete frequencies have been examined in the experiments, the probe simply has been calibrated at the frequencies of interest, rather than attempting to use damping.

The microphone probe assemblies have been calibrated using a standard B&K microphone probe calibrator, using standard B&K procedures as follows. Care is taken to insure that the probe tip is maintained in the uniform sound field produced by the calibrator. With the probe assembly inserted into the calibration assembly, the frequency of the sine random generator is set using a counter. The output of the B&K type 1024 sine random generator is fully compressed and compression slowly reduced until the desired calibration level is reached. The rms voltage of the reference microphone and the probe assembly are recorded. The effective sensitivity of each of the microphone probe assemblies is calculated from the following formula:

$$S_p = \frac{S_r V_r}{V_p}$$

where S_p = Sensitivity of probe microphone (N/M^2)

S_r = Sensitivity of reference microphone (N/M^2)

V_r = RMS voltage of reference microphone

V_p = RMS voltage of probe microphone

Note that since the same amplifier is used in measuring both the reference microphone and probe microphone voltages, any errors associated with the amplifier gain will cancel. In these experiments, the microphone probe assemblies have been calibrated at 840, 2640 and 3150 Hz.

In the hard-walled experiments it was possible to use one microphone probe assembly. This reduced the amplitude and phase errors associated with using many probes and amplifiers. In the experiments using a soft-walled test section one microphone probe block has been used together with many permanently-installed microphone probe tips. Care has been taken to insure that the length of each probe tip is within a $\pm$ .010-inch tolerance. Each probe tip has been individually calibrated in the probe block with respect to both amplitude and phase. The sensitivity of each of the probe tips is within 5% of the average value, and the phase shift associated with individual probe tips is within the $\pm$ 2 degrees recording accuracy.

2.3.3 Acoustical source electronics

As described previously, the electronic driver instrumentation consists of the SD 104A-5 sweep oscillator, the SD 104-A amplitude servo-monitor, one channel of the SD 122 tracking filter, a phase shifter, a power amplifier, the reference microphone probe and a signal conditioning amplifier.

The output of the reference probe-microphone assembly is fed via the SD 122 tracking filter (with a 10 Hz bandwidth) to the servo-input of the SD 105-A servo-monitor. An initial voltage setting is then selected which is within the rating of the acoustical drivers. The servo-control then maintains the SPL constant at the reference microphone probe.

2.3.4 Data acquisition system

The data acquisition electronics consist of the data microphone probe assembly and its signal conditioning amplifier, the SD 122 tracking filter and the SD 127 controller. The microphone probe signal is filtered and amplified by the signal conditioning amplifier. Limited filtering is effected by this amplifier. The filtering for data acquisition is accomplished by use of the SD 122 tracking filter. A bandwidth of 2 Hz has been used in the SD 122 tracking filter. Thus, data has been obtained only within $\pm$ 1 Hz of the signal supplied to the acoustic drivers.

The rms value of the amplified and conditioned output is measured with a true rms voltmeter. Under no-flow conditions relative rms values of amplitude are limited only by the accuracy of the digital voltmeter. This error is typically less than .1%.

Phase, relative to the reference probe, is obtained by utilizing the phase capabilities of the SD 127 MZ/TFA controller and can be recorded to an accuracy of $\pm$ 2°.

2.4 Experimental Set-up

In some of the experimental tests an attempt was made to minimize the presence of higher modes in the acoustic signal that enters the test section. The oscillator was set to the chosen frequency, which was verified with the aid of a counter, and the servo controls that regulate the sound pressure level amplitude were by-passed. Each of the four acoustic driver units was tested independently to determine the amplifier and phase-shifter settings required to produce specified signals at a measuring station. The measuring station for this set-up procedure was at the same circumferential location as the acoustic driver being investigated. For the soft-walled test section, these set-up measurements were made at the downstream end of the signal-insertion section, and for the the hard-walled test section the measurements were made at the first station (station 1) of the test section. After the capabilities of each acoustic driver unit had been determined, each was supplied, in turn, with the same signal from the oscillator, and the amplifier and phase shifter for each driver unit were set to produce identical acoustic signals at each unit's measuring station.

All four acoustic drivers were then connected in parallel, to be driven by the same oscillator, and the system returned to servo control following the normal procedures outlined in the SD manual. The servo control

operated to maintain the sound pressure level constant during the tests.

There was, of course, some interaction between the acoustic drivers. The impedance seen by one acoustic driver was altered by the acoustic signals coming from the other three acoustic drivers. Consequently, the phase of the signal obtained was somewhat different from the arbitrarily selected phase angle used in the set-up procedure. Thus, the dominant acoustic signal was the plane mode, with relatively smaller amplitudes of the spinning modes present.

2.5 Summary

An acoustic duct facility has been constructed for studies of sound propagation through mean flows that possess both axial and transverse velocity gradients. The design of the duct facility controls the mean flow so that the mean boundary layer in the test section is thin, and controls the ambient noise levels through the use of line mufflers and an anechoic termination. The annular test section can be selected to have either a rigid or lined outer wall; the cross-sectional area can be either constant or variable by selection of a straight or variable-radius inner wall, which is rigid. The duct liner consists of a 40-Rayl Feltmetal facing sheet that covers .625-inch cellular cavities. The duct has been instrumented to permit acquisition of narrow band data for determination of the relative amplitudes and phases of the acoustic disturbance along the outer wall of the test section. The test sections are provided with sufficient microphone probe locations to permit resolution of the modal content of the acoustic signal up to the third circumferential mode.

3. Hard-Walled Annular Ducts Without Flow

In this section, an analytic solution is determined to the problem of sound propagation in hard-walled annular ducts with slowly-varying cross sectons in the absence of mean flow. Experimental studies of propagation in the hard-walled duct are described, and the experimental and analytical results are compared.

3.1 Theory

In the absence of mean flow and for negligible dissipation, the propagation of sound in a hard-walled annular duct can be mathematically described by the wave equation

$$\nabla^2\phi - \frac{1}{c^2}\frac{\partial^2\phi}{\partial t^2} = 0 \tag{1}$$

subject to the boundary conditions

$$\frac{\partial\phi}{\partial r} = \varepsilon R_1' \frac{\partial\phi}{\partial x} \text{ at } r = R_1(x_1) \tag{2}$$

$$\frac{\partial\phi}{\partial r} = \varepsilon R_2' \frac{\partial\phi}{\partial x} \text{ at } r = R_2(x_1) \tag{3}$$

where $\phi(x,r,\theta,t)$ is the potential function, ε is a small dimensionless parameter, $x_1 = \varepsilon x$ is a long scale describing the slow axial variations of the duct cross-section, R_1 and R_2 are the inner and outer radii of the duct, and primes denote differentiation with respect to the argument.

An approximate solution to Eqs. (1)-(3) is sought by using the method of multiple scales[45] in the form

$$\phi(x,r,\theta,t) = [\psi_0(x_1,r) + \varepsilon\psi_1(x_1,r) + \ldots]\exp[i(\eta + m\theta)] \tag{4}$$

The spinning mode number m is an integer and

$$\frac{\partial \eta}{\partial t} = -\omega \ , \quad \frac{\partial \eta}{\partial x} = k(x_1) \tag{5}$$

where ω is the sound frequency, which is assumed to be constant, and $k(x_1)$ is the wavenumber. The axial and time derivatives become

$$\frac{\partial}{\partial t} = -\omega \frac{\partial}{\partial \eta}$$
$$\frac{\partial}{\partial x} = k \frac{\partial}{\partial \eta} + \epsilon \frac{\partial}{\partial x_1} \tag{6}$$

Substituting Eqs. (4)-(6) into Eqs. (1)-(3) and equating coefficients of like powers of ϵ, one obtains

Order ϵ^0

$$\frac{\partial^2 \psi_0}{\partial r^2} + \frac{1}{r}\frac{\partial \psi_0}{\partial r} + \left(\frac{\omega^2}{c^2} - k^2 - \frac{m^2}{r^2}\right)\psi_0 = 0 \tag{7}$$

$$\frac{\partial \psi_0}{\partial r} = 0 \quad \text{at} \quad r = R_1 \tag{8}$$

$$\frac{\partial \psi_0}{\partial r} = 0 \quad \text{at} \quad r = R_2 \tag{9}$$

Order ϵ^1

$$\frac{\partial^2 \psi_1}{\partial r^2} + \frac{1}{r}\frac{\partial \psi_1}{\partial r} + \left(\frac{\omega^2}{c^2} - k^2 - \frac{m^2}{r^2}\right)\psi_1 = -2ik \frac{\partial \psi_0}{\partial x_1} - ik_1' \psi_0 \tag{10}$$

$$\frac{\partial \psi_1}{\partial r} = ikR_1' \omega_0 \text{ at } r = R_1 \tag{11}$$

$$\frac{\partial \psi_1}{\partial r} = ikR_2' \psi_0 \text{ at } r = R_2 \tag{12}$$

The solution of Eqs. (7)-(9) is

$$\psi_0 = A_{mn}(x_1)\Psi_{mn}(r;x_1) \tag{13}$$

$$\Psi_{mn} = J_m(\gamma_{mn}r) - \frac{J_m'(\gamma_{mn}R_1)}{Y_m'(\gamma_{mn}R_1)} Y_m(\gamma_{mn}r) \tag{14}$$

The γ_{mn} are the roots of

$$J_m'(\gamma R_2)Y_m'(\gamma R_1) - J_m'(\gamma R_1)Y_m'(\gamma R_2) = 0 \tag{15}$$

and the wavenumber k_{mn} is related to γ_{mn} by

$$k_{mn}^2 = \frac{\omega^2}{c^2} - \gamma_{mn}^2 \tag{16}$$

In Eq. (13), $A_{mn}(x_1)$ is undetermined at this level of approximation; it is determined by imposing a solvability condition at the next level of approximation.

With ψ_0 and k_{mn} known, the inhomogeneous Eqs. (10)-(12) have a solution if, and only if, their right-hand sides satisfy a solvability condition, since their homogeneous parts have a nontrivial solution. To determine this solvability condition, multiply Eq. (10) by $r\psi_0$, integrate the result by parts from $r = R_1$ to $r = R_2$ to transfer the derivatives from ψ_1 to ψ_0, and use Eqs. (7)-(9) to obtain

$$R_2\psi_0 \frac{\partial\psi_1}{\partial r}\bigg|_{r=R_2} - R_1\psi_0 \frac{\partial\psi_1}{\partial r}\bigg|_{r=R_1} = -i\int_{R_1}^{R_2} r \frac{\partial}{\partial x_1} \times (k_{mn}\psi_0^2)dr \tag{17}$$

Substituting for $\partial\psi_1/\partial r$ at $r = R_1$ and R_2 from Eqs. (11) and (12) into Eq. (17), we have

$$k_{mn}R_2R_2'\psi_0^2\big|_{r=R_2} - k_{mn}R_1R_1'\psi_0^2\big|_{r=R_1} + \int_{R_1}^{R_2} r \frac{\partial}{\partial x_1} \times (k_{mn}\psi_0^2)dr = 0 \tag{18}$$

Using Leibnitz' rule, we rewrite Eq. (18) as

$$\frac{\partial}{\partial x_1}\left[k_{mn}\int_{R_1}^{R_2} r\psi_0^2 dr\right] = 0 \tag{19}$$

or

$$A_{mn}^2 k_{mn}\int_{R_1}^{R_2} r\Psi_{mn}^2 dr = \text{constant} \tag{20}$$

Since $\partial\psi_0/\partial r = 0$ at $r = R_1$ and R_2,

$$\int_{R_1}^{R_2} r\Psi_{mn}^2 dr = \frac{1}{2} R_2^2\left(1 - \frac{m^2}{\gamma_{mn}^2 R_2^2}\right)\Psi_{mn}\Big|_{r=R_2} - \frac{1}{2} R_1^2 \times \left(1 - \frac{m^2}{\gamma_{mn}^2 R_1^2}\right)\Psi_{mn}^2\Big|_{r=R_1}$$

Hence,

$$A_{mn} = \frac{D_{mn}(x_{1_r})}{D_{mn}(x_1)} A_{mn}(x_{1_r}) \tag{21}$$

where x_{1_r} is a reference axial location, the complex amplitudes $A_{mn}(x_{1_r})$ at the reference location must be found experimentally, and

$$D_{mn}^2 = \frac{1}{2} k_{mn}\left(R_2^2 - \frac{m^2}{\gamma_{mn}^2}\right)\left[J_m(\gamma_{mn}R_2) - \frac{J_m'(\gamma_{mn}R_2)}{Y_m'(\gamma_{mn}R_2)} Y_m(\gamma_{mn}R_2)\right] - \frac{1}{2} k_{mn}\left(R_1^2 - \frac{m^2}{\gamma_{mn}^2}\right)\left[J_m(\gamma_{mn}R_1) - \frac{J_m'(\gamma_{mn}R_1)}{Y_m'(\gamma_{mn}R_1)} Y_m(\gamma_{mn}R_1)\right] \tag{22}$$

Thus, the complex acoustic pressure variation of a single mode at the outer wall is given by

$$p_{mn}(x,R_2,t) = -i\omega A_{mn}(x_{1_r}) \frac{D_{mn}(x_{1_r})}{D_{mn}(x_1)} \Psi_{mn}(R_2;x_1) \times$$

$$\exp[i(\int_{x_r}^{x} k_{mn}dx + m\theta - \omega t)] \qquad (23)$$

where the eigenfunction Ψ_{mn} is defined by Eq. (14) and the axial amplitude variation is defined by Eq. (22). This may be re-written as

$$p_{mn}(x,R_2,t) = B_{mn} \frac{D_{mn}(x_{1_r})}{D_{mn}(x_1)} \frac{\Psi_{mn}(R_2;x_1)}{\Psi_{mn}(R_2;x_{1_r})} \times$$

$$\exp[i(\int_{x_r}^{x} k_{mn}dx + m\theta - \omega t)] \qquad (24)$$

where the constant B_{mn} is determined experimentally and is the complex amplitude of the mode at the reference station. The acoustic pressure is summed over all modes present in the duct, and the result is expressed in terms of an amplitude and phase of the total signal for comparison with the experimental data in Section 3.3.

3.2 Preliminary Investigations Using the Hard-Walled Test Section

To facilitate the comparison of experimental and theoretical results, it is desirable to obtain experimental data for conditions which are not close to a mode cut-on frequency. By considering only well cut-on modes, strong reflections leading to upstream propagating modes and strong axial standing waves are avoided. Thus a preliminary investigation was conducted to determine the conditions for which strong standing waves occur for cases with and without mean flow. These results are easily compared with the theoretical hard-walled cut-on frequencies, giving a relatively simple check of the instrumentation and the validity of the theoretical modelling of the experimental facility. Finally, the frequencies at which more extensive and detailed tests were to be conducted are identified in this section.

3.2.1 Low-frequency standing waves

Since the acoustical horn on the end of the duct is least efficient at low frequencies, the system has been checked for standing waves at a frequency below the cut-on frequency of the first circumferential mode. A frequency of 840 Hz was selected for this examination, and the experiments were conducted using the straight centerbody. Acoustic pressures were measured at each axial location and were found to be within $\pm$ 0.5 dB in amplitude. It was

concluded that no axial standing waves existed. Since the efficiency of the acoustical horn would increase with increasing frequency, it was also concluded that no substantial standing waves existed in the frequency range of interest, provided that all propagating modes were well cut on.

3.2.2 Cut On of Higher Circumferential Modes

At frequencies close to the cut-on frequencies of the circumferential modes, strong reflections from the duct termination are anticipated, and it was desired to avoid conducting the experiments at these frequencies. The cut-on frequency is defined as the frequency at which the axial wavenumber for that mode is zero; that is, the wave is not a propagating wave. For a circular, annular duct having hard walls, the acoustic waves at cut on may be visualized as m-lobed circumferential spinning waves of constant amplitude along the axial length.

Plumblee et al[41] have shown that the cut-on frequencies may be obtained experimentally by sweeping an acoustic driver through the appropriate frequency range and monitoring the pressure amplitude at some downstream station. Using this procedure, the strong reflections that occur near cut-on frequencies generate large pressure amplitudes within the duct which are easily detected.

Figure 7 gives the voltage output from the measuring-microphone amplifier, and thus provides an indication of the pressure amplitude as a function of the exciting frequency. These measurements were made in the hard-walled test section with the straight centerbody (1.5-inch radius) installed. The cut-on frequencies correspond to the peaks and are clearly visible. The amplitudes shown in Fig. 7 have not been corrected for the response of the microphone probe. Since the relation between the voltage output and the pressure amplitude is not constant over the entire frequency range, the results in Fig. 7 cannot be used in a quantitative manner to calculate sound pressure amplitudes. All the peaks observed in Fig. 7 agree with those expected for the hard-walled annular duct. Theoretically, the cut-on frequencies may be obtained by setting the wavenumber, k_{mn}, equal to zero in the eigenvalue equation

$$k_{mn}^2 = \frac{\omega^2}{c^2} - \gamma_{mn}^2 \tag{25}$$

where ω is the circular frequency, c is the speed of sound of the medium, and γ_{mn} is the characteristic number. The characteristic numbers, γ_{mn}, are the roots of the equation

$$J_m'(\gamma R_1)Y_m'(\gamma R_2) - J_m'(\gamma R_2)Y_m'(\gamma R_1) = 0 \tag{26}$$

The freqencies satisfying this equation (the cut-on frequencies) for the hard-walled test section are given in Table 1.

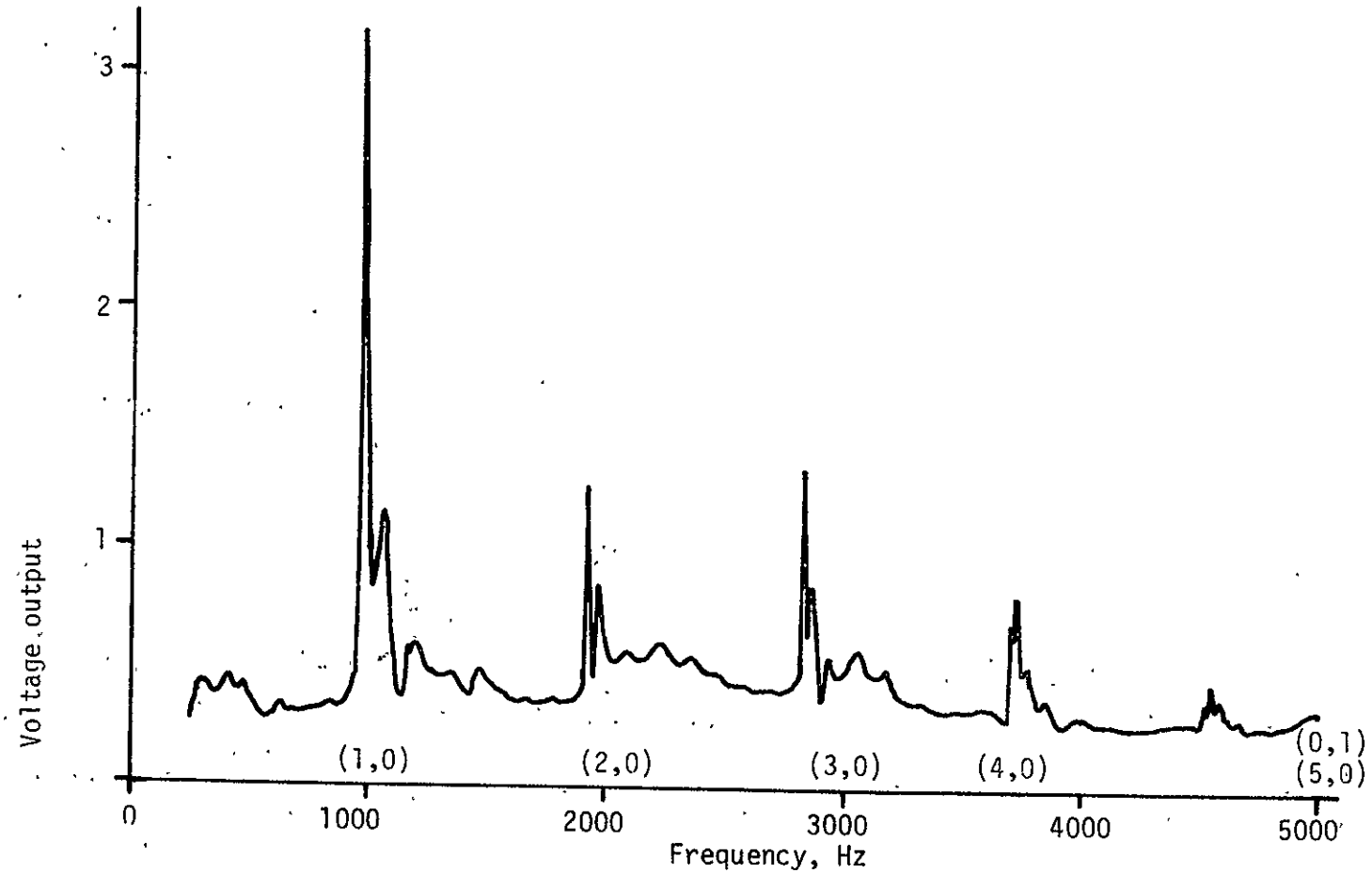

Figure 7. Frequency characterization of hard-wall test section with uniform centerbody installed.

Table 1. Theoretical cut-on frequencies for a hard-walled duct with R_2 = 3.05".

Mode Number* m,n	Cut-on Frequencies, Hz	
	Inner radius R_1 = 1.0"	Inner radius R_1 = 1.5"
0,0	-	-
0,1	3356	4336
0,2	6518	8558
0,3	9713	12802
0,4	12920	-
1,0	1066	939
1,1	3615	4459
1,2	6639	8616
1,3	9791	12840
1,4	12977	-
2,0	2024	1856
2,1	4317	4813
2,2	7002	8789
2,3	10024	12955
3,0	2870	2736
3,1	5262	5366
3,2	7597	9073
3,3	10412	13143
4,0	3657	3573
4,1	6252	6071
4,2	8405	9461
4,3	10954	13405
5,0	4417	4372
5,1	7185	6880
5,2	9356	9946
5,3	11651	13755
6,0	5167	5143
6,1	8061	7748
6,2	10345	10521

*m - Circumferential mode number
n - Radial mode number

The agreement between the theoretical and experimental values is good. The resonant frequencies, which are approximately three percent higher than the theoretical cut-on frequencies, are sharply defined. The three percent shift in the frequency of peak response is a consequence of damping and is consistent with the observations of an earlier study (Ref. 41, pp. 53-55). For this particular hub-to-tip ratio, no radial modes were encountered before the third circumferential mode cut-on frequency.

Figure 8 is a similar plot showing the variation of the amplitude with frequency for the system with the variable-area centerbody installed. In the signal-insertion section, the variable centerbody has a radius of 1 inch. This smaller hub-to-tip ratio shifts the cut-on frequencies of the fundamental radial modes (n=0) to higher values and lowers the cut-on frequencies of the higher radial modes (see Table 1). The shift of the resonance of the spinning modes to higher frequencies is apparent in a comparison of Figs. 7 and 8. As before, the resonance peaks appear at frequencies that are three percent higher than the hard-walled cut-on frequencies. The first radial-mode cut-on frequency in the signal-insertion section is lowered from 4336 Hz to 3356 Hz, and this appears as a sharp valley in the amplitude spectrum at 3450 Hz (three percent higher than 3356 Hz). Although the first radial mode is cut on in the signal-insertion section at this frequency, it cuts off in the variable-area

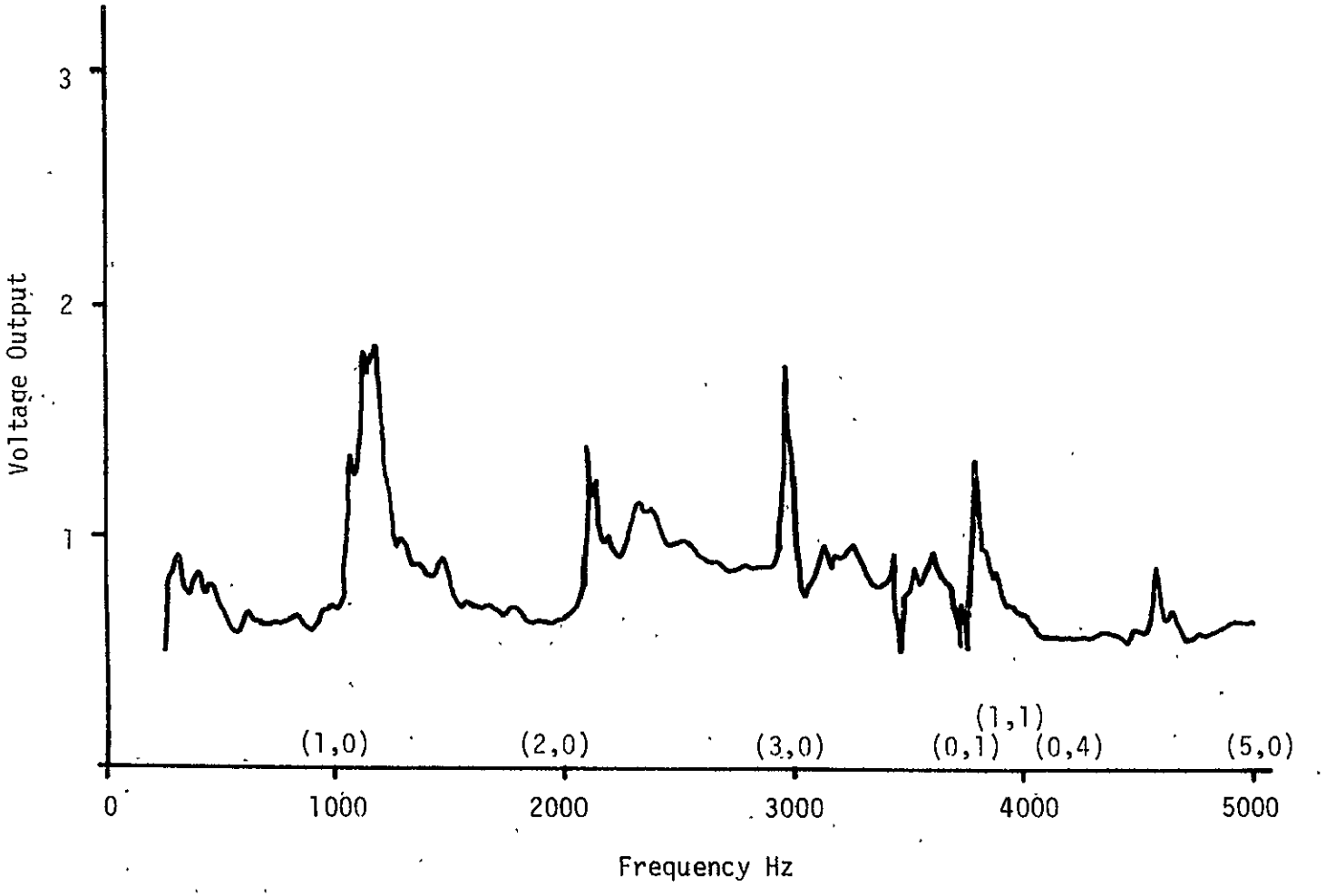

Figure 8. Frequency characterization of hard-wall test section with variable area centerbody installed.

section just downstream; the reflection from the variable-area centerbody at the cut-off point apparently causes a partial cancellation of the signal upstream. The sharp valley at 3720 Hz corresponds to cut on of the (1,1) mode. The variable-area centerbody introduces a slight resonance in the region of 2300-2450 Hz; the origin of this resonance is unclear, and it was decided to avoid further testing in this range. Using the results of these two figures and attempting to avoid resonance conditions, we decided to carry out detailed experimental studies at three frequencies: one, 840 Hz, just below cut on of the first spinning mode; a second, 2640 Hz, just before cut on of the third spinning mode; a third, 3150 Hz, between cut on of the third spinning mode and the first radial mode.

3.2.3. Preliminary Tests with Mean Flow

When air is flowing through the test section, the cut-off frequencies are changed. Theory predicts that the effective cut-on frequency will vary with flow velocity as

$$f_c' = f_c \sqrt{1 - M^2} \qquad (27)$$

where f_c is the original cut-on frequency without flow.

Tests were run using the variable-area centerbody in both the soft-walled and hard-walled test sections. The tests confirmed the shifts in the resonance frequencies and showed a strong resonance for the first radial mode, unlike

the no-mean-flow cases. The test frequency of 3150 Hz was selected in an attempt to avoid this strong resonance.

Measurements also were made to determine the effect of the mean flow on the control of the input signals. As noted in Section 2, the input drivers could be controlled to minimize the presence of the circumferential modes; the acoustical wave at station 1 could be maintained plane within $\pm$ 2 dB in amplitude and $\pm$ 15° in phase for the 3150 Hz test frequency, and within $\pm$ 0.1 dB in amplitude and a $\pm$ 2° in phase for the 840 Hz signal. Because of the difference in impedance presented to the sound sources, the relative amplitudes of the higher modes increased somewhat as the free-stream velocity increased.

3.3. Comparison of Experimental and Theoretical Results

The theoretical prediction method described in Section 3.1 predicts the attenuation and phase shift of each acoustic mode as it propagates through the test section, provided the relative amplitude of each mode is known.

In order to establish the modal content of the signal, detailed measurements of amplitude and phase around the circumference at station 1 are necessary. Since the highest test frequency (3150 Hz) allows the third circumferential mode to propagate, at least seven measurements of amplitude and phase are required. The duct instrumentation was designed to provide this data. A least-squares technique is used to obtain the complex constants B_{mn} of Eq. (24). Once these constants are determined, the acoustical pressure at the outer wall at the downstream locations are obtained using Eq. (24).

The first experiments performed were those using a hard-walled test section and a variable-area centerbody. Figures 9a and 9b show the circumferential variation of the pressure amplitude and phase, respectively, at the outer walls for three axial stations for an input frequency of 840 Hz. Only one mode, the plane mode, is cut on at this frequency. Both the amplitude and the phase measurements are in good agreement with the theoretical predictions. The theory shows the intensification of the signal as it propagates from station 1 to station 3 although it slightly overpredicts the increase.

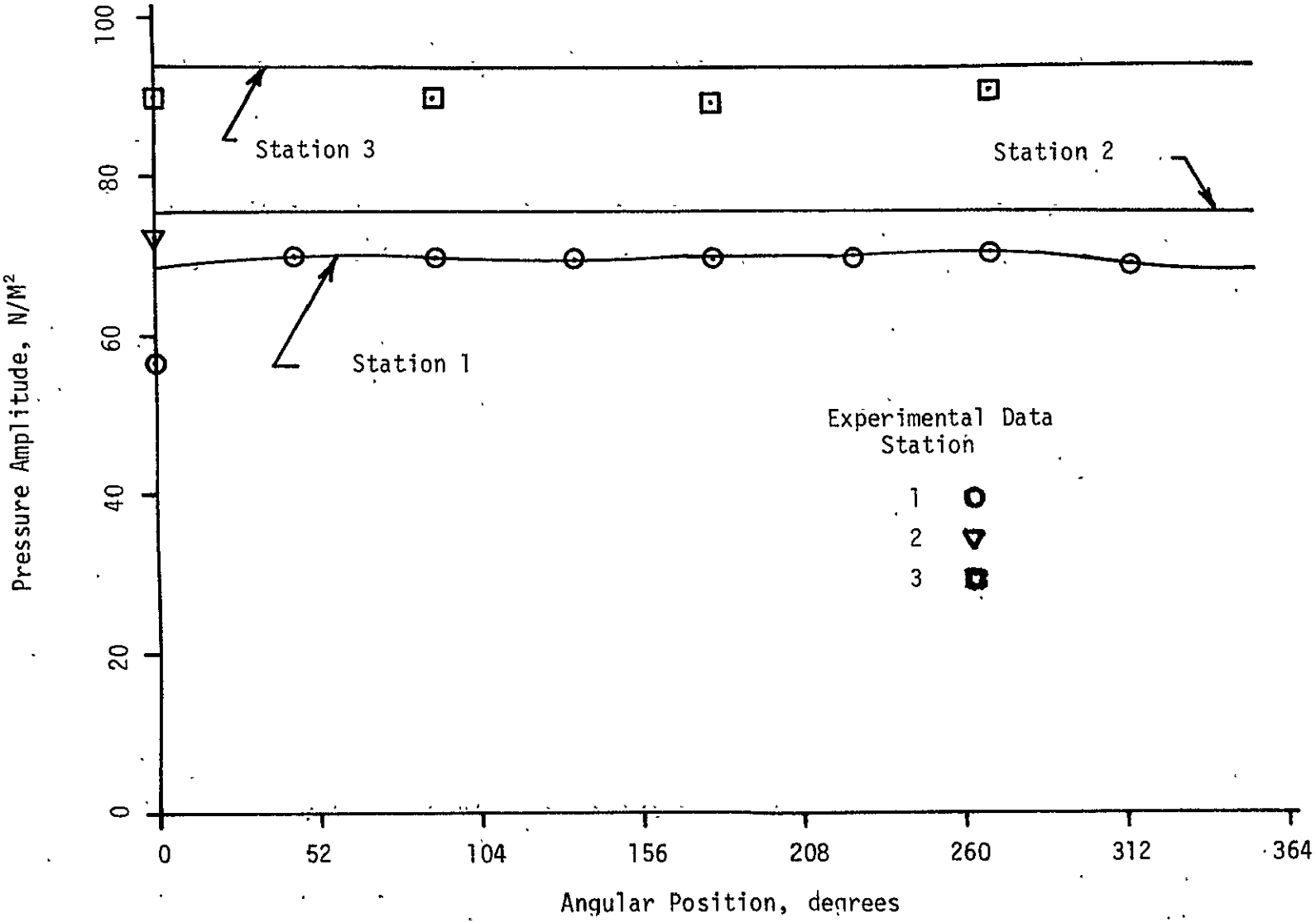

Figure 9a. Comparison of the theoretical and experimental pressure amplitudes for the hard-walled case; M = 0 and f = 840Hz

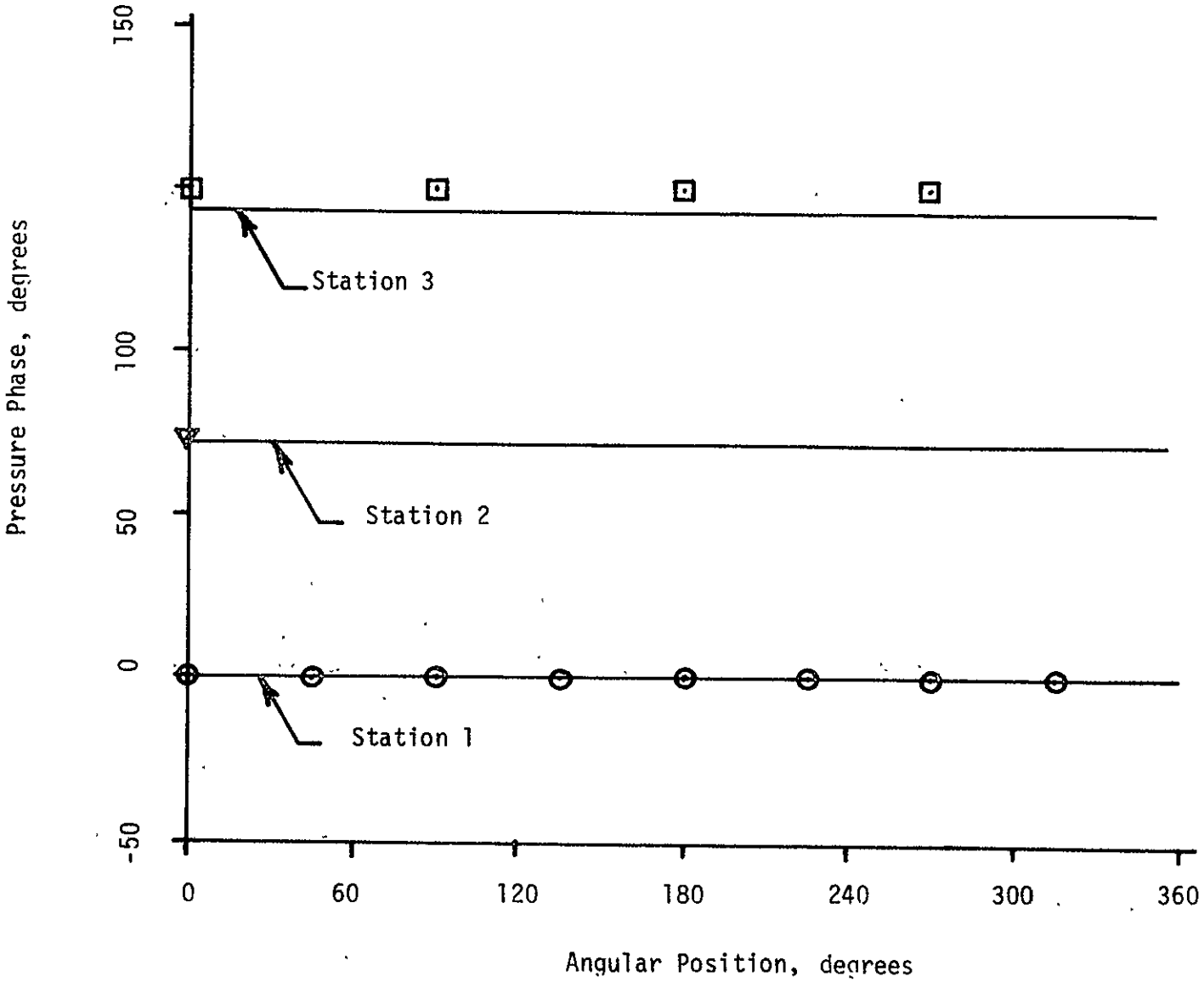

Figure 9b. Comparison of the theoretical and experimental pressure phases for the hard-walled case; M = 0 and f = 840 Hz.

Figures 10a and 10b are similar plots for an input frequency of 2640 Hz. Three modes (plane, 1st circumferential, and 2nd circumferential) are cut on at this frequency. Both the amplitude and the phase predictions agree very well with the measured values. The measured increase in the acoustic intensity as well as the decrease in the circumferential variation of the pressure are both predicted by the theory.

Figures 11a and 11b show results for an input frequency of 3150 Hz. Four modes (plane, 1st, 2nd, and 3rd circumferential) are cut on at this frequency. Although there is a reasonable agreement between the measured and predicted phases, the circumferential variation of the pressure amplitudes is not adequately predicted by the theory. Nevertheless, the theory does correctly show that the circumferential average of the pressure amplitude increases as the signal propagates down the duct.

It is apparent from all three cases that more probe positions are needed at downstream locations especially if significant components of higher spinning modes are present. Consequently, the lined-duct tests, which were conducted later, included more probe locations at stations 2 and 3.

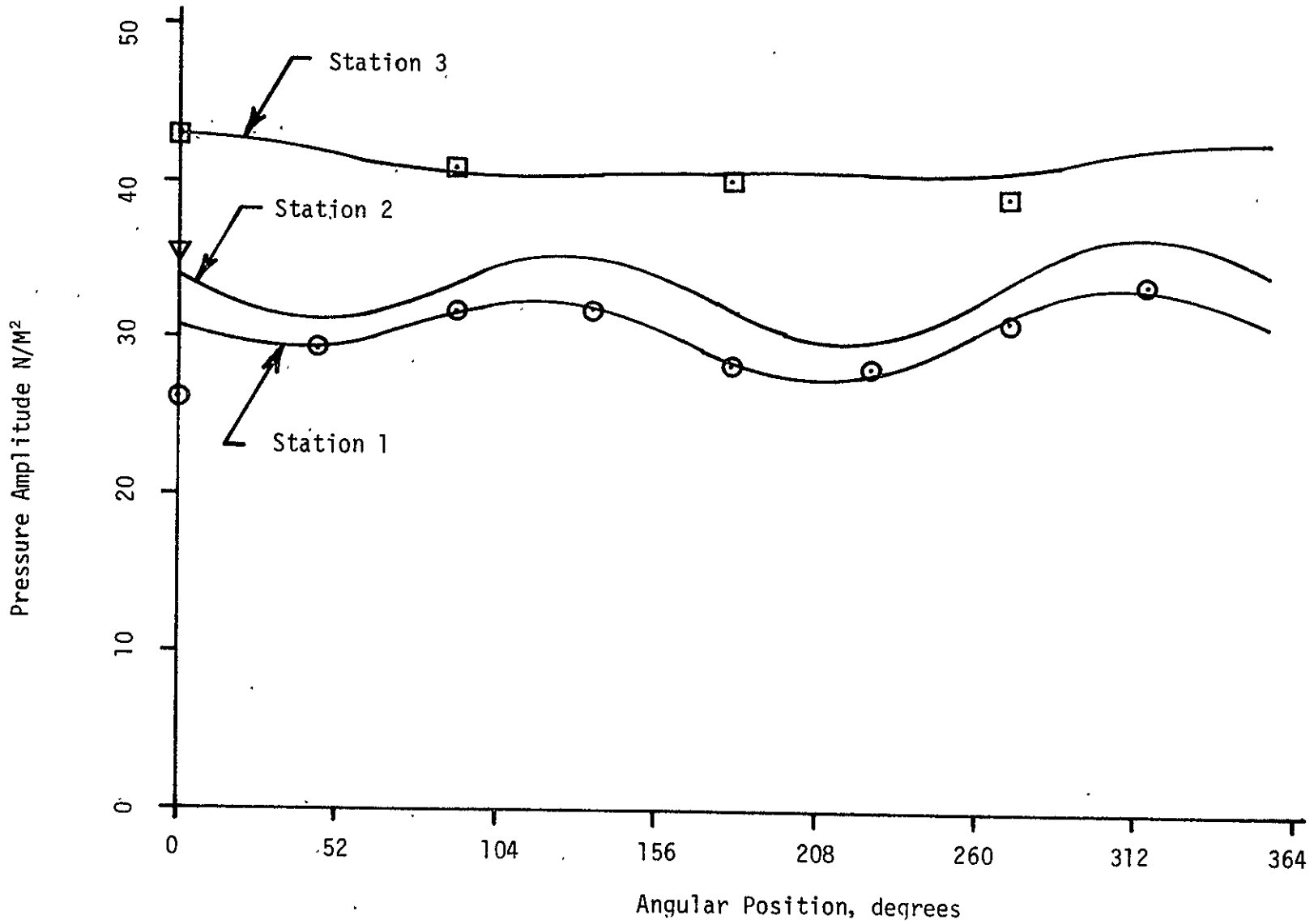

Figure 10a. Comparison of the theoretical and experimental pressure amplitudes for the hard-walled case; M = 0 and f = 2640 Hz.

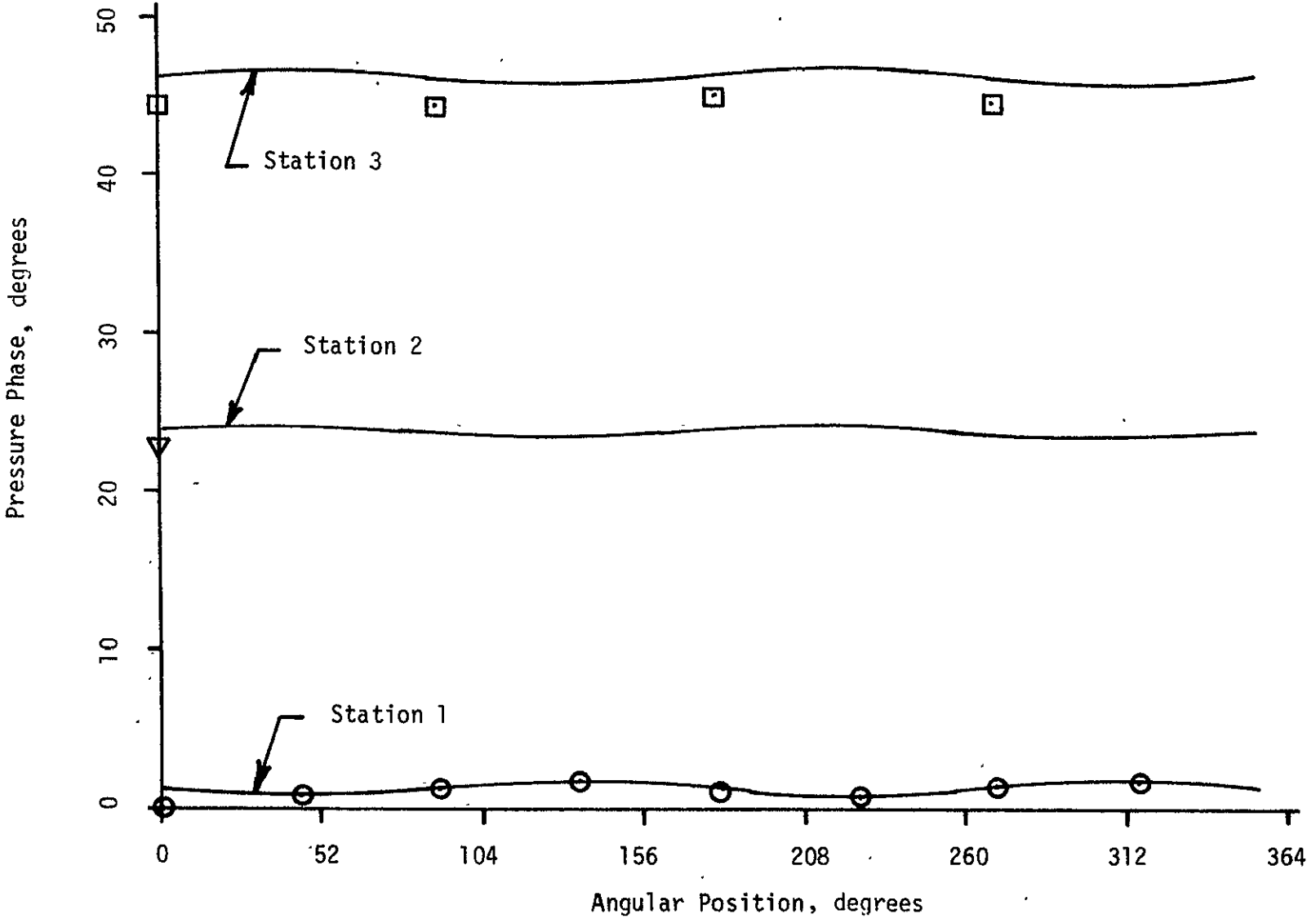

Figure 10b. Comparison of the theoretical and experimental pressure phases for the hard-walled case; M = 0 and f = 2640 Hz.

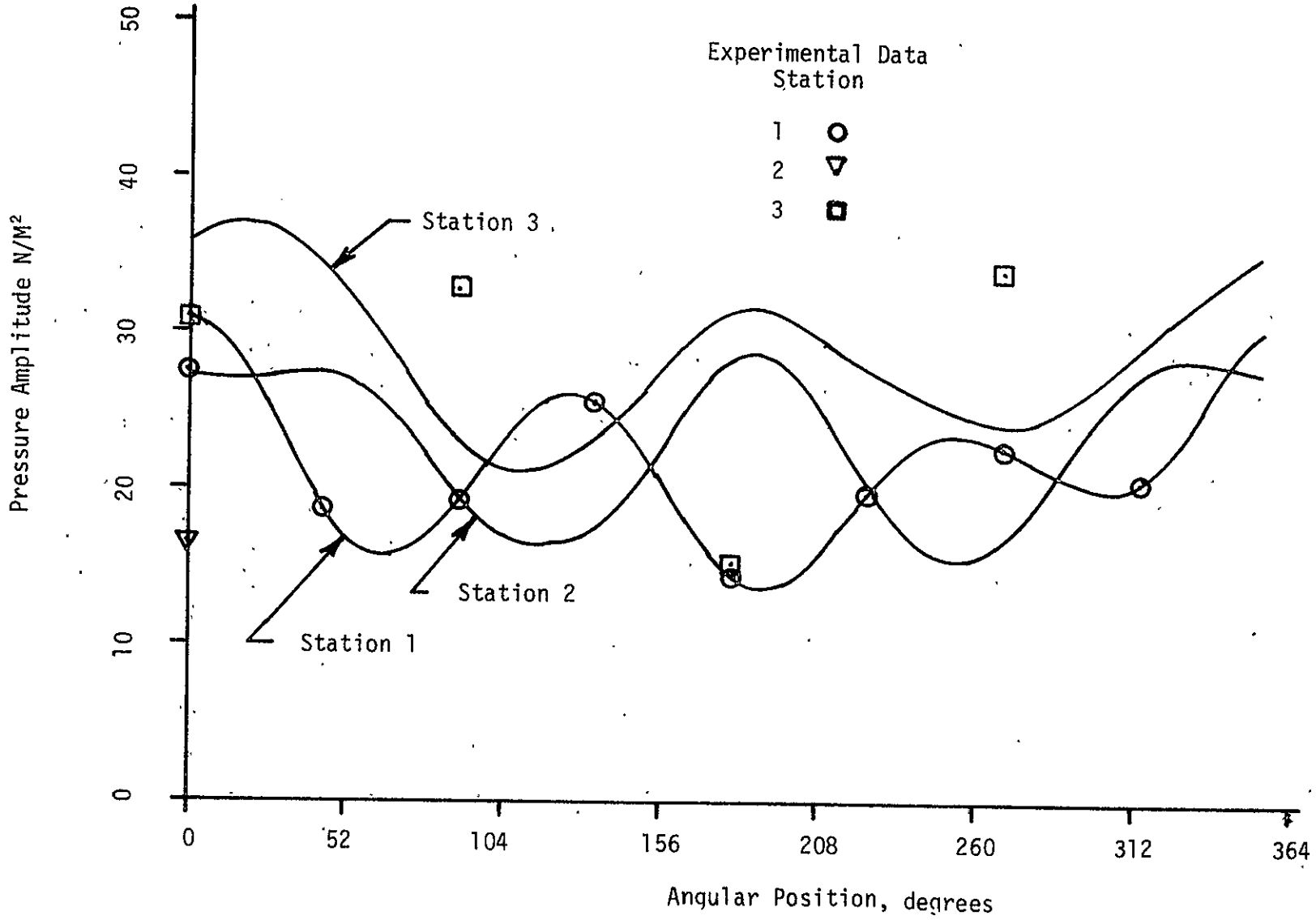

Figure 11a. Comparison of the theoretical and experimental pressure amplitudes for the hard-walled case; M = 0 and f = 3150 Hz.

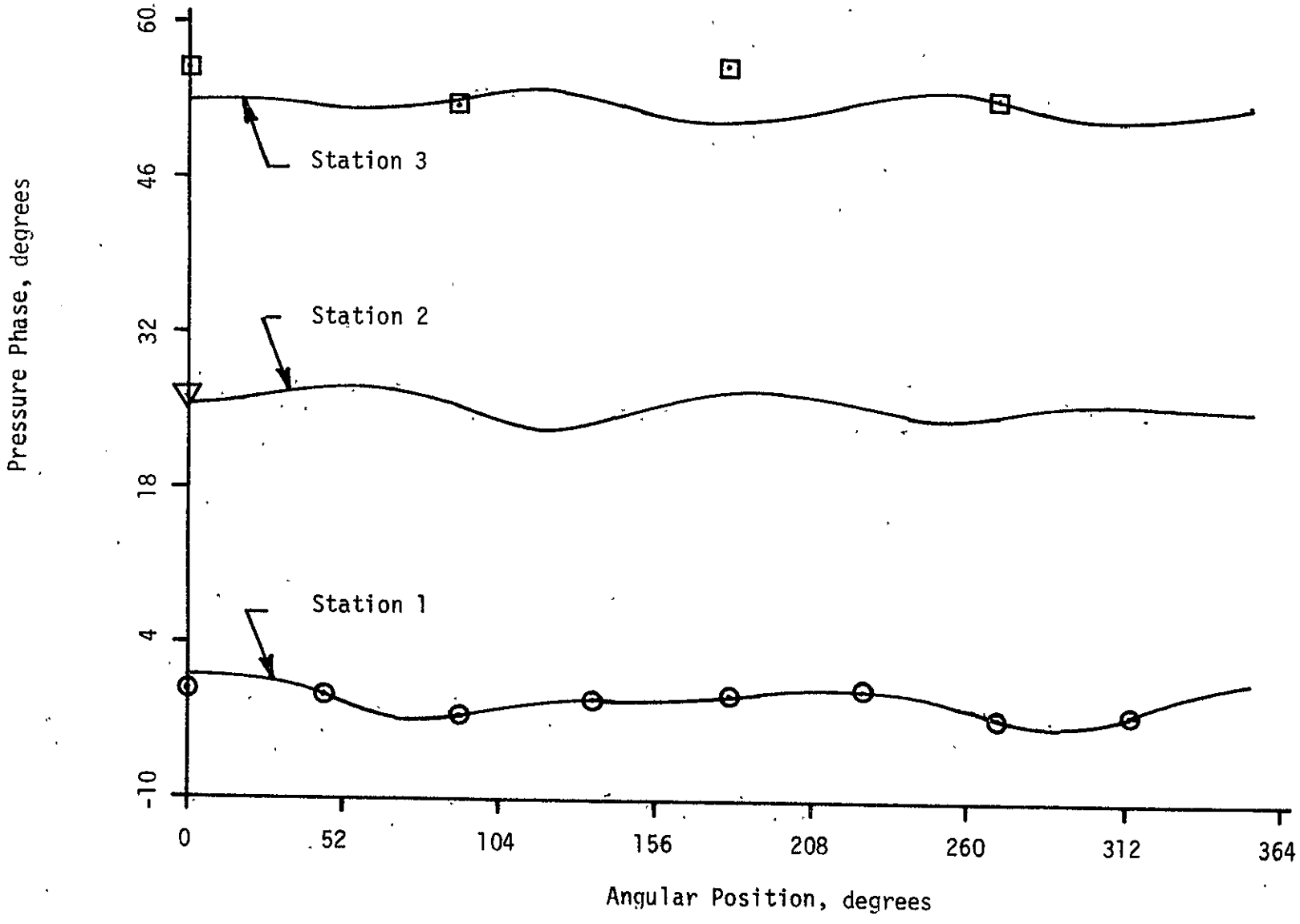

Figure 11b. Comparison of the theoretical and experimental pressure phases for the hard-walled case; M = 0 and f = 3150 Hz.

4. Lined Annular Ducts Without Flow

In this section, an analytic expression is derived for the propagation and attenuation of sound waves in annular lined ducts having slowly-varying cross sections and in the absence of mean flow. Experimental studies of propagation in the lined duct are described, and the experimental and theoretical results are compared.

4.1 Theoretical Considerations

In the absence of a mean flow and viscous dissipation, the mathematical statement of the problem can be written as

$$\nabla^2\phi - \frac{1}{c^2}\frac{\partial^2\phi}{\partial t^2} = 0 \tag{28}$$

$$\frac{\partial\phi}{\partial r} - \frac{\beta_1(x_1)}{c}\frac{\partial\phi}{\partial t} = \varepsilon R_1' \frac{\partial\phi}{\partial x} \quad \text{at } r = R_1(x_1) \tag{29}$$

$$\frac{\partial\phi}{\partial r} + \frac{\beta_2(x_1)}{c}\frac{\partial\phi}{\partial t} = \varepsilon R_2' \frac{\partial\phi}{\partial x} \quad \text{at } r = R_2(x_1) \tag{30}$$

where $\beta_1(x_1)$ and $\beta_2(x_1)$ are the admittances of the two walls.

An approximate solution is sought to Eqs. (28)-(30) by using the method of multiple scales in the form

$$\psi(x,r,\theta,t) = [\psi_0(x_1,r) + \varepsilon\psi_1(x_1,r) + \ldots]\exp[i(\eta + m\theta)] \tag{31}$$

where m is an integer and

$$\frac{\partial\eta}{\partial t} = -\omega, \quad \frac{\partial\eta}{\partial x} = k(x_1) \tag{32}$$

with ω being the sound frequency; k is the complex wave-number in the streamwise direction whose imaginary part represents the attenuation of the sound. Substituting Eqs. (31) and (32) into Eqs. (28)-(30), using Eq. (6), and equating coefficients of like powers of ε, we obtain

Order ε^0

$$\frac{\partial^2\psi_0}{\partial r^2} + \frac{1}{r}\frac{\partial\psi_0}{\partial r} + \left(\frac{\omega^2}{c^2} - k^2 - \frac{m^2}{r^2}\right)\psi_0 = 0 \tag{33}$$

$$\frac{\partial\psi_0}{\partial r} + \frac{i\omega\beta_1}{c}\psi_0 = 0 \quad \text{at } r = R_1 \tag{34}$$

$$\frac{\partial\psi_0}{\partial r} - \frac{i\omega\beta_2}{c}\psi_0 = 0 \quad \text{at } r = R_2 \tag{35}$$

Order ε

$$\frac{\partial^2\psi_1}{\partial r^2} + \frac{1}{r}\frac{\partial\psi_1}{\partial r} + \left(\frac{\omega^2}{c^2} - k^2 - \frac{m^2}{r^2}\right)\psi_1 = -2ik\frac{\partial\psi_0}{\partial x_1} - ik'\psi_0 \tag{36}$$

$$\frac{\partial\psi_1}{\partial r} + \frac{i\omega\beta_1}{c}\psi_1 = ikR_1\psi_0 \text{ at } r = R_1 \tag{37}$$

$$\frac{\partial\psi_1}{\partial r} - \frac{i\omega\beta_2}{c}\psi_1 = ikR_2\psi_0 \text{ at } r = R_2 \tag{38}$$

The solution of Eqs. (33)-(35) is

$$\psi_0 = A(x_1)\Psi(r;x_1) \tag{39}$$

where

$$\Psi = J_m(\gamma_{mn}r) - \frac{\gamma_{mn}J_m'(\gamma_{mn}R_1) + \frac{i\omega\beta_1}{c}J_m(\gamma_{mn}R_1)}{\gamma_{mn}Y_m'(\gamma_{mn}R_1) + \frac{i\omega\beta_1}{c}Y_m(\gamma_{mn}R_1)}Y_m(\gamma_{mn}r) \tag{40}$$

$$\gamma_{mn}^2 = \frac{\omega^2}{c^2} - k_{mn}^2 \tag{41}$$

and the γ_{mn} are the roots of

$$[\gamma J_m'(\gamma R_2) - \frac{i\omega\beta_2}{c} J_m(\gamma R_2)][\gamma Y_m'(\gamma R_1) + \frac{i\omega\beta_1}{c} Y_m(\gamma R_1)]$$
$$= [\gamma J_m'(\gamma R_1) + \frac{i\omega\beta_1}{c} J_m(\gamma R_1)][\gamma Y_m'(\gamma R_2)$$
$$- \frac{i\omega\beta_2}{c} Y_m(\gamma R_2)] \qquad (42)$$

With ψ_0 and k_{mn} known, Eqs. (36)-(38) have a solution if, and only if, their inhomogeneous parts satisfy a solvability condition. To determine this solvability condition, multiply Eq. (36) by $r\psi_0$, integrate the result by parts from $r = R_1$ to $r = R_2$ to transfer the derivatives from ψ_1 to ψ_0, use Eq. (33), and obtain

$$[r\psi_0 \frac{\partial\psi_1}{\partial r} - r\psi_1 \frac{\partial\psi_0}{\partial r}]_{r=R_1}^{r=R_2} = -i \int_{R_1}^{R_2} r \frac{\partial}{\partial x_1}(k\psi_0^2)dr \qquad (43)$$

Substitution for $\frac{\partial\psi_0}{\partial r}$ and $\frac{\partial\psi_1}{\partial r}$ at $r = R_1$ and R_2 from Eqs. (34), (35), (37), and (38) into Eq. (43) results in

$$k_{mn}R_2R_2^1\psi_0^2\Big|_{r=R_2} - k_{mn}R_1R_1^1\psi_0^2\Big|_{r=R_1} + \int_{R_1}^{R_2} r\cdot\frac{\partial}{\partial x_1}(k_{mn}\psi_0^2)dr = 0 \qquad (44)$$

Using Leibnitz' rule and the fact that $\psi_0 = A_{mn}\Psi$, rewrite Eq. (44) as

$$\frac{\partial}{\partial x_1}[A_{mn}^2 k_{mn} \int_{R_1}^{R_2} r\Psi^2 dr] = 0 \qquad (45)$$

Hence,

$$A_{mn} = \frac{D_{mn}(x_{1_r})}{D_{mn}(x_1)} A_{mn}(x_{1_r}) \tag{46}$$

where x_{1_r} is a reference station, the complex amplitudes $A_{mn}(x_{1_r})$ at the reference location are determined experimentally, and

$$D_{mn}^2 = \frac{k_{mn}R_2^2}{2\gamma_{mn}^2}\left[\gamma_{mn}^2 - \frac{\omega^2\beta_2^2}{c^2} - \frac{m^2}{R_2^2}\right]\Psi^2(R_2;x_1) - \frac{k_{mn}R_1^2}{2\gamma_{mn}^2}\left[\gamma_{mn}^2 - \frac{\omega^2\beta_1^2}{c^2} - \frac{m^2}{R_1^2}\right]\Psi^2(R_1;x_1) \tag{47}$$

Analogous to the discussion in Section 3, the development of the acoustic pressure at the outer wall leads to

$$p_{mn}(x,r_2,t) = B_{mn}\frac{D_{mn}(x_{1_r})}{D_{mn}(x_1)}\frac{\Psi_{mn}(R_2;x_1)}{\Psi_{mn}(R_2;x_{1_r})} \times \exp\left[i\left(\int_{x_r}^{x} k_{mn}dx + m\theta - \omega t\right)\right] \tag{48}$$

where B_{mn} is the complex mode amplitude at the reference station. The pressure is summed over all modes, and the result is expressed in terms of an amplitude and phase for the total signal. These amplitudes and phases are compared with the experimental data in Section 4.3.

4.2 Experimental Investigation

4.2.1 Introduction

The soft-walled experiments were performed using the apparatus as described in Section 2. Both straight and tapered centerbodies were used so that cases for both variable area and constant area were included.

The introduction of a soft-walled test section brings with it several complications. First, the impedance of the wall is no longer well-known. Also, the insertion of a soft-walled section in a tube which is otherwise hard-walled gives rise to impedance discontinuites (and thus reflections) at the hard-wall to soft-wall joints.

Thus, the three necessary steps in this investigation are (1) determine if any problems with standing waves occur, (2) find the impedance of the soft-walled section as installed and calculate the basic facing-sheet properties (resistance and characteristic frequency) from the impedance, and (3) measure the acoustic pressures and phases for the variable-area case. The results from this last step are compared with the theoretical predictions.

4.2.2 Standing-Wave Investigation

The experimental approach to standing-wave detection is basically the same as that outlined for the hard-walled experiments. An acoustical driver, located at the 12:00

o'clock position, is operated at constant voltage as the frequency is slowly swept from 500 Hz to 5000 Hz. An acoustical probe simultaneously detects the sound-pressure level at the discrete axial locations. The amplified microphone output is passed through a 10 Hz tracking filter and it is recorded. The result is an uncalibrated pressure amplitude vs. frequency plot with the peaks indicating resonance frequencies.

The results of this test, when conducted with the soft-walled test section and the uniform centerbody are shown in Figs. 12 and 13. Figure 12 was obtained in the signal-insertion section. Comparison of this result with the result shown in Fig. 7 for the hard-walled test section shows several interesting features. It is evident that peaks corresponding to the hard-walled cut-on frequencies are present; however, these response peaks are broader than in the hard-walled case. The peaks at 1600-1700 Hz increased markedly over that observed with the hard-walled test section perhaps as a consequence of reflection at the hard-wall, lined-wall junction. There is also a similar increase in the peak centered at 3075 Hz, which is of concern for tests that were run at 3150 Hz. A stronger response is also observed at about 4700 Hz, but this is well above the test frequencies and is not of concern for interpretation of the test data.

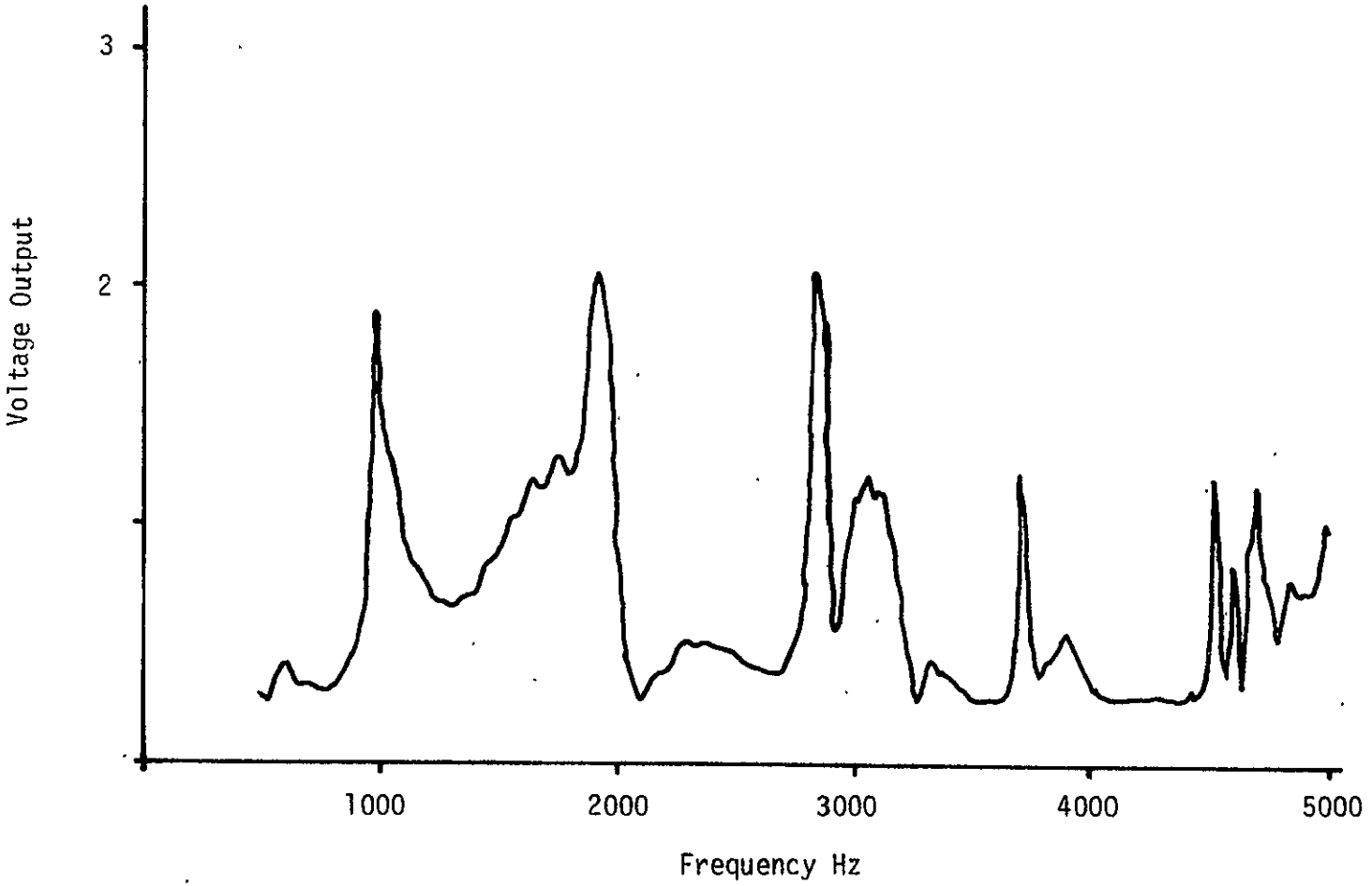

Figure 12. Frequency characterization with soft-walled test section and uniform centerbody installed; measured in signal insertion section.

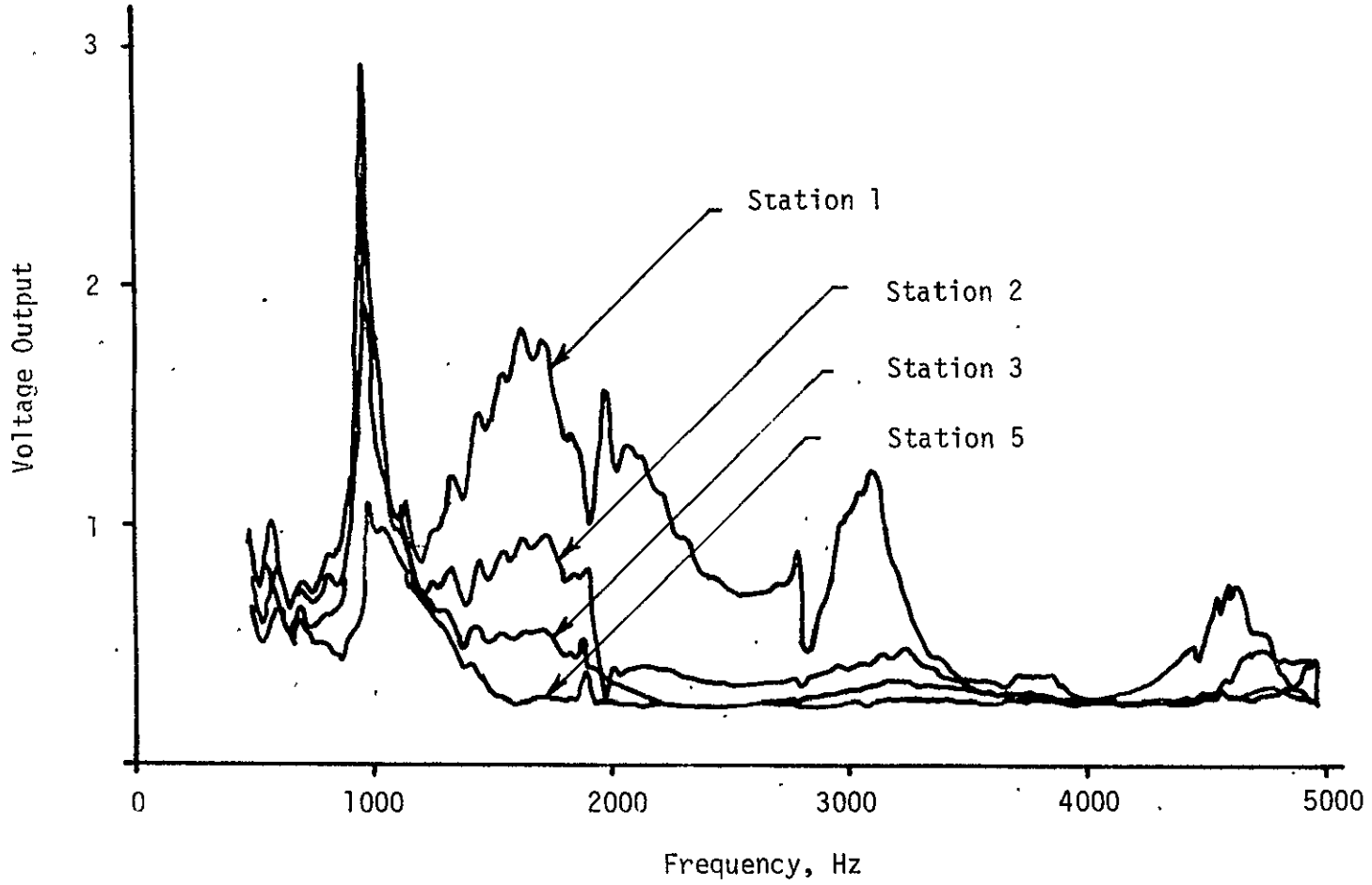

Figure 13. Frequency characterization of soft-walled test section with uniform centerbody installed; measured in lined section.

Traces of the system response at downstream locations within the test section are shown in Fig. 13. Examination of Fig. 13 shows that the pressure amplitude decreases as expected as the probe is moved down the soft-walled test section farther from the signal-insertion section. This attenuation occurs in all regions, but is most evident in the frequency range of 2000-3200 for which the liner was designed. Again, this is in line with expectations from theoretical considerations.

The response peaks centered at 1600 Hz and 3100 Hz are relatively more prominent at the start of the lined section (Fig. 13) than they are in the hard signal-insertion section (Fig. 12), but they are rapidly attenuated by the liner.

A similar system response curve with the variable-area centerbody installed is given in Fig. 14. The results shown in Fig. 14 were obtained in the signal-insertion section. The installation of the variable-area centerbody results in two additional resonances in the frequency range 3400-3700 Hz that correspond to cut on of radial modes. There is also some shift in the relative strengths of the standing waves. However, the basic response is quite similar to the response observed with the straight centerbody installed. The relative response observed at station 1 in the test section with the tapered centerbody installed is almost identical to that obtained with the straight centerbody installed and is not shown.

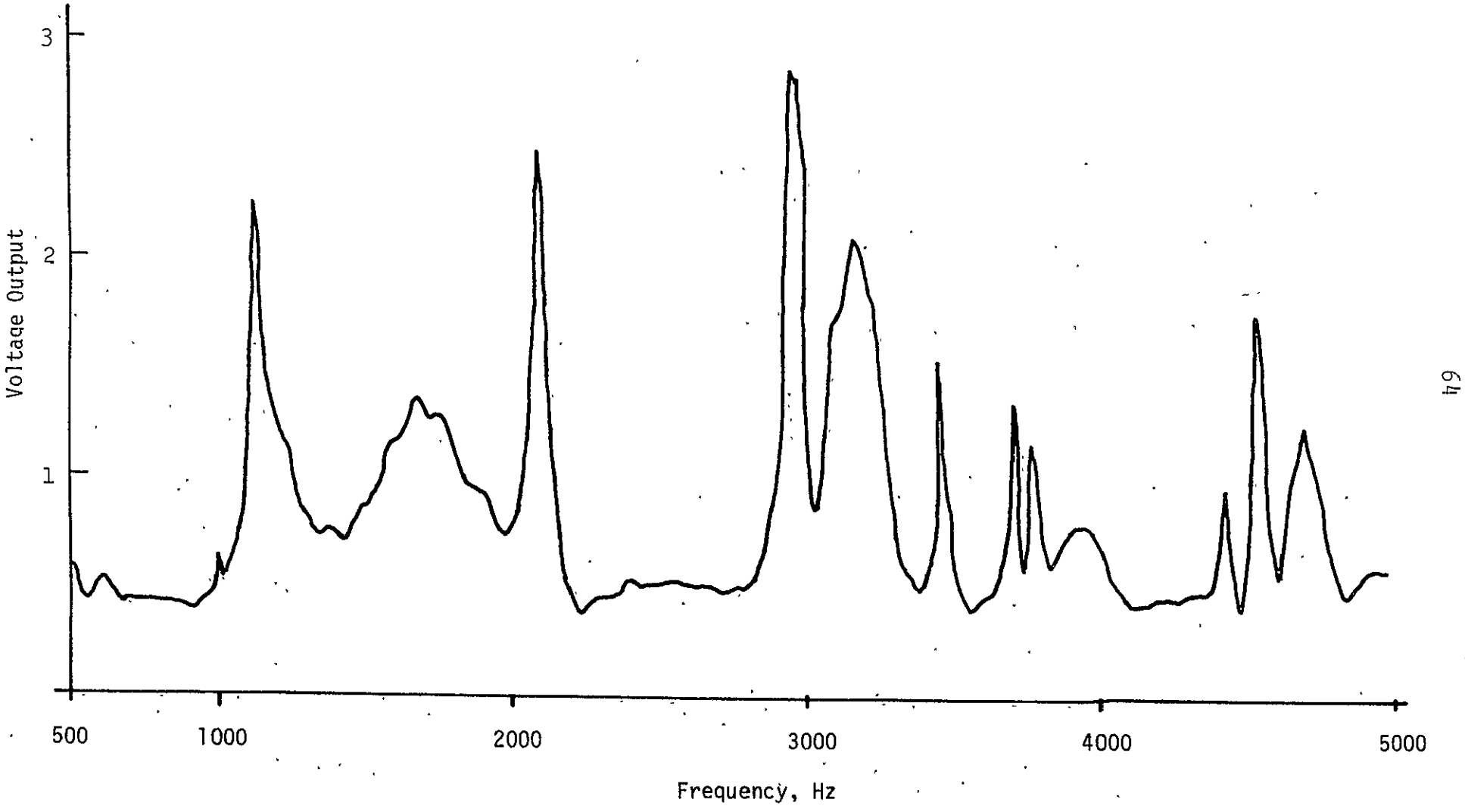

Figure 14. Frequency characterization of soft-walled test section with variable centerbody installed.

These preliminary investigations into standing waves indicate that few problems are expected at the frequencies 840 and 2640 Hz. However, difficulties in comparing the test results at 3150 Hz with the theoretical predictions may be encountered since the theoretical model does not account for the reflections.

4.2.3 Determination of Liner Properties

Determination of the acoustic properties of the liner presented some difficulties, even though the effect of the backing cavities can be modelled simply by theoretical means and the resistance of the facing-sheet material was specified as 40 rayls by the supplier. The reactance of the facing-sheet material was unknown, and it was readily apparent that the facing-sheet material is inhomogeneous. In addition, the bonding of the facing sheet to the backing cavities undoubtably altered the effective resistance of the material through blockage of some pores. Consequently, test data from the duct for cases with no mean flow and with a straight centerbody installed have been used to determine effective properties of the liner section. The liner properties established in this manner are then used in making theoretical predictions for variable-area cases both with and without mean flow. This procedure is considered acceptable since the primary purpose of the tests is to establish the ability of the theoretical model to predict the effect of axial gradients on the acoustic propagation.

The experimental data at station 1 provide the modal content of the signal entering the lined section. The standard theory for wave propagation in straight ducts provides the attenuation and phase changes of each mode for an assumed value of the liner impedance. The acoustic signal predicted at station 3 in this manner is then compared with the experimental measurements. The liner impedance Z is varied to obtain the best fit of the theoretical and experimental results at each of the three test frequencies: 840 Hz, 2650 Hz and 3150 Hz. The admittance $\beta = 1/Z$ that is found in this manner for each of the three test frequencies is listed in Table 2.

These values of admittance are then related to the physical characteristics of the liner to check whether the admittances are consistent with the known behavior of point-reacting liners. The dimensionless impedance Z of a point-reacting liner is usually modelled by the formula

$$Z = R_s(1 - i\omega/\omega_0) + Z_c \qquad (49)$$

where R_s is the dimensionless resistance of the facing sheet, ω_0 is the characteristic frequency of the facing sheet, and Z_c is the dimensionless impedance of the backing cavities. The impedance of the backing cavities is a known function of the circular frequency ω and the cavity depth h; the functional form involves the Bessel functions of the

Table 2. Liner properties at test frequencies

Frequency	Admittance β_2	Facing Sheet Properties	
		R_s	ω_0 rad/sec
840	(0.10,-0.26)	1.3	30,000
2640	(0.77,-0.02)	1.29	25,370
3150	(0.69, 0.12)	1.41	50,280

Admittance values calculated using $R_s = 1.3$ and $\omega_0 = 30{,}000$ are

Frequency	β_2
840	(.10,-.26)
2640	(.75,-.095)
3150	(.75, .13)

first and second kinds of order zero since the radial variation of the pressure in the cavities is given by[1]

$$p = AJ_0(\frac{\omega r}{c}) + BY_0(\frac{\omega r}{c}) \tag{50}$$

The radial particle velocity v is then

$$v = -\frac{i}{\rho_0 c}\left[AJ_0'(\frac{\omega r}{c}) + BY_0'(\frac{\omega r}{c})\right] \tag{51}$$

Requiring the radial velocity to vanish at $r = R_2 + h$ and evaluating the dimensionless impedance $Z = p/\rho_0 cv$ at $r = R_2$, one obtains the impedance of the backing cavity as

$$Z_c = i\ J_0(\frac{\omega R_2}{c})Y_0'[\frac{\omega}{c}(R_2 + h)] - J_0'[\frac{\omega}{c}(R_2 + h)] \times$$

$$Y_0'(\frac{\omega R_2}{c}) \,/\, J_0'(\frac{\omega R_2}{c})Y_0'[\frac{\omega}{c}(R_2 + h)]$$

$$- J_0'[\frac{\omega}{c}(R_2 + h)]Y_0'(\frac{\omega R_2}{c}) \tag{52}$$

With Z_c determined from Eq. (52), the experimentally-determined values of Z were substituted into Eq. (49) and the facing-sheet resistance and characteristic frequency were determined. The values of R and ω_0 that are found from the experimental data are listed in Table 2. The nominal value of the dimensionless resistance of the facing sheet material as supplied by the manufacturer is approximately 1.0. Since some reduction of the porosity of the material occurred during its bonding to the backing cavities, the resistance values of approximately 1.3 at the two lower test frequencies seem reasonable. Similarly the agreement in the values of ω_0 at these two test frequencies is considered satisfactory. At the test frequency 3150 Hz there is more discre-

pancy in the predicted liner properties. As noted earlier, of the test section and the inability of the theory to predict reflections, cause some doubts as to the adequacy of the theory at this test frequency; thus, R = 1.3 and ω_0 = 30,000 rad/sec are taken to be the values of the facing-sheet parameters.

The values of the liner admittance corresponding to R = 1.3 and ω_0 = 30,000 rad/sec have been recalculated and are listed in Table 2. The comparison between the experimental and calculated pressure amplitudes and phases are shown in Figs. 15, 16, and 17 for each of the three test frequencies. It is readily apparent the circumferential variation of the signal could not be modelled even for this simple case; indeed, in the 840 Hz case, the signal has a larger m = 1 component at station 3 than at station 1. This is entirely inconsistant with the standard theory and can be explained only in terms of the observed inhomogeneities of the liner material. The soft-walled liner was fabricated in two separate halves that were bolted together; the results shown in these figures strongly indicate that the two halves have somewhat different acoustic properties. Thus, the values of liner admittance have been selected to provide an average fit to the data. Consequently, the comparison between theory and experiment for the variable-area cases with and without mean flow that are presented in later sections can be expected to show only general trends and not the specific circumferential variation of the pressure amplitude.

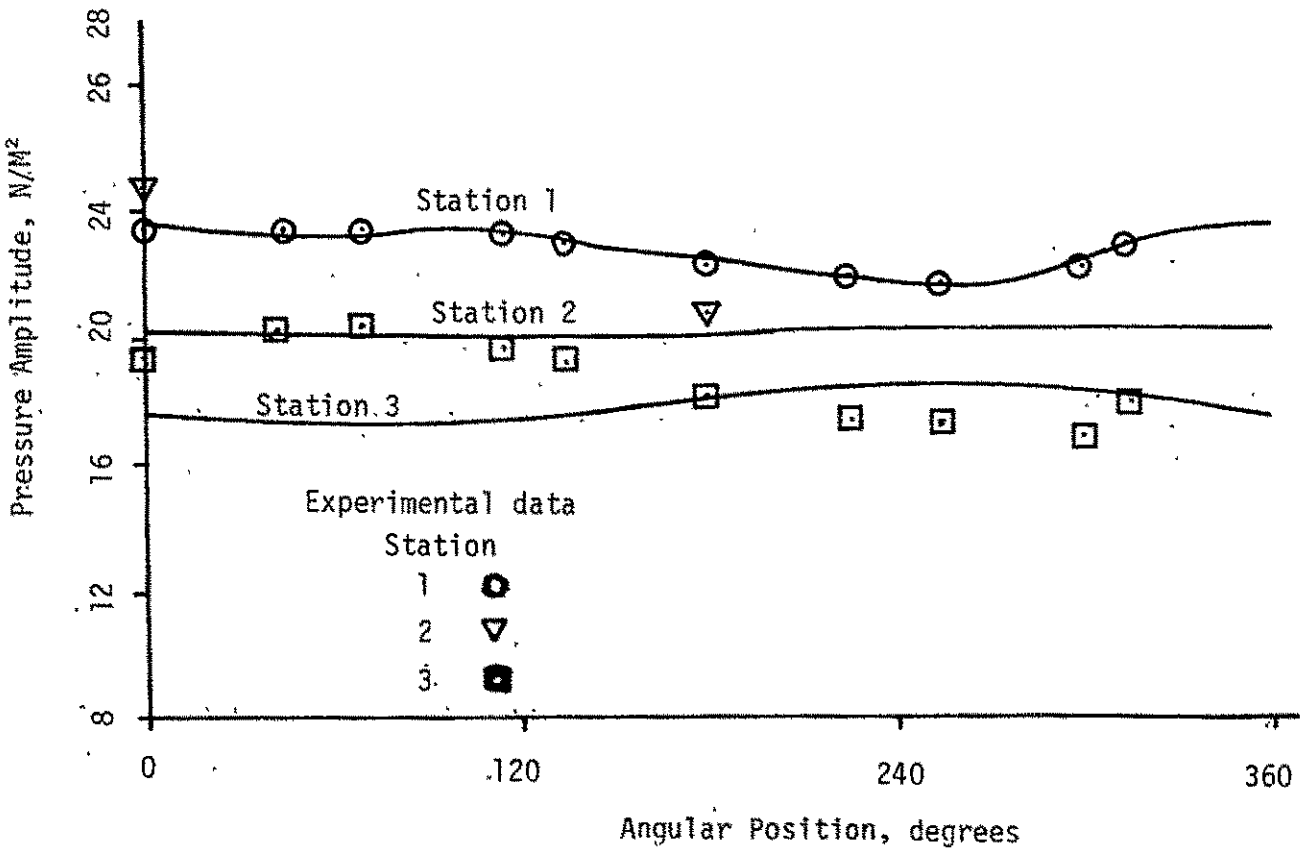

Figure 15a. Comparison of the theoretical and experimental pressure amplitudes with uniform centerbody installed; M = 0, β = .1 - .26i, f = 840Hz.

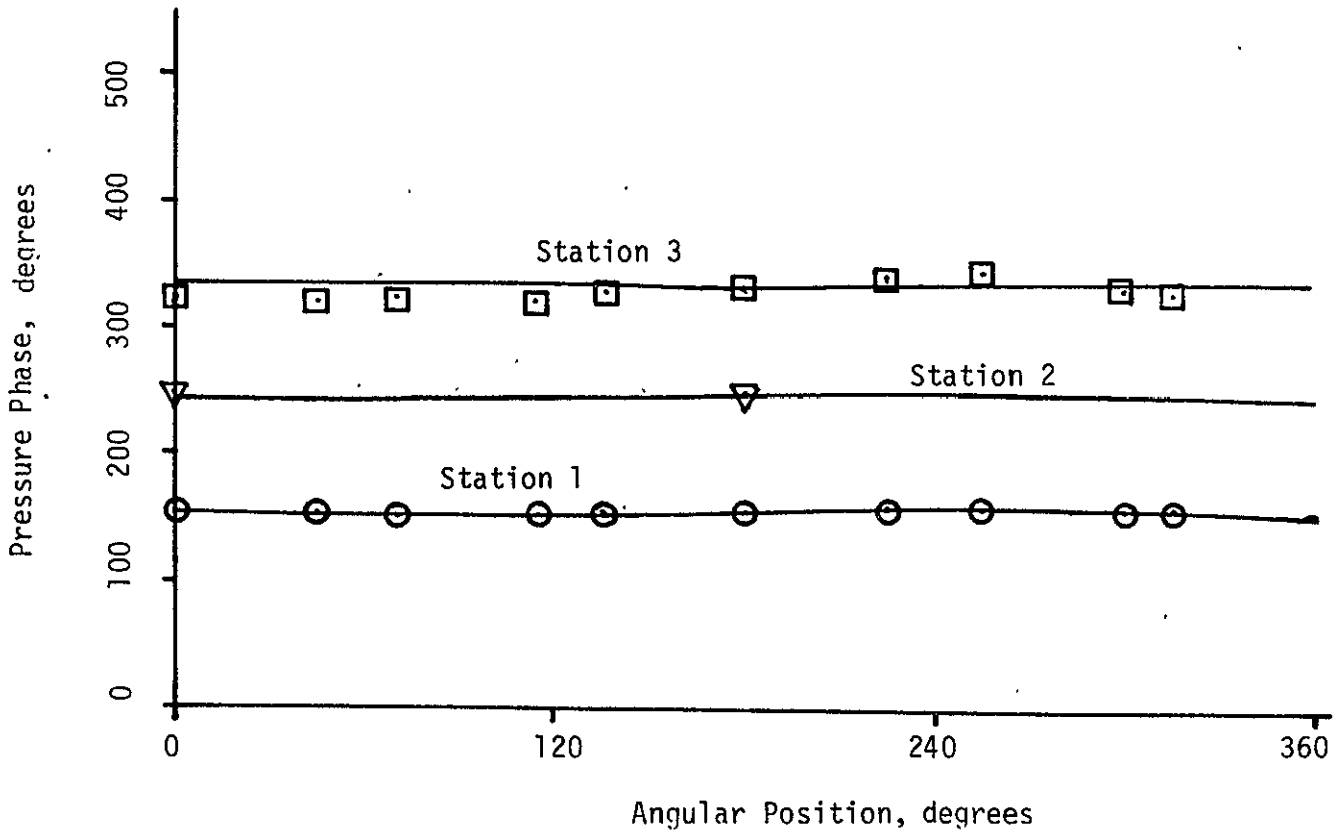

Figure 15b. Comparison of the theoretical and experimental pressure phases with uniform centerbody installed; M = 0, β = .1 - .26i, f = 840Hz.

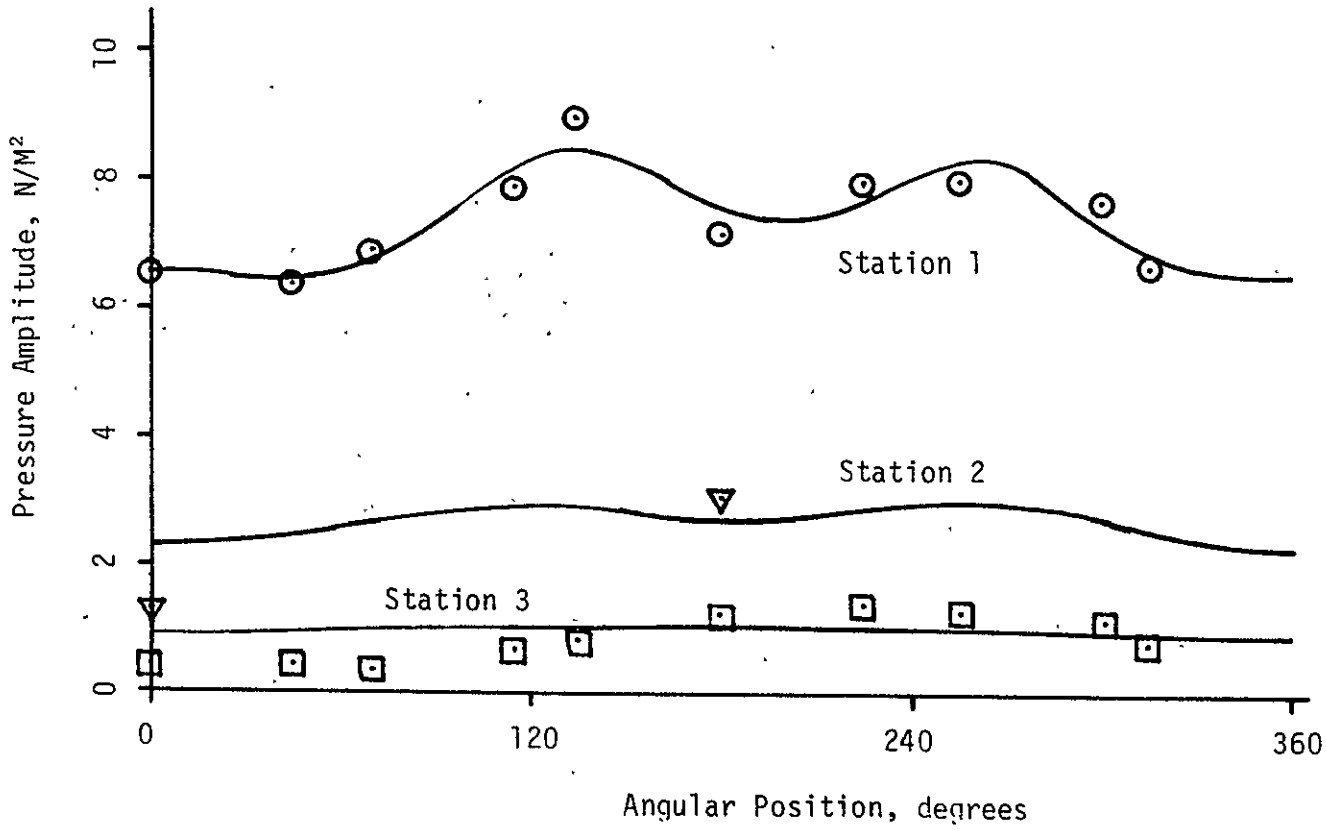

Figure 16a. Comparison of the theoretical and experimental pressure amplitudes with uniform centerbody installed; M = 0, β = .75 - .095i, f = 2640Hz.

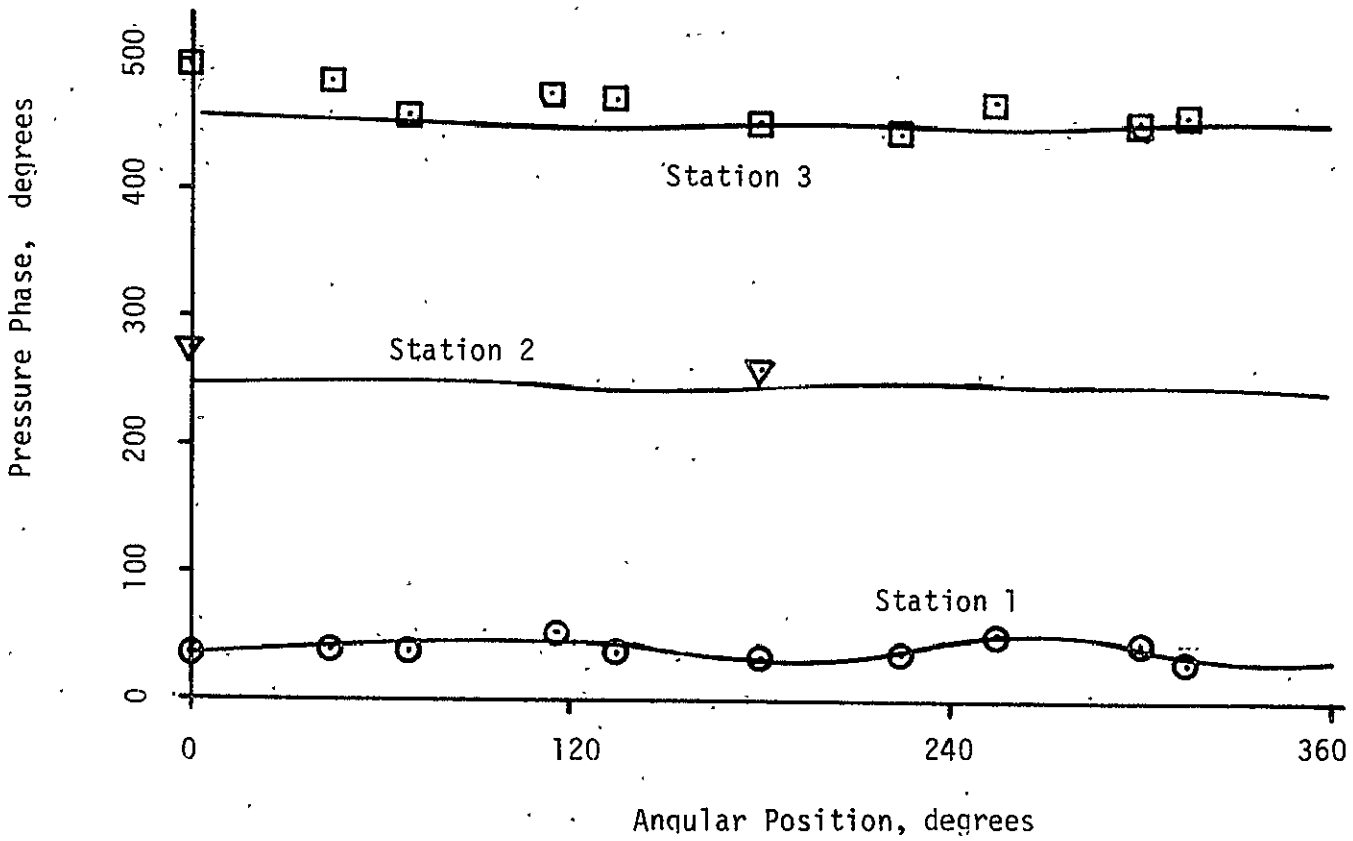

Figure 16b. Comparison of the theoretical and experimental pressure phases with uniform centerbody installed; M = 0, β = .75 - .095i, f = 2640Hz.

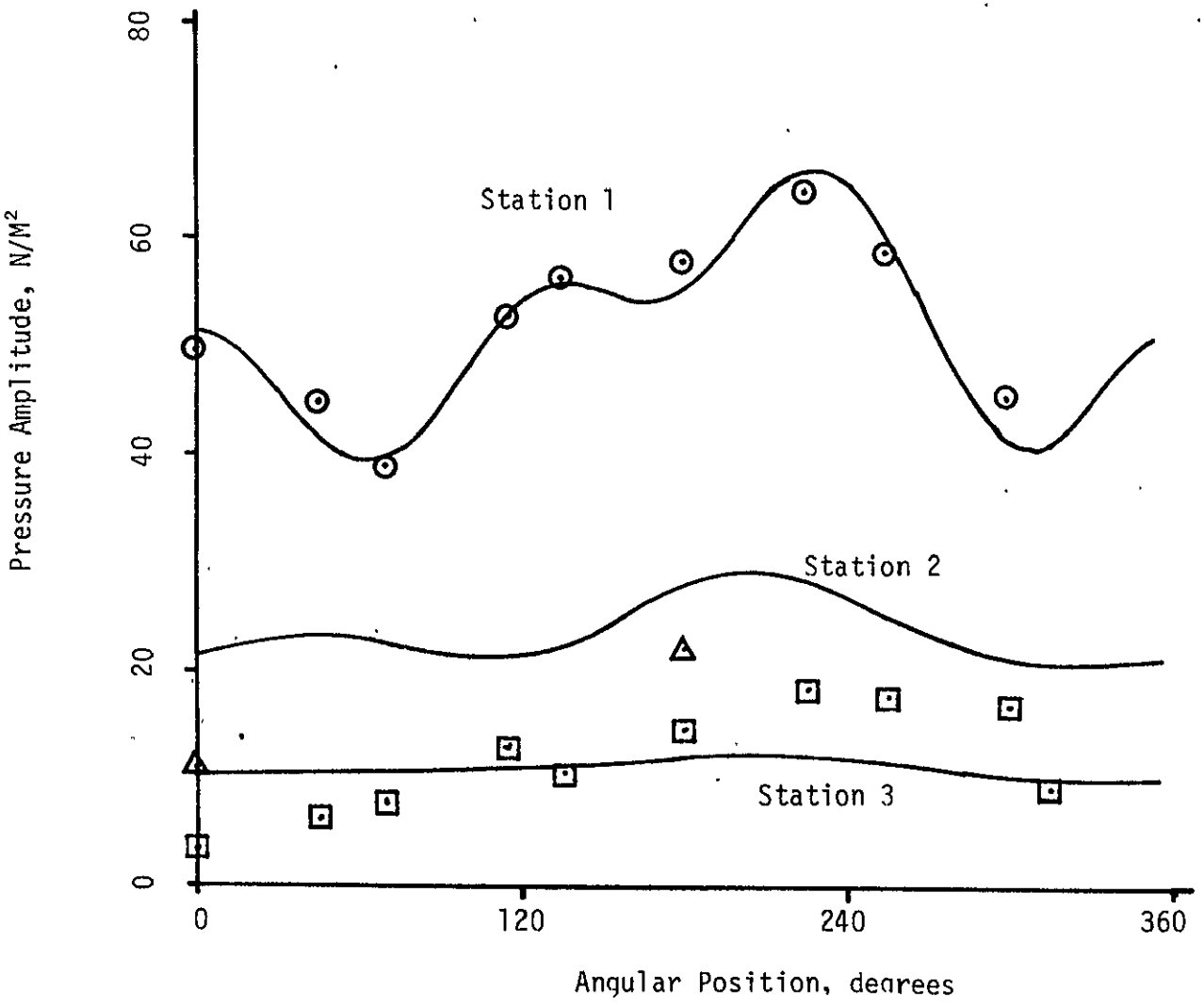

Figure 17a. Comparison of the theoretical and experimental pressure amplitudes with uniform centerbody installed; M = 0, β = .75 + .13i, f = 3150Hz.

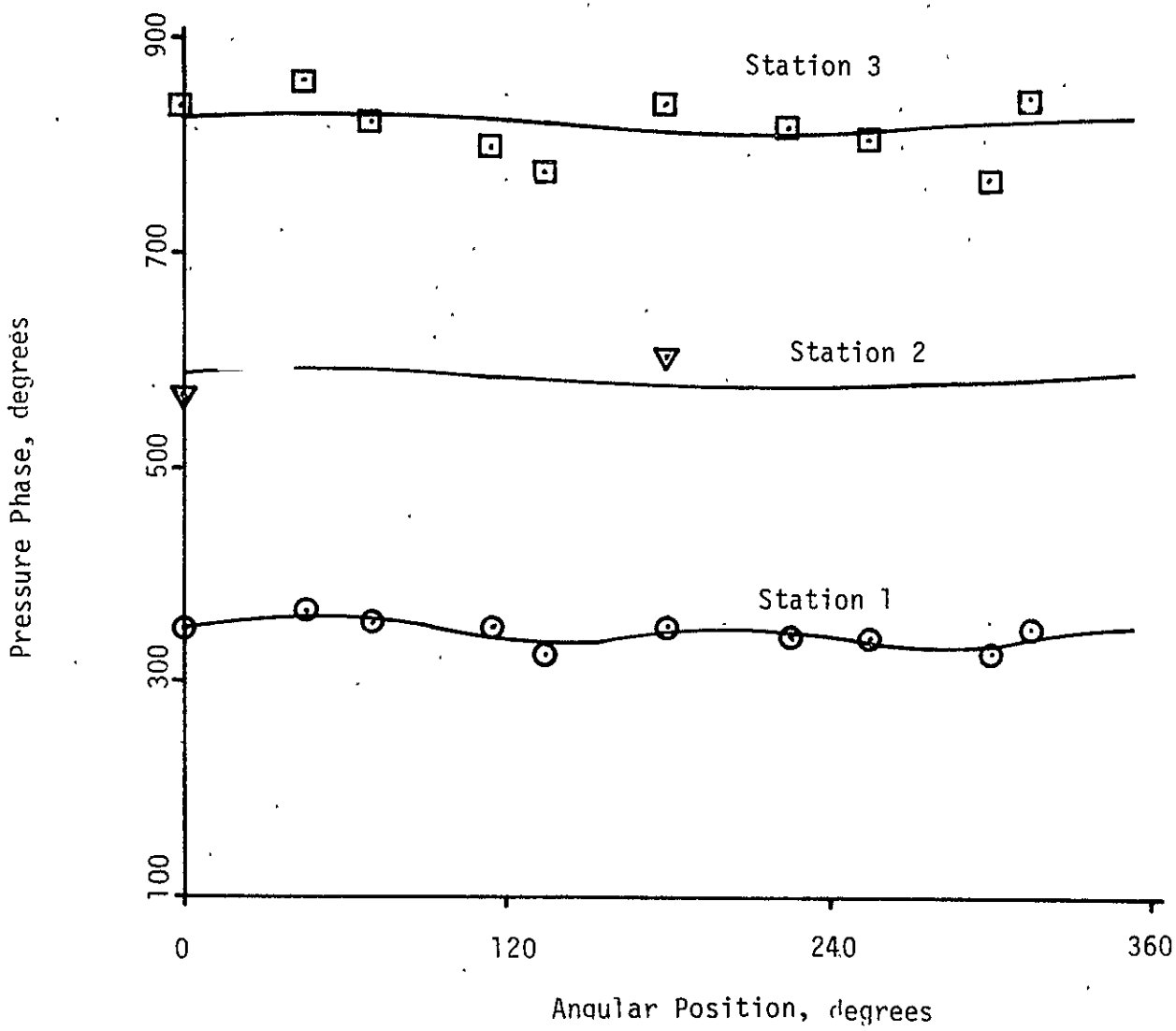

Figure 17b. Comparison of the theoretical and experimental pressure phases with uniform centerbody installed; M = 0 β = .75 + .13i, f = 3150Hz.

4.3 Comparison of Experimental and Theoretical Results

The liner properties estimated in the previous section have been used in the theoretical-prediction method described in Section 4.1. The acoustic amplitude and phase of each mode is determined experimentally at station 1, and the theory is used to predict the signal amplitude and phase at downstream stations.

The results for a variable-area centerbody without flow are shown in Figs. 18, 19, and 20 for the frequencies 840 Hz, 2640 Hz, and 3150 Hz, respectively. The case of 2640 Hz yields agreement that is as good as the agreement in the straight-walled case; although the circumferential variation is not predicted, the overall attenuation rate and the phase shift of the 2640 Hz signal are adequately modelled. However, the overall attenuation rate is overpredicted for both the 840 Hz and 3150 Hz cases, and the phase shift of the 840 Hz signal is underpredicted. Surprisingly, the results for cases with flow that are reported in Section 5 exhibit better agreement between theory and experiment.

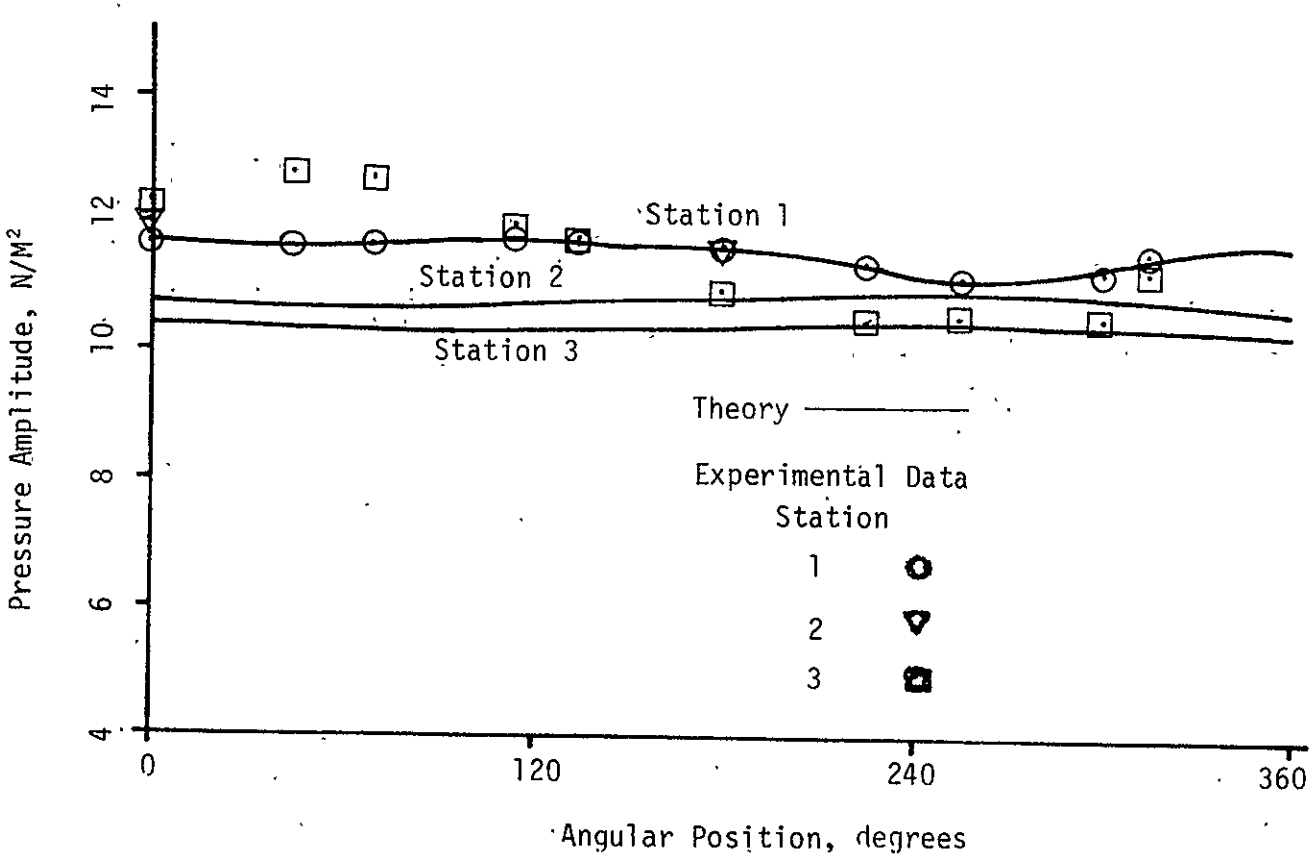

Figure 18a. Comparison of the theoretical and experimental pressure amplitudes with the variable centerbody installed; M = 0, β = .10 - .26i, f = 840Hz.

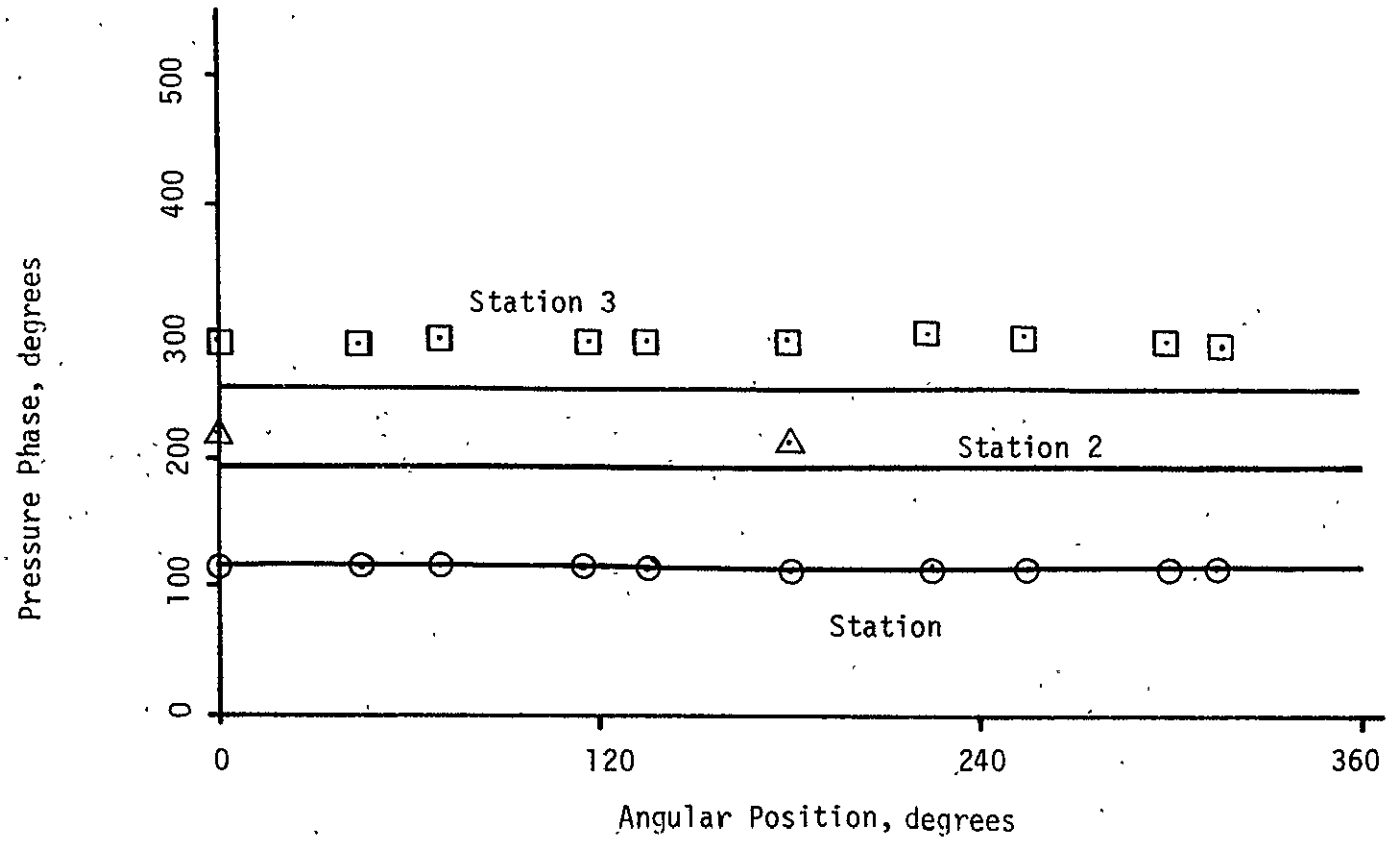

Figure 18b. Comparison of the theoretical and experimental pressure phases with the variable centerbody installed; M = 0, β = .10 - .26i, f = 840Hz.

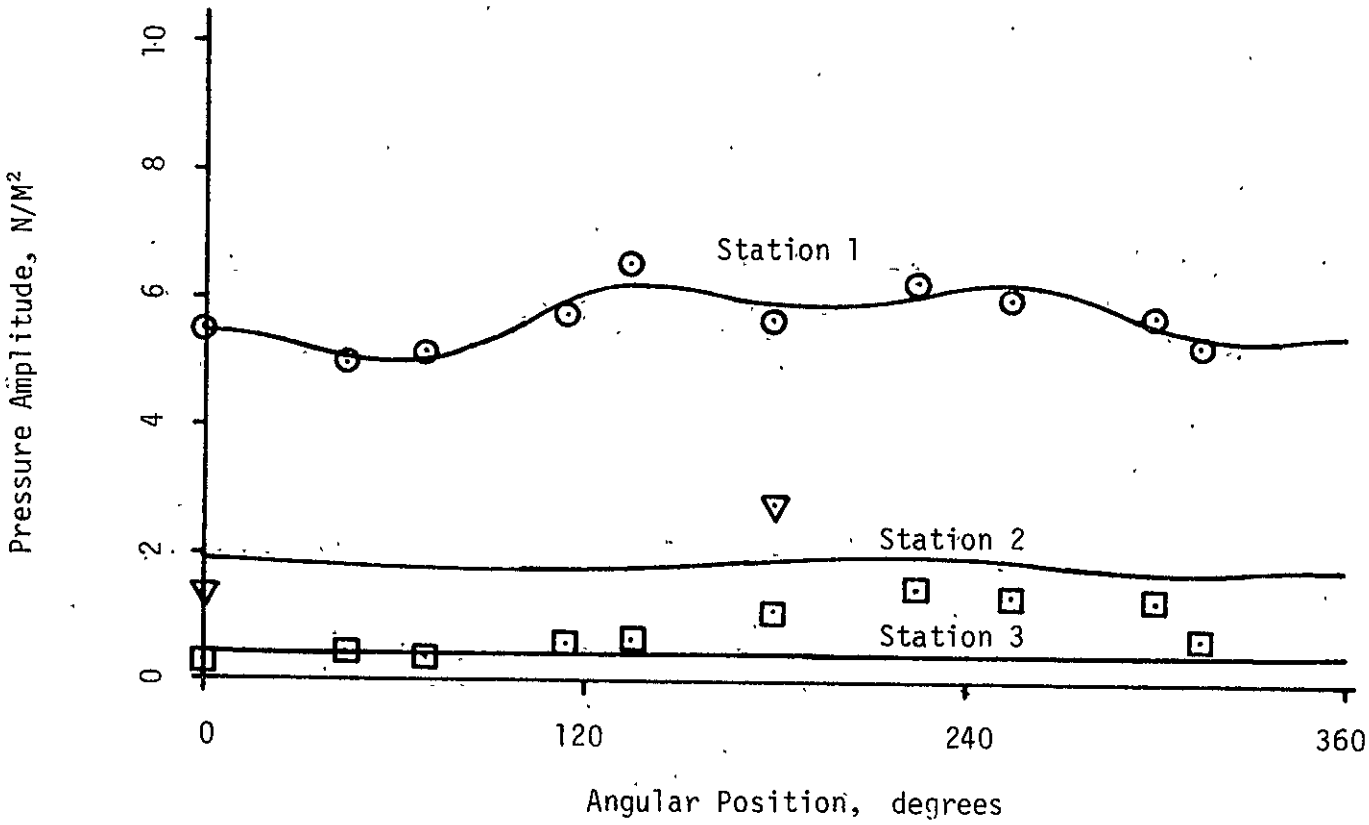

Figure 19a. Comparison of the theoretical and experimental pressure amplitudes with the variable centerbody installed; $M = 0$, $\beta = .75 - .095i$, $f = 2640$ Hz.

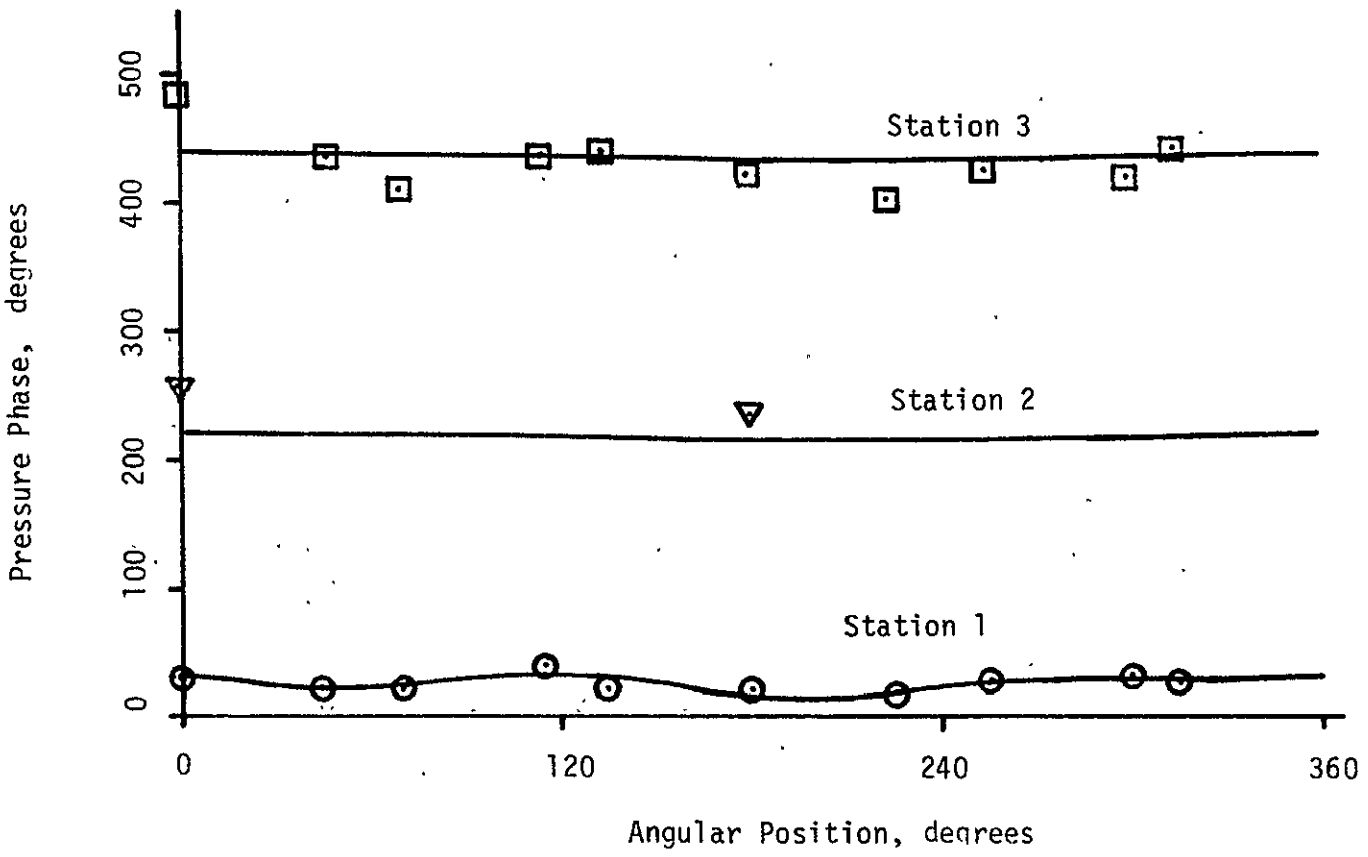

Figure 19b. Comparison of the theoretical and experimental pressure phases with the variable centerbody installed, M = 0, β = .75 - .095i, f = 2640Hz.

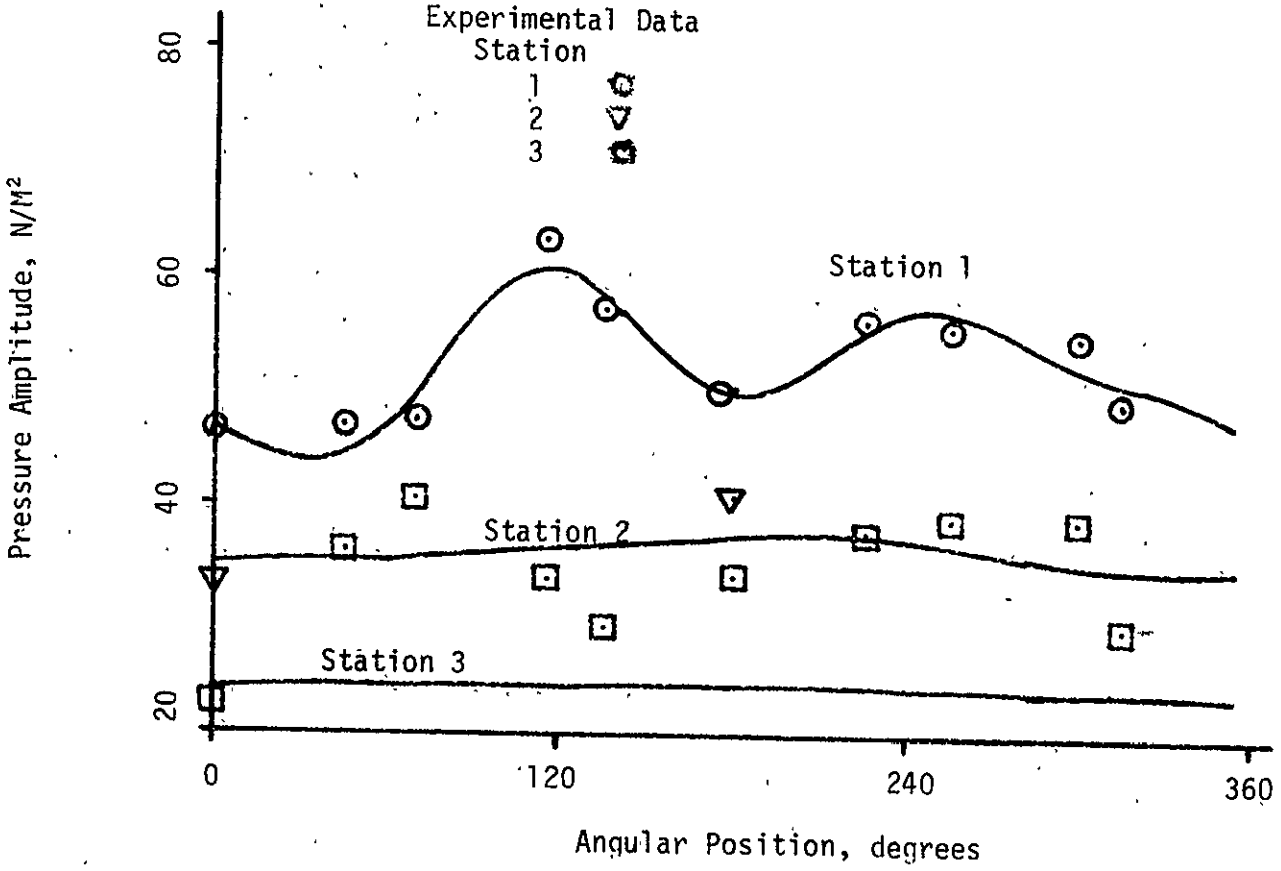

Figure 20a. Comparison of the theoretical and experimental pressure amplitudes with the variable centerbody installed, M = 0 β = .75 + .13i, f = 3150 Hz.

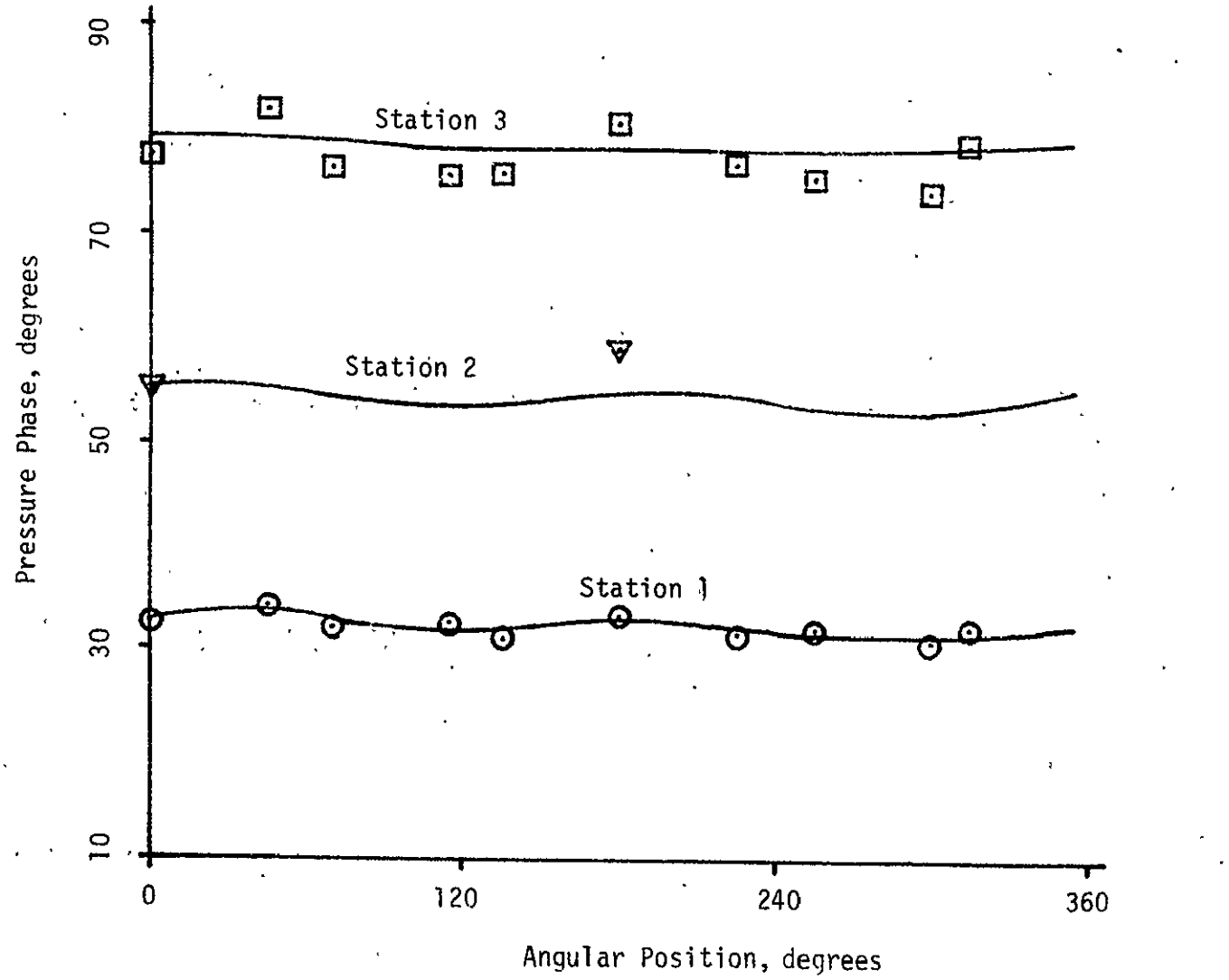

Figure 20b. Comparison of the theoretical and experimental pressure phases with the variable centerbody installed; M = 0 β = .75 + .13i, f = 3150 Hz.

5. Annular Ducts with Flow

In this section the theory for wave propagation through ducts that carry a mean flow is summarized, the mean-flow model used in the numerical studies is described, and the comparison between experimental and theoretical results is discussed. The theoretical development closely follows the development described in Ref. 34; thus it is described here only in a summary form. The implementation of the analysis in a computer code differs in some details from the method discussed in Ref. 34; however, the changes were introduced only to simplify the specification of the mean flow. Since the changes have no effect on the accuracy of the calculated results, they are not described here, and the reader is referred to Ref. 34 for the procedure details.

5.1 Theoretical Solution

5.1.1 Problem formulation

We consider the transmission and attenuation of acoustic waves in an annular duct having a slowly-varying cross section and carrying a sheared mean flow. The mean flow has constant density ρ_0 and pressure p_0. Moreover, the mean flow is slightly nonparallel; that is, the mean-velocity components along and normal to the duct centerline are assumed to have the form $U(x_1,r)$ and $\varepsilon V(x_1,r)$, where $x_1 = \varepsilon x$ is a slow scale and ε is a small dimensionless parameter representing, for example, the maximum slope of the wall.

We assume that each flow quantity is the sum of a mean part and an acoustic part; that is, we express the flow quantities as

$$U(x_1,r) + \varepsilon_1 u(x,r,\theta,t),\ \varepsilon V(x_1,r) + \varepsilon_1 v(x,r,\theta,t),$$
$$\varepsilon_1 w(x,r,\theta,t),\ p_0 + \varepsilon_1 p(x,r,\theta,t),\ \rho_0 + \varepsilon_1 \rho(x,r,\theta,t) \tag{53}$$

where ε_1 is a small dimensionless parameter characterizing the amplitude of the acoustic wave. Substituting Eq. (53) into the Euler equations and subtracting the mean-flow quantities, we obtain

$$\frac{\partial \rho}{\partial t} + U\frac{\partial \rho}{\partial x} + \rho_0\left(\frac{\partial u}{\partial x} + \frac{\partial v}{\partial r} + \frac{1}{r}\frac{\partial w}{\partial \theta} + \frac{v}{r}\right) = -\varepsilon V\frac{\partial \rho}{\partial r} + O(\varepsilon_1) + O(\varepsilon\varepsilon_1) \tag{54}$$

$$\frac{\partial u}{\partial t} + U\frac{\partial u}{\partial x} + V\frac{\partial U}{\partial r} + \frac{1}{\rho_0}\frac{\partial p}{\partial x} = -\varepsilon\left[V\frac{\partial u}{\partial r} + u\frac{\partial U}{\partial x_1} + \frac{\rho}{\rho_0}\left(U\frac{\partial U}{\partial x_1} + V\frac{\partial U}{\partial r}\right)\right] + O(\varepsilon_1) + O(\varepsilon\varepsilon_1) \tag{55}$$

$$\frac{\partial v}{\partial t} + U\frac{\partial v}{\partial x} + \frac{1}{\rho_0}\frac{\partial p}{\partial r} = -\varepsilon\frac{\partial}{\partial r}(vV) + O(\varepsilon^2) + O(\varepsilon_1) + O(\varepsilon\varepsilon_1) \tag{56}$$

$$\frac{\partial w}{\partial t} + U\frac{\partial w}{\partial x} + \frac{1}{\rho_0 r}\frac{\partial p}{\partial \theta} = -\varepsilon\left(\frac{Vw}{r} + V\frac{\partial w}{\partial r}\right) + O(\varepsilon^2) + O(\varepsilon_1) + O(\varepsilon\varepsilon_1) \tag{57}$$

For an inviscid, adiabatic acoustic disturbance, the equation of state gives

$$p = \rho c^2 \tag{58}$$

where c is the mean speed of sound. The expansion will be carried out to $O(\varepsilon)$ in Eqs. (54)-(57), so that ε_1 must be less than or equal to $O(\varepsilon^2)$ for consistency.

The problem formulation is completed by specification of boundary conditions: the duct walls are lined with point-reacting acoustic materials whose specific acoustic admittances β_1 and β_2 may vary slowly with the axial distance, $\beta_j = \beta_j(x_1)$. For a no-slip mean flow, a requirement of continuity of particle displacement gives

$$(v - \varepsilon R_j' u)/p = (-1)^j(\beta_j/\rho_0 c) + O(\varepsilon^2) \text{ at } r = R_j \qquad (59)$$

where R_1 and R_2 are the inner and outer radii of the duct.

5.1.2 Method of Solution

Lengths, velocities, time and pressure are made dimensionless using a characteristic length L, the speed of sound c, L/c and $\rho_0 c^2$ as reference values. The method of multiple scales determines an asymptotic solution of Eqs. (54)-(58), subject to the boundary conditions (59), of the form

$$\begin{aligned} p(x,r,\theta,t) &= \rho_0 c^2 F(x_1,r;\varepsilon)\exp(i\eta) \\ v(x,r,\theta,t) &= cG(x_1,r;\varepsilon)\exp(i\eta) \\ u(x,r,\theta,t) &= cH(x_1,r;\varepsilon)\exp(i\eta) \\ w(x,r,\theta,t) &= cS(x_1,r;\varepsilon)\exp(i\eta) \end{aligned} \qquad (60)$$

where

$$\partial\eta/\partial t = -\omega, \quad \partial\eta/\partial x = k_0(x_1), \quad \partial\eta/\partial\theta = m \qquad (61)$$

with constant ω. Here ω is the frequency, m is an integer, the real part of k_0 is the wavenumber, and the imaginary part of k_0 is the attenuation rate, α_0.

The modal description of acoustic waves has been employed in Eqs. (60). Hence, for each value of the circumferential mode number m there will exist an infinite number of radial modes (including those beyond cutoff) corresponding to distinct values of the complex wavenumber k_0. For strong axial variations of the duct, the radial modes interact as they propagate through the duct. However, for the slow variations assumed in this investigation the coupling of the radial modes can be neglected and the various modes studied independently. Thus, Eqs. (60) describe a single arbitrary mode.

The separation of the acoustic disturbance into independent modes also contains an implicit assumption that such modes are distinct. In those cases in which two parallel-duct modes have identical eigenvalues, the modes interact to produce a linear amplification in the axial direction in addition to the attenuation contained in the exp(iη) factor (Tester[46] or Zorumski and Mason[47]). In a duct whose properties vary in the axial direction, the difference between two eigenvalues is a slowly-varying function; as the difference becomes smaller, the interaction between the two modes, which approaches the linear amplification factor as the difference vanishes, requires a modification of Eq. (60) to account for the additional axial amplitude variations of the modes (Section 5.2). However, no theory to account for the transition from independent duct modes to the linear ampli-

fication interaction is now available, and thus we must exclude an analysis of such cases from the current study.

In terms of x_1 and η, the time and spatial derivatives are

$$\begin{aligned} \partial/\partial t &= -\omega(\partial/\partial\eta) \\ \partial/\partial\theta &= m(\partial/\partial\eta) \\ \partial/\partial x &= k_0(\partial/\partial\eta) + \varepsilon(\partial/\partial x_1) \end{aligned} \tag{62}$$

The functions F, G, H, and S are expanded in the form

$$\begin{aligned} F &= F_0(x_1,r) + \varepsilon F_1(x_1,r) + \ldots \\ G &= G_0(x_1,r) + \varepsilon G_1(x_1,r) + \ldots \\ H &= H_0(x_1,r) + \varepsilon H_1(x_1,r) + \ldots \\ S &= S_0(x_1,r) + \varepsilon S_1(x_1,r) + \ldots \end{aligned} \tag{63}$$

As described in Ref. 34, the expansion of Eqs. (54)-(58) according to Eqs. (60)-(63) leads to the following problems for the pressure functions F_0 and F_1:

$$L(F_0) \equiv \frac{1}{r}\frac{\partial}{\partial r}\left(\frac{r}{\hat{\omega}^2}\frac{\partial F_0}{\partial r}\right) + \frac{1}{\hat{\omega}^2}\left(\hat{\omega}^2 - k_0^2 - \frac{m^2}{r^2}\right)F_0 = 0 \tag{64}$$

$$\frac{\partial F_0}{\partial r} + (-1)^{j+1} i\omega\beta_j F_0 = 0 \text{ at } r = R_j \tag{65}$$

and

$$L(F_1) = I(F_0,U,V,k_0) \tag{66}$$

$$\frac{\partial F_1}{\partial r} + (-1)^{j+1} i\omega\beta_j F_1 = B_j(F_0,U,V,k_0,R_j') \text{ at } r = R_h \tag{67}$$

where

$$\hat{\omega} = \omega - kU \tag{68}$$

The functionals I and B_j contain the effects of the axial gradients of the flow; the specific forms of these functions may be found in Ref. 34. The slow scale x_1 appears impli-

citly in Eqs. (64) and (65). If U, R_j, and β_j are independent of x_1, Eqs. (64) and (65) reduce to those used extensively in the literature to analyze the wave propagation in uniform annular ducts carrying sheared mean flow and lined with materials having uniform acoustic properties. For a given ω, $U(x_1)$, $\beta_j(x_1)$ and $R_j(x_1)$, Eqs. (64) and (65) can be solved to determine the eigenvalue $k_0(x_1)$ and its corresponding eigenfunction $\psi(r;x_1)$. The solution can be expressed as

$$F_0 = A(x_1)\psi(r;x_1) \tag{69}$$

where $A(x_1)$ is still an undetermined function at this level of approximation. It is determined by the nature of the solution to Eqs. (66) and (67). Since F_0 and k_0 are solutions of the homogeneous parts of Eqs. (66) and (67), the inhomogeneous equations (66) and (67) have a solution if, and only if, a solvability condition is satisfied. This solvability condition yields the desired equation for $A(x_1)$.

To determine this condition, we multiply Eq. (66) by $r\psi(r;x_1)$. Integrating the resulting equation by parts from $r = R_1$ to $r = R_2$ and using the definition of the operator L from Eq. (64), we obtain

$$\left[\frac{r}{\hat{\omega}^2}\left(\psi \frac{\partial F_1}{\partial r} - F_1 \frac{\partial \psi}{\partial r}\right)\right]_{R_1}^{R_1} = \int_{R_1}^{R_2} rI\psi dr \tag{70}$$

Using the boundary conditions from Eq. (65) and (67) and substituting for F_0 from Eq. (69), one obtains an equation for the amplitude variation in the form

C-2

$$f(x_1)\frac{dA}{dx_1} + g(x_1)A = 0 \tag{71}$$

which has the solution

$$A(x_1) = A_0\exp[i\ k_1 dx_1] = A_0\exp[i\varepsilon\ k_1 dx] \tag{72}$$

where

$$k_1 = ig(x_1)/f(x_1) \tag{73}$$

The functions $f(x_1)$ and $g(x_1)$ are integrals across the duct width of ψ, U, V, k_0 and their derivatives. The integrals require numerical evaluation; the specific forms of these functions can be found in Ref. 34. Thus the dimensional acoustic pressure variation is given by

$$p(x,r,\theta,t) = A_0\rho_0 c^2\ \psi(r;x_1)\exp i[\ (k_0 + \varepsilon k_1)dx - \omega t + m\theta] + O(\varepsilon) \tag{74}$$

where $\psi(r;x_1)$ and $k_0(x_1)$ are calculated at each station in the duct as if the duct walls and mean flow were parallel, and $k_1(x_1)$ contains the effects of the axial derivatives of the mean flow and duct properties. If the εk_1 term is omitted from Eq. (74), the representation of the acoustic signal is referred to as the quasi-parallel approximation since it assumes that the acoustic propagation locally is the same as in a parallel duct. One objective of this study is to obtain a comparison of the results of both the quasi-parallel model (i.e., k_0) and the non-parallel model, (i.e., $k_0 + \varepsilon k_1$) with experimental data in order to establish the validity of the theory. These comparisons are described in Section 5.3.

5.2 Optimum Liner Properties

Computations based on the method described above have attempted to determine the effect of axial gradients on "optimum" liner properties (defined here as those properties that produce maximum attenuation of the least attenuated mode), since parallel-flow studies[48,49] have shown that the optimum properties are strongly dependent on parameters such as boundary-layer thickness. However, the computed results develop a singular behavior as the "optimum" properties are approached. Figure 21 shows results which exhibit such behavior; for this specific case, the duct has a constant cross-sectional area, the boundary layer is growing, and the liner properties are those that a parallel-flow analysis identified as "optimum" for the boundary-layer thickness that occurs at $x = 1.5$. Thus the liner is off optimum except at the midpoint where the eigenvalues of two modes become equal. The resulting singular behavior has been found to be a consequence of a weak nonuniformity in the parallel-flow analysis when two modes are equal. The usual theory assumes that the modes are independent. However, if two eigenvalues k_a and k_b are nearly the same, say $k_b = k_a + \Delta$, then

$$p = A\psi_a(r)e^{ik_a x} + B\psi_b(r)e^{ik_b x} e^{-i\omega t+im\theta} \quad (75)$$

becomes

$$p = e^{ik_a x} \left(A + Be^{ix_1}\right)\psi_a(r) + C\psi_c(r)e^{ix_1} \; e^{-i\omega t + im\theta} \quad (76)$$

where $x_1 = \Delta x$ and ψ_c is related to the derivative of ψ_a with respect to the eigenvalue. Thus, if the two modes are distinct, but close, the acoustic signal has a slow amplitude variation with axial distance due to the interaction of the two modes in addition to the slow, non-parallel variation included in Eq. (74). When the two modes are exactly equal, Tester[46] and Zorumski and Mason[47] have shown that the appropriate acoustic description takes the form

$$p = e^{ik_a x} \left(A + Bx\right)\psi_a(r) + C\psi_c(r) \; e^{-i\omega t + im\theta} \quad (77)$$

As "optimum" liner properties are approached and the two modes approach one another, the interaction between them becomes stronger until it leads to a linear amplification factor when the modes are identical. It should be noted that this occurs in a very small neighborhood of the optimum admittance value. Although the attenuation over a finite length section may differ from the "optimal" prediction based on a parallel analysis due to the neglect of the linear amplification term, the largest attenuation will still be located very close to the admittance value calculated without considering the mode interaction. This is reflected in the results shown in Fig. 21; the local optimum liner properties are nearly the same over the entire axial distance $0<x<3$, yet the singularity develops only very close to the point where the liner admittance exactly equals the optimum value.

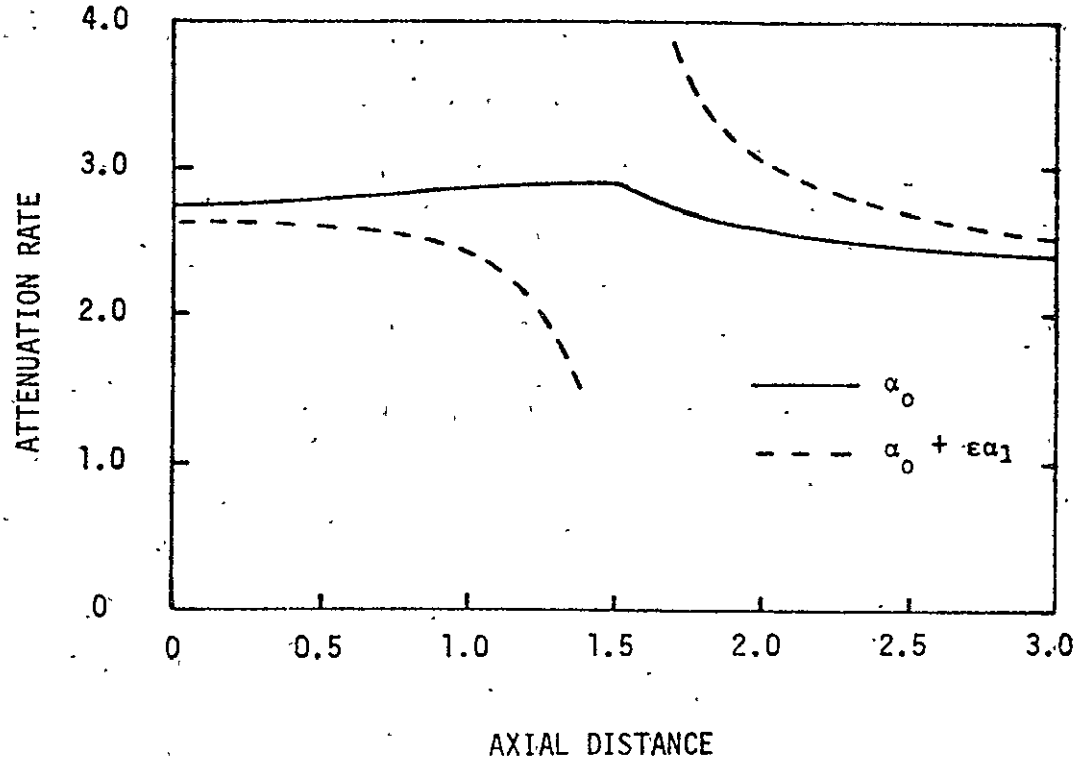

Figure 21. Singular behavior of nonparallel effects at a multiple eigenvalue; M = - 0.3, ω = 5, HTR = 0.5, varying boundary-layer thickness.

Thus the nonuniformity in the parallel-duct theory is very weak; however, in any perturbation analysis, nonuniformities become more singular in the higher-order terms -- in this case in the nonparallel results. The singular behavior exhibited in Fig. 21 is seen to approximately the $k_1 = (i/\varepsilon)/(x-x_s)$ behavior that would be required to obtain the linear amplification of Eq. (77) from the slow variation of Eq. (74). A result that bridges the singularity in the curve requires the development of a nonparallel-duct theory that accounts for the interaction of nearly-equal modes and thus bridges the gap between the classic independent-mode results and the linear-amplification results for multiple eigenvalues. Such an analysis would be analogous to that used by Nayfeh[50] to investigate the nonlinear propagation of a wave packet in a rigid duct. If we consider only linear, monochromatic waves, such an analysis would yield an amplitude function that is governed by an equation of the form

$$h(x)\frac{d^2A}{dx^2} + f(x)\frac{dA}{dx} + g(x)A = 0 \qquad (78)$$

The presence of the d^2A/dx^2 term, which is generally small, becomes important when $f(x)$ approaches zero [$f(x_1) \to 0$ is responsible for the singular behavior of k_1 in Eq. (74)] and accounts for the linear amplification factor when a multiple root occurs.

5.3 Comparison with Experimental Results

The computer code described in Ref. 34 that implements the theory outlined in Section 5.1 has been adapted to the flow and wave propagation in the experimental facility described in Section 2. The mean flow is assumed to be uniform across the duct width except for boundary layers at the two walls. The integral method of Alber[51] has been used to predict the boundary-layer thicknesses on the two walls for the flow conditions at which tests were run. The acoustic studies at the three test frequencies of 840 Hz, 2460 Hz and 3150 Hz have shown that the mean boundary-layer thickness, which is small, has little effect on the acoustic propagation for the test conditions of the experimental facility. Thus the refractive effects within the duct are primarily due to the axial velocity gradients that occur.

5.3.1 Straight-wall Cases

The liner properties used in the theoretical study are the same as those estimated in Section 4.2.3 on the basis of no-mean-flow results. Comparisons between theory and experiment have been made for cases in which the duct carries a mean flow. Two cases, in which the mean-flow velocity is approximately 105 feet per second and 200 feet per second, have been considered for each of the three test frequencies.

The theoretical results in these cases agree with the experimental data as well as the original no-mean-flow

results from which the liner admittance was estimated. Several examples are shown in Figures 22-24. As noted in Section 4, the amplitudes of the pressure disturbance have a strong m = 1 component at station 3 that is not predicted by the theory, due to the inhomogeneous liner properties. However, the average attenuation of the duct is predicted quite well; in the cases that are not shown in Figs. 22-24 the agreement is as good as for the cases shown, and the results for the phase of the acoustic disturbance are excellent in all cases. The basic conclusion from these results is that the liner admittance is not altered significantly by the presence of the mean flow.

5.3.2 Variable-area Cases

For the variable-area centerbody, the flow in the signal-insertion section upstream of the variable-area test section was maintained at nominal values of either 105 feet per second or 184 feet per second. The flow within the test section reached a maximum value of approximately 300 feet per second for the faster of the two cases. This keeps the Mach number below 0.3 and permits comparison with the incompressible theoretical model.

Both the quasi-parallel approximation and the non-parallel perturbation approximation were calculated for comparison with the experimental data and both theoretical curves are shown in those cases in which they differ. Figures 25 and 26 show results for 840 Hz at flow speeds of

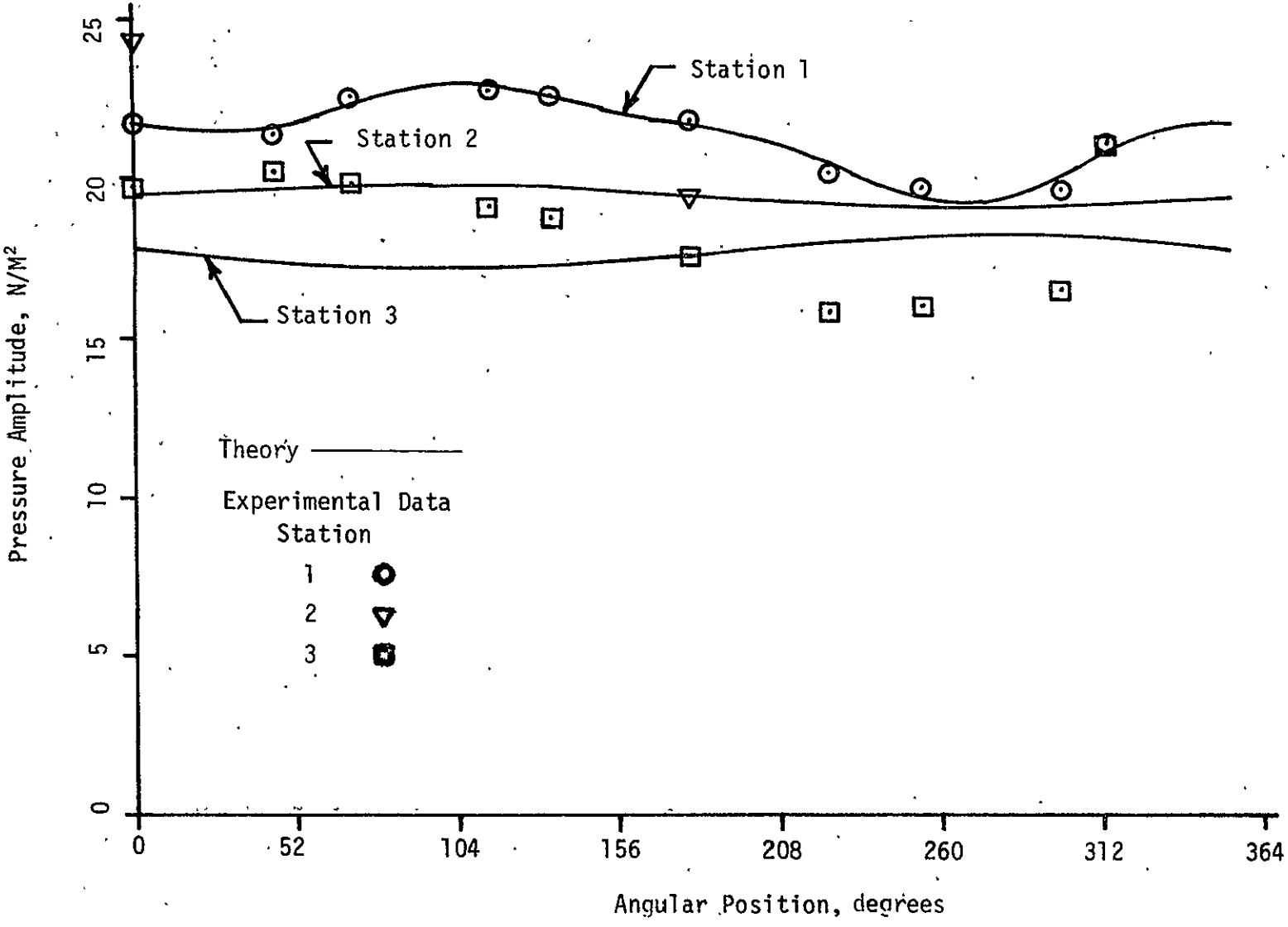

Figure 22. Comparison of the theoretical and experimental pressure amplitudes with the uniform centerbody installed; v = 105ft/sec, β = .10 - .26i, f = 840Hz.

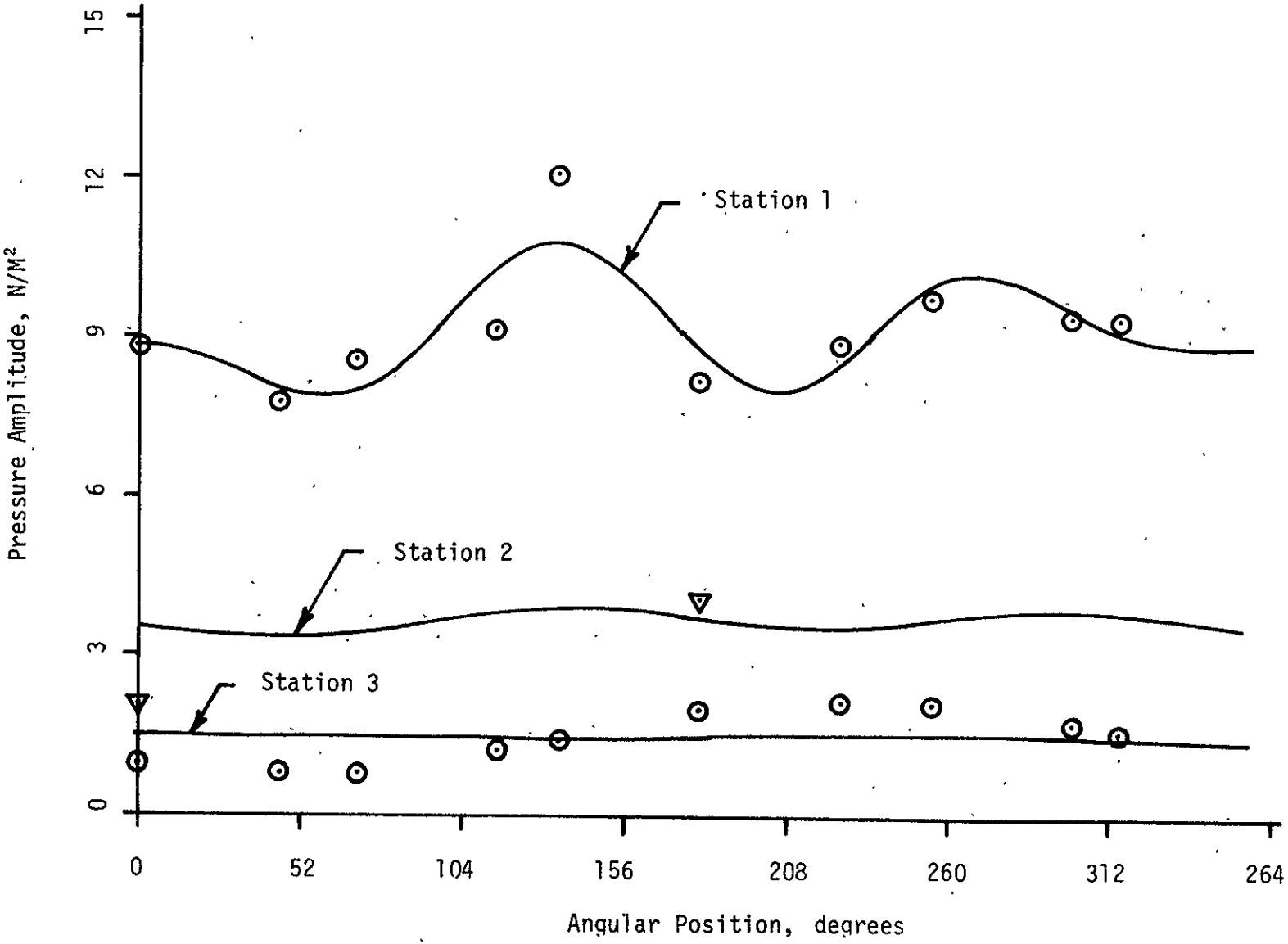

Figure 23. Comparison of the theoretical and experimental pressure amplitudes with the uniform centerbody installed; v = 105ft/sec., β = .75 - .095i, f = 2640 Hz.

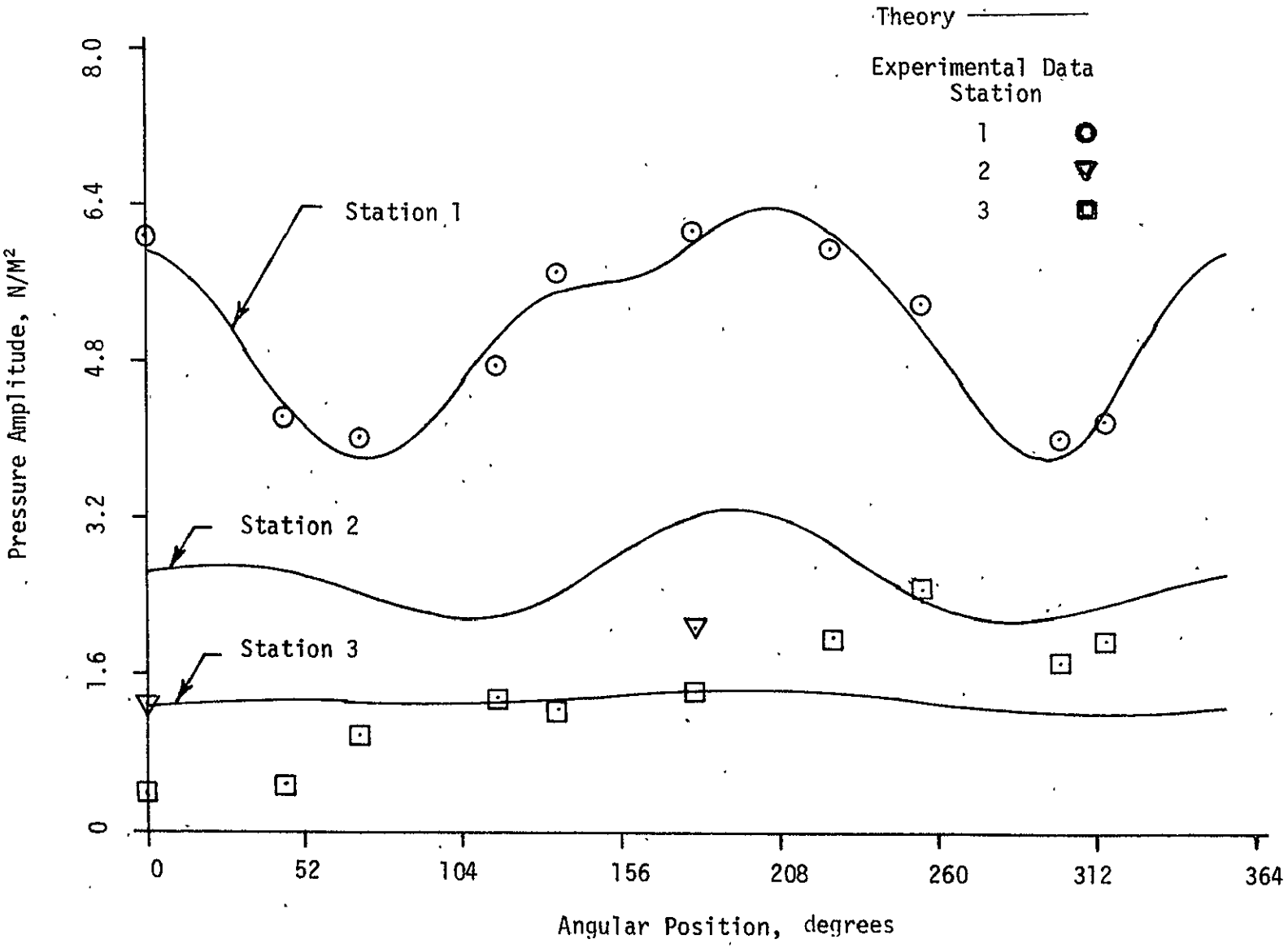

Figure 24. Comparison of the theoretical and experimental pressure amplitudes with the uniform centerbody installed; v = 184ft/sec., β = .75 + .13i, f = 3150 Hz.

105 feet per second and 184 feet per second, respectively. As before, the liner inhomogeneities generate a strong m = 1 circumferential-mode component at the third station. However, for the lower speed, the average attenuation rate is predicted very well by the non-parallel theory in contrast with the quasi-parallel theory which overpredicts the attenuation rate (Fig. 25a). Both theoretical models give the same phase shift (Fig. 25b). At the higher speed, the experimental pressure amplitude (Fig. 26a) has a somewhat erratic circumferential variation that provides little help in validating one theoretical result to the exclusion of the other. Both theoretical results give good agreement with the measured phases, as shown in Fig. 26b.

At the higher frequencies, the results are also good. Figures 27 and 28 present comparisons between theory and experiment for flow velocities of 105 feet per second and 184 feet per second respectively. The pressure amplitudes are shown in Figs. 27a and 28a, and the agreement is satisfactory in both cases; there is no appreciable difference between the two theoretical results. However, the phase predictions from the quasi-parallel theory and the non-parallel theory are slightly different for this case, and in both Figs. 27b and 28b, the non-parallel results are seen to be slightly better.

At the highest frequency of 3150 Hz, the two theoretical results are nearly identical. The comparison with experimental data is shown in Figs. 29 and 30. The overall

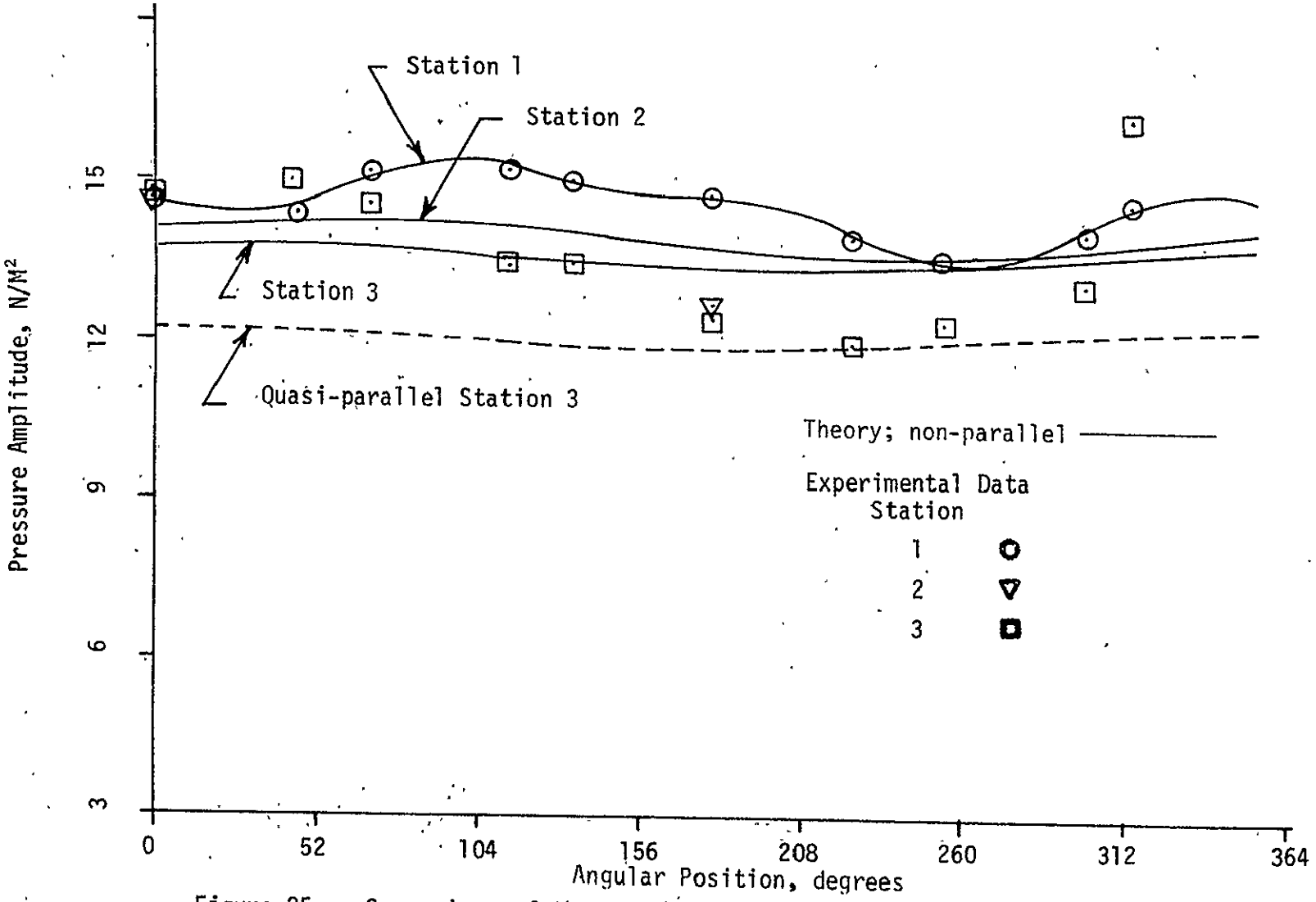

Figure 25a. Comparison of the quasi-parallel, nonparallel and experimental pressure amplitudes with the variable centerbody installed; v = 105ft/sec., f = 840 Hz, $\bar{\beta}$ = .1 - .26i.

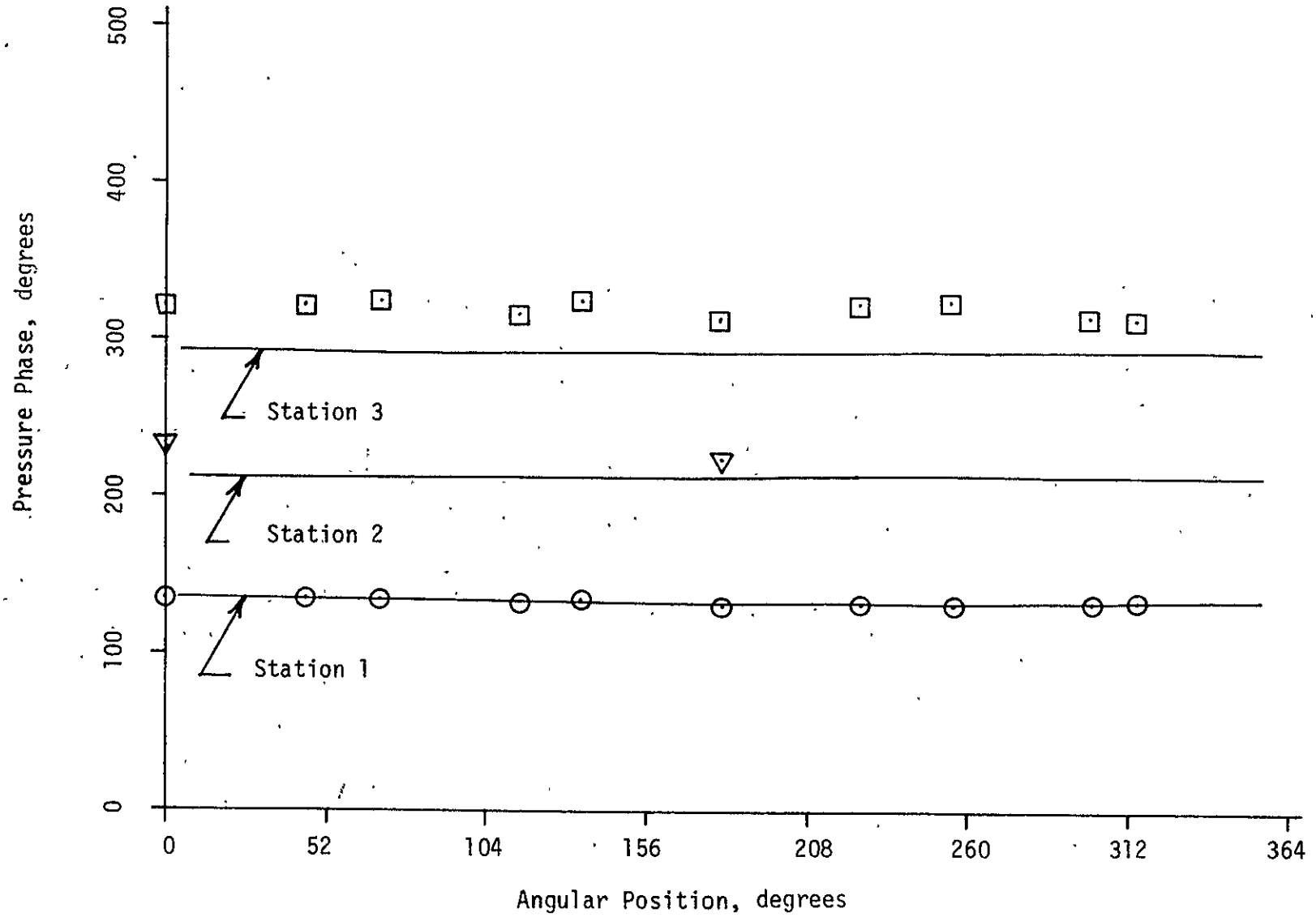

Figure 25b. Comparison of the theoretical and experimental pressure phases with the variable centerbody installed; v = 105ft/sec., f = 840Hz, β = .1 - .26i.

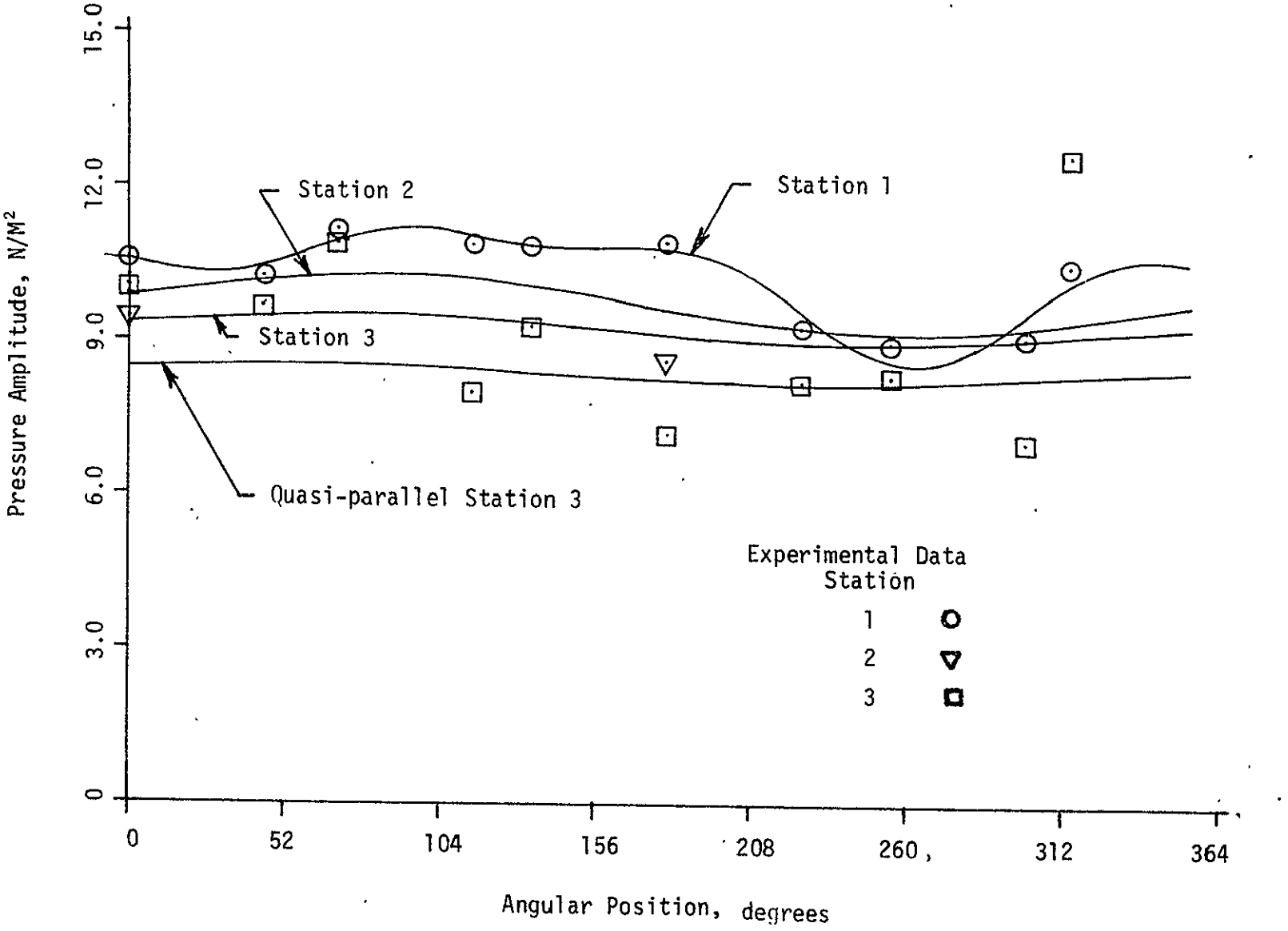

Figure 26a. Comparison of the quasi-parallel, nonparallel and experimental pressure amplitudes with the variable centerbody installed; v = 184ft/sec., f = 840Hz, β = .1 - .26i.

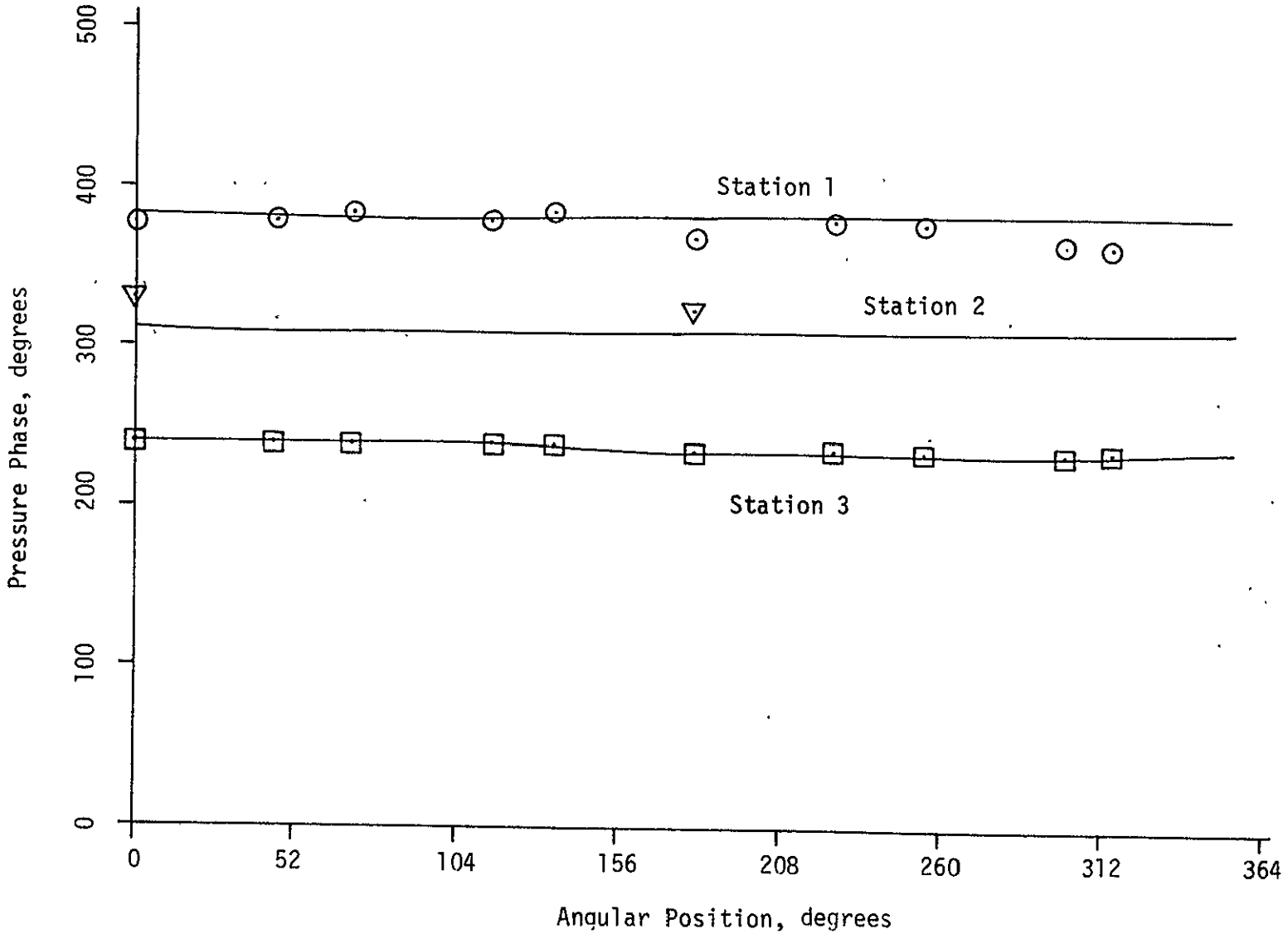

Figure 26b. Comparison of the theoretical and experimental pressure phases with the variable centerbody installed; v = 184ft/sec., f = 840Hz, R = 1 - 26i

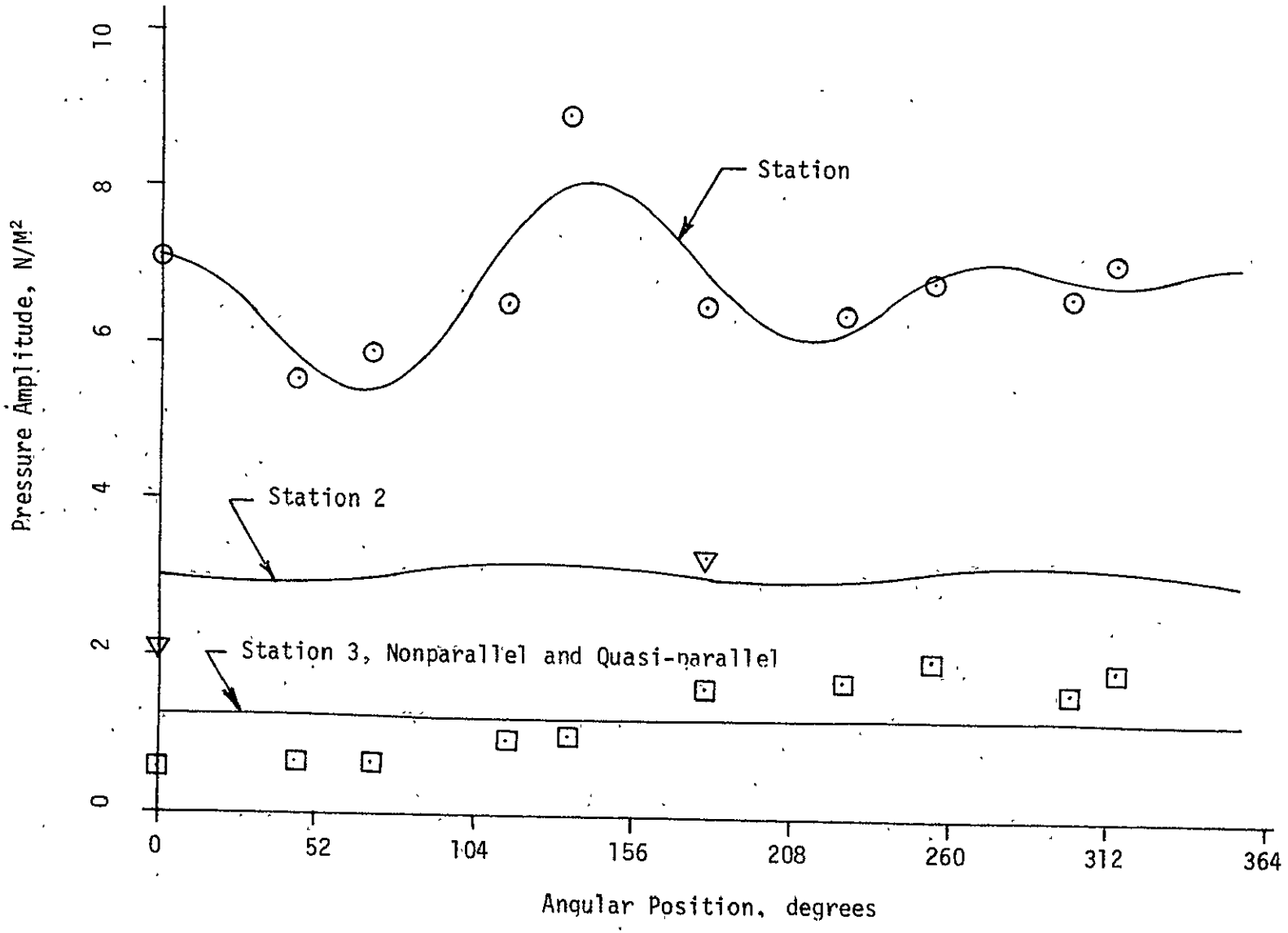

Figure 27a. Comparison of the quasi-parallel, nonparallel and experimental pressure amplitudes with the variable centerbody installed; v = 105ft/sec., f = 2640 Hz, β = .75 - .095i.

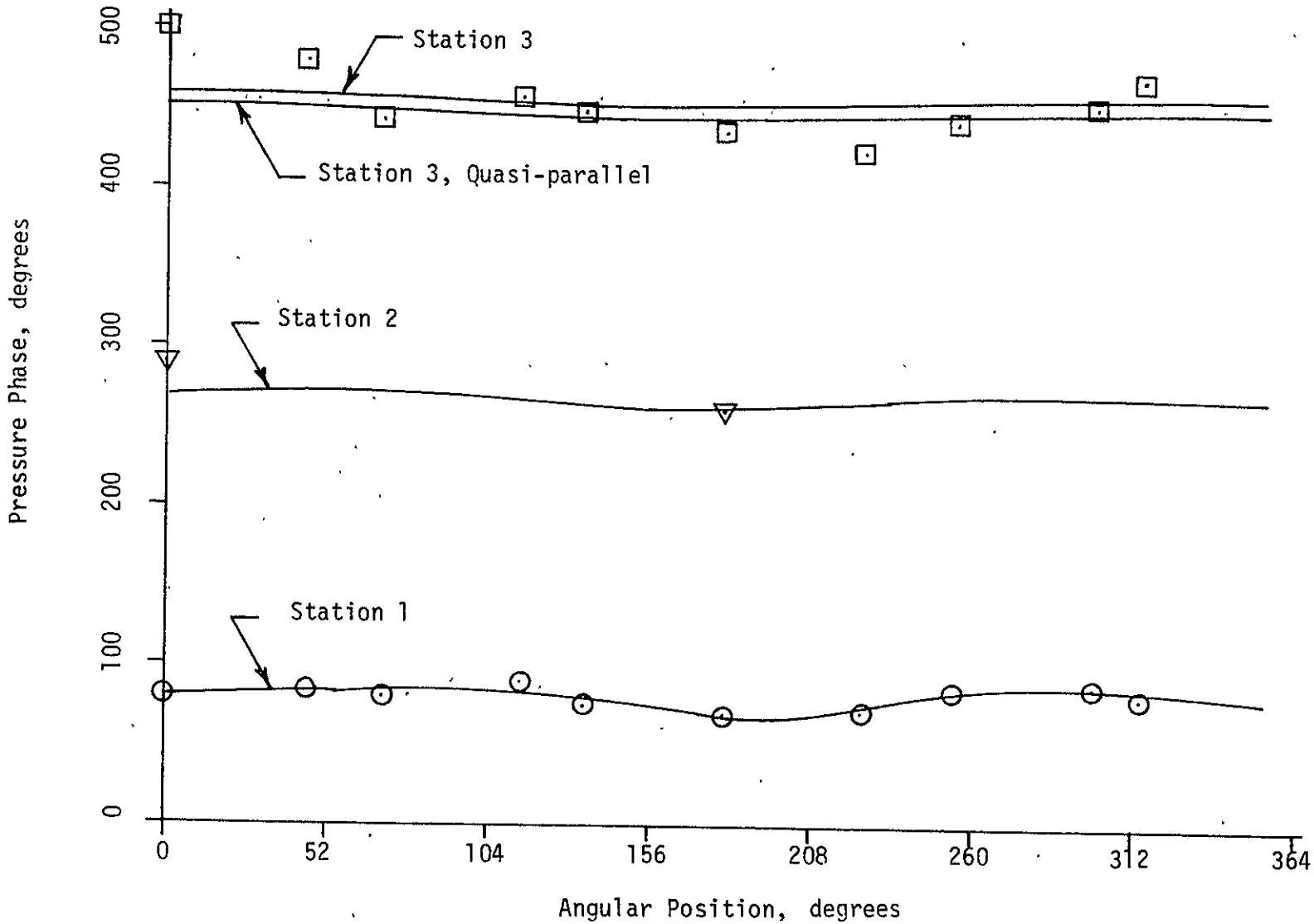

Figure 27b. Comparison of the quasi-parallel, nonparallel and experimental pressure phases with the variable centerbody installed; v = 105ft/sec., f = 2640 Hz, β = .75 - .095i.

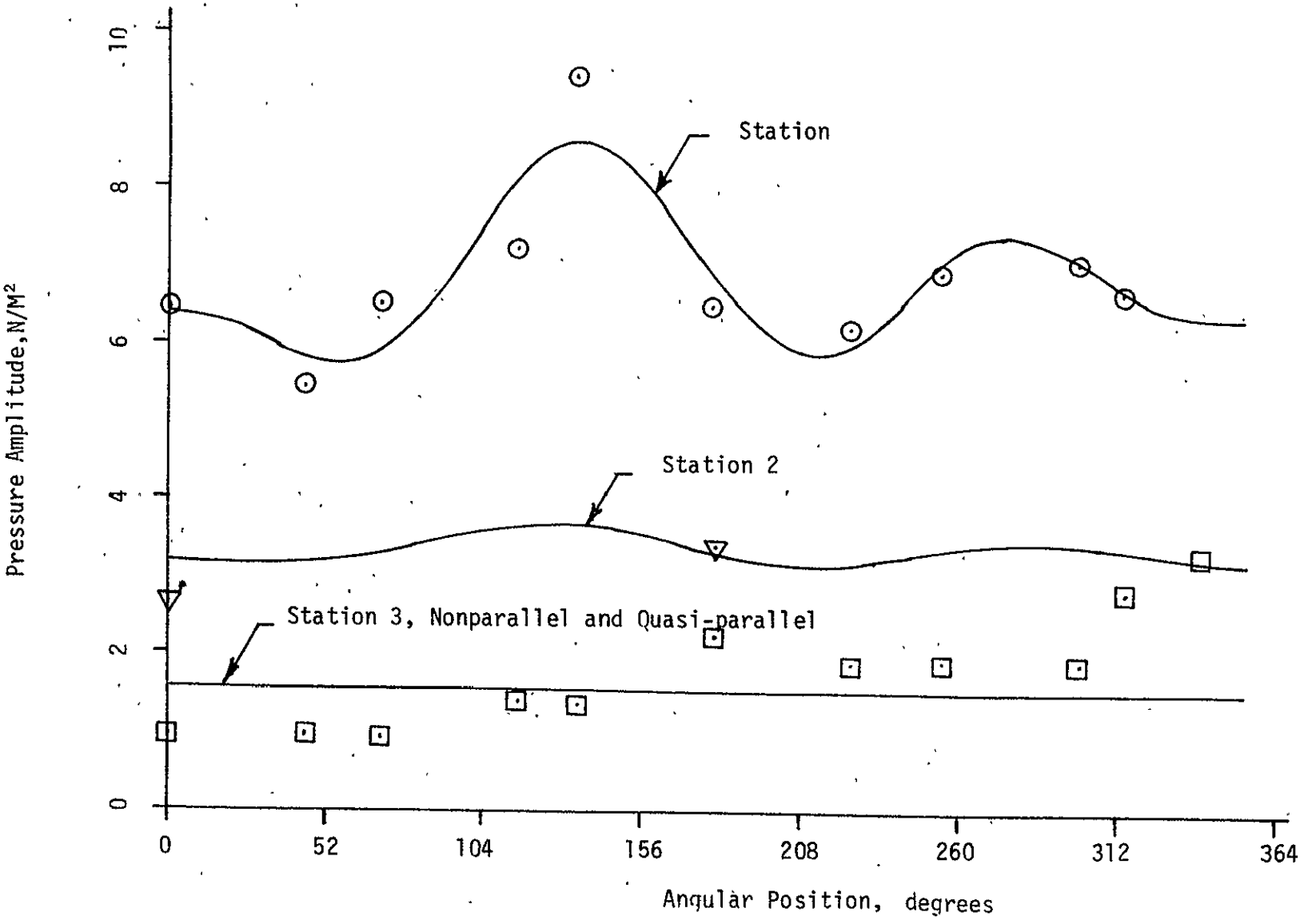

Figure 28a. Comparison of the quasi-parallel, nonparallel and experimental pressure amplitudes with the variable centerbody installed; v = 184ft/sec., f = 2640 Hz, β = .75 - .095i.

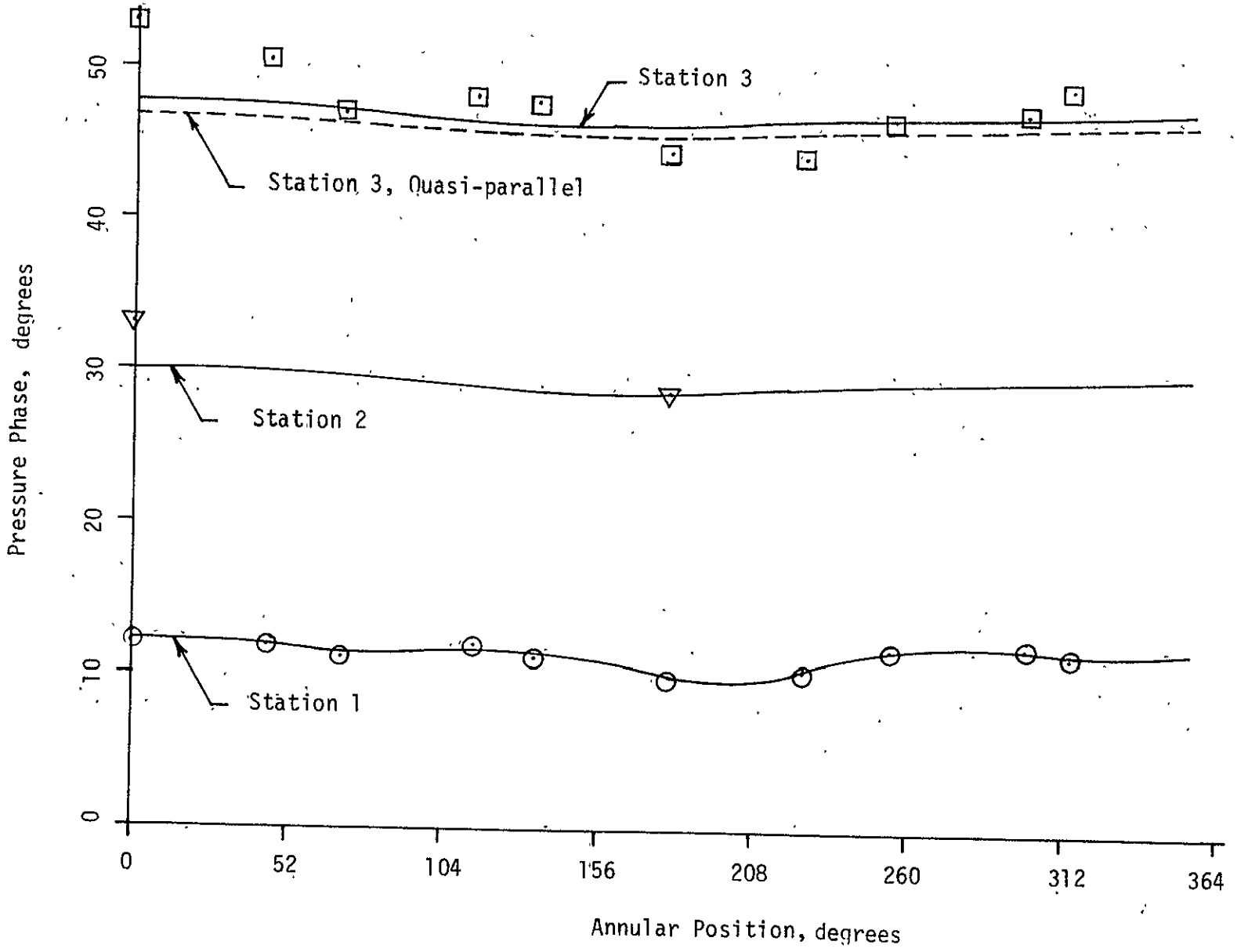

Figure 28b. Comparison of the quasi-parallel, nonparallel and experimental pressure phases with the variable centerbody installed; v = 184ft/sec., f = 2640 Hz, β = .75 - .095i.

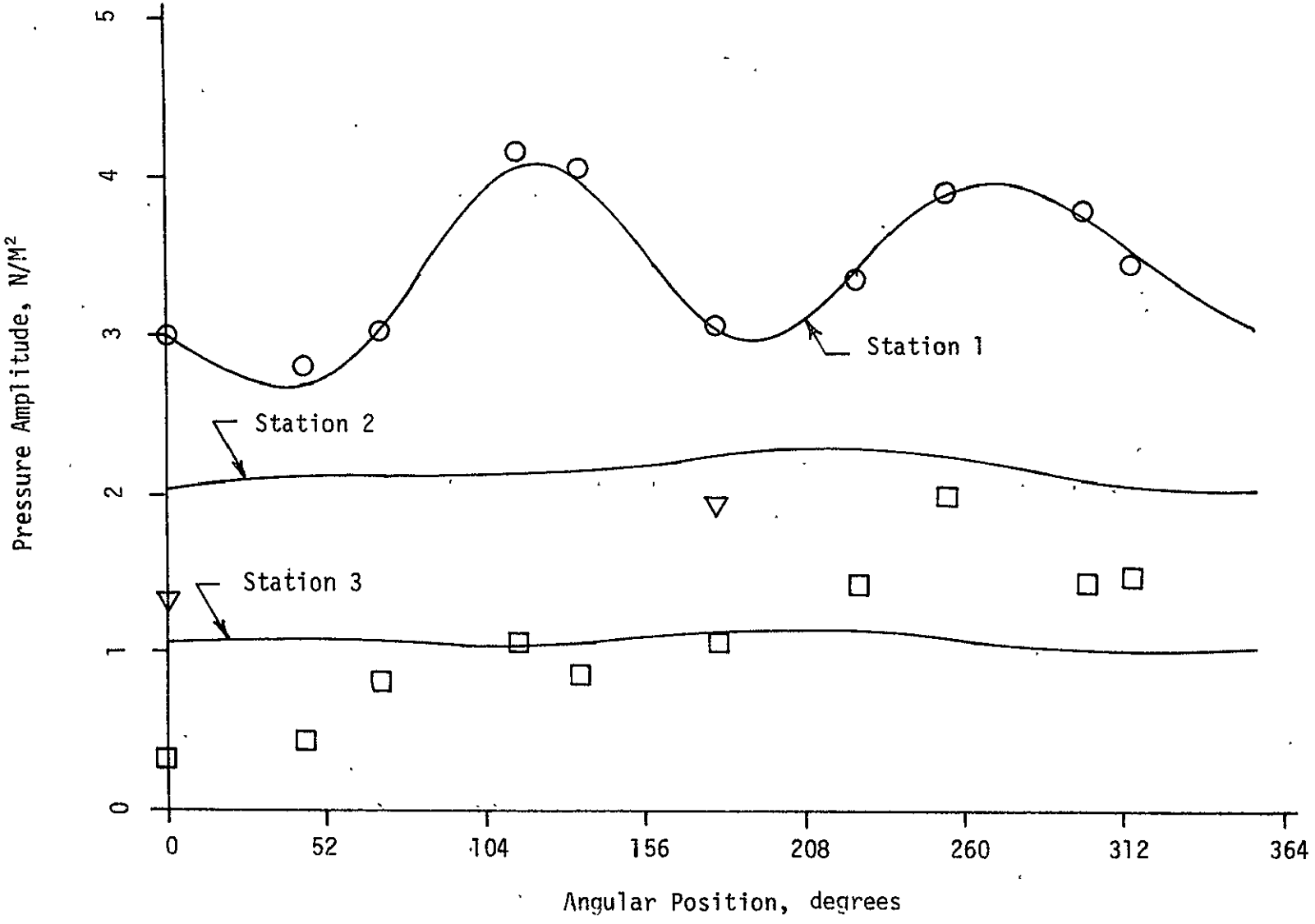

Figure 29a. Comparison of the theoretical and experimental pressure amplitude with the variable centerbody installed; v = 105ft/sec., f = 3150 Hz, β = .75 + .13i.

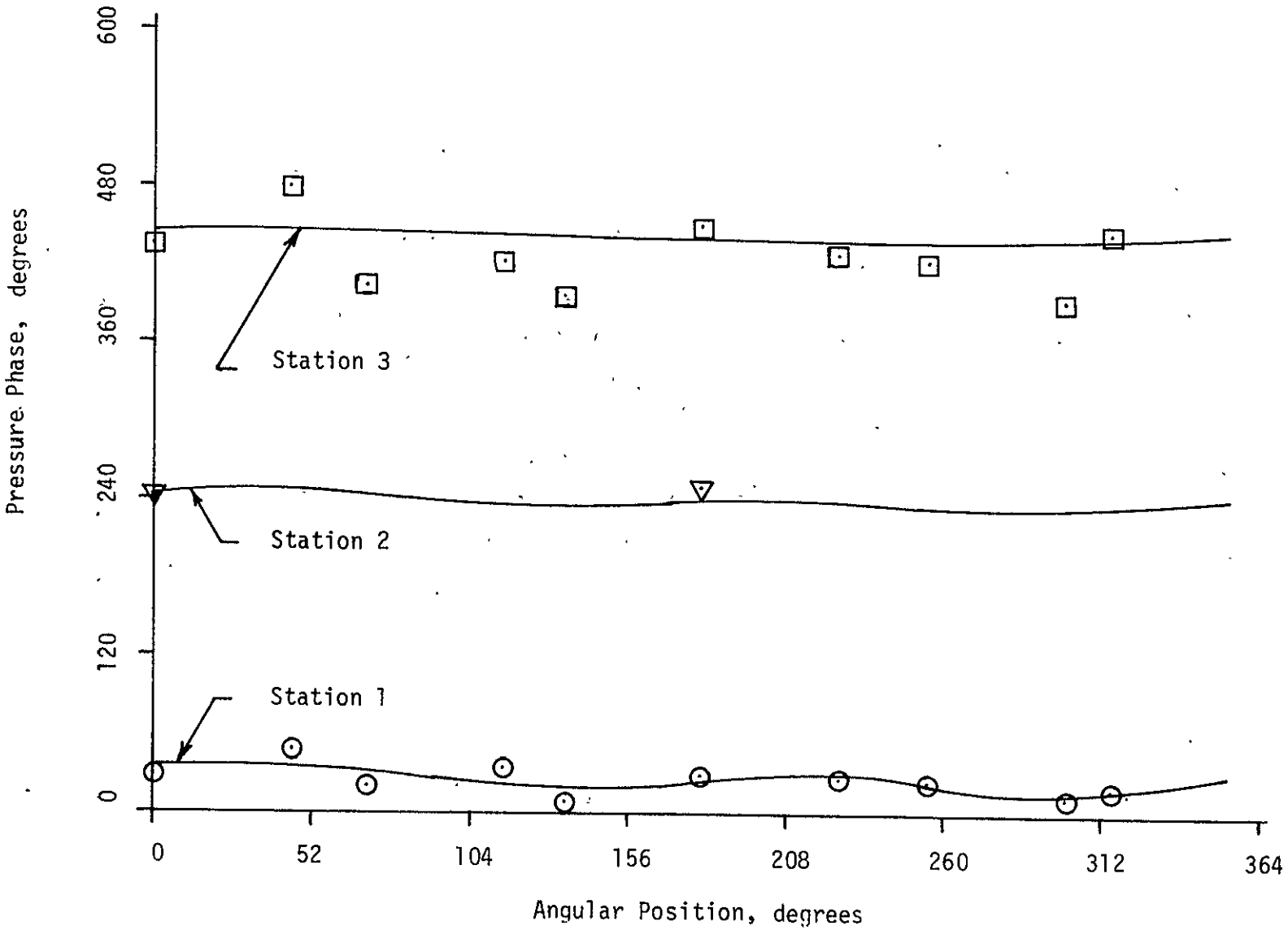

Figure 29b. Comparison of the theoretical and experimental pressure phase with the variable centerbody installed; v = 105ft/sec., f = 3150 Hz, $\beta = .75 + .13i$.

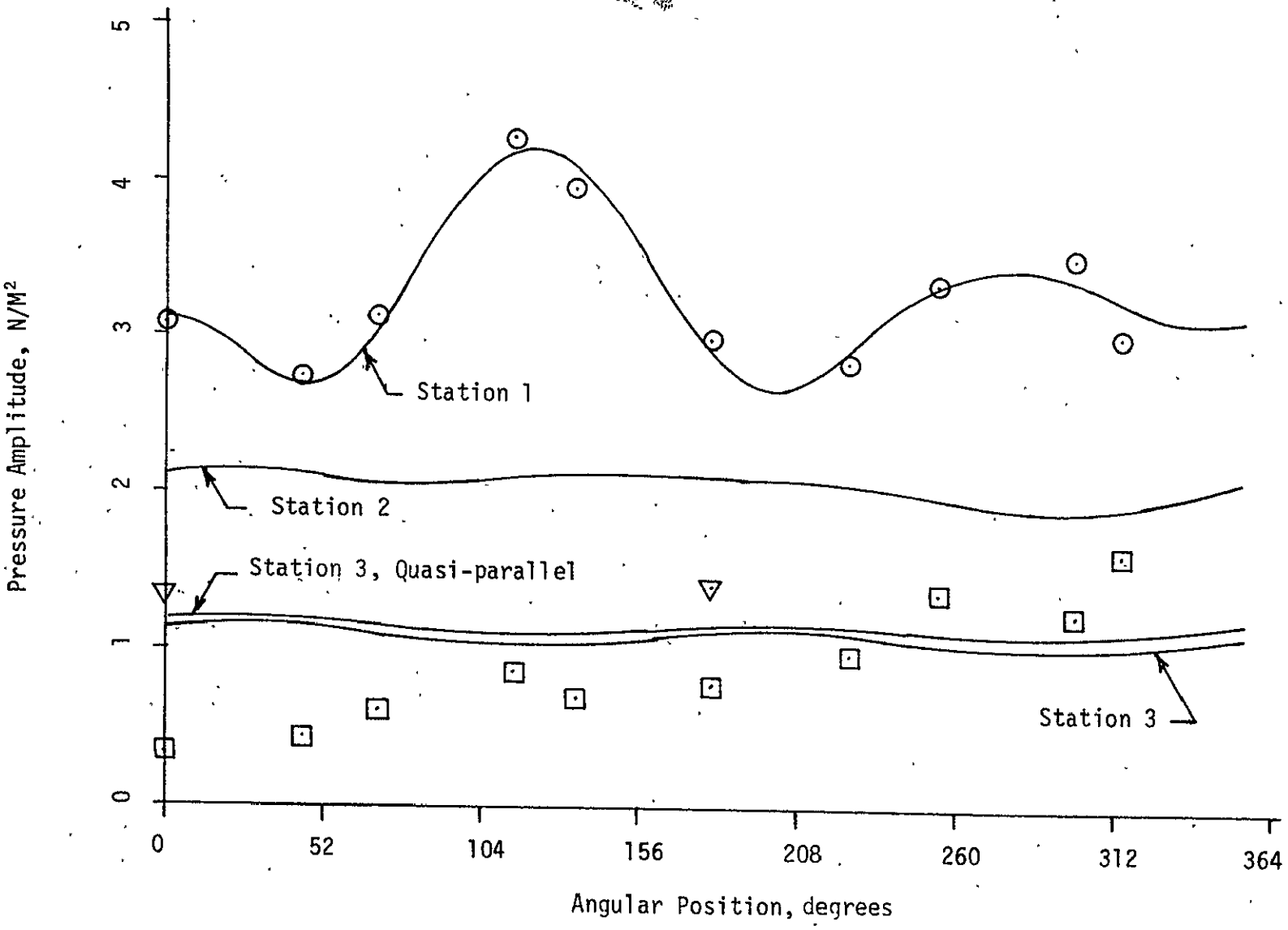

Figure 30a.. Comparison of the theoretical and experimental pressure amplitude with the variable centerbody installed; v = 184ft/sec., f = 3150Hz, β = .75 + 13i.

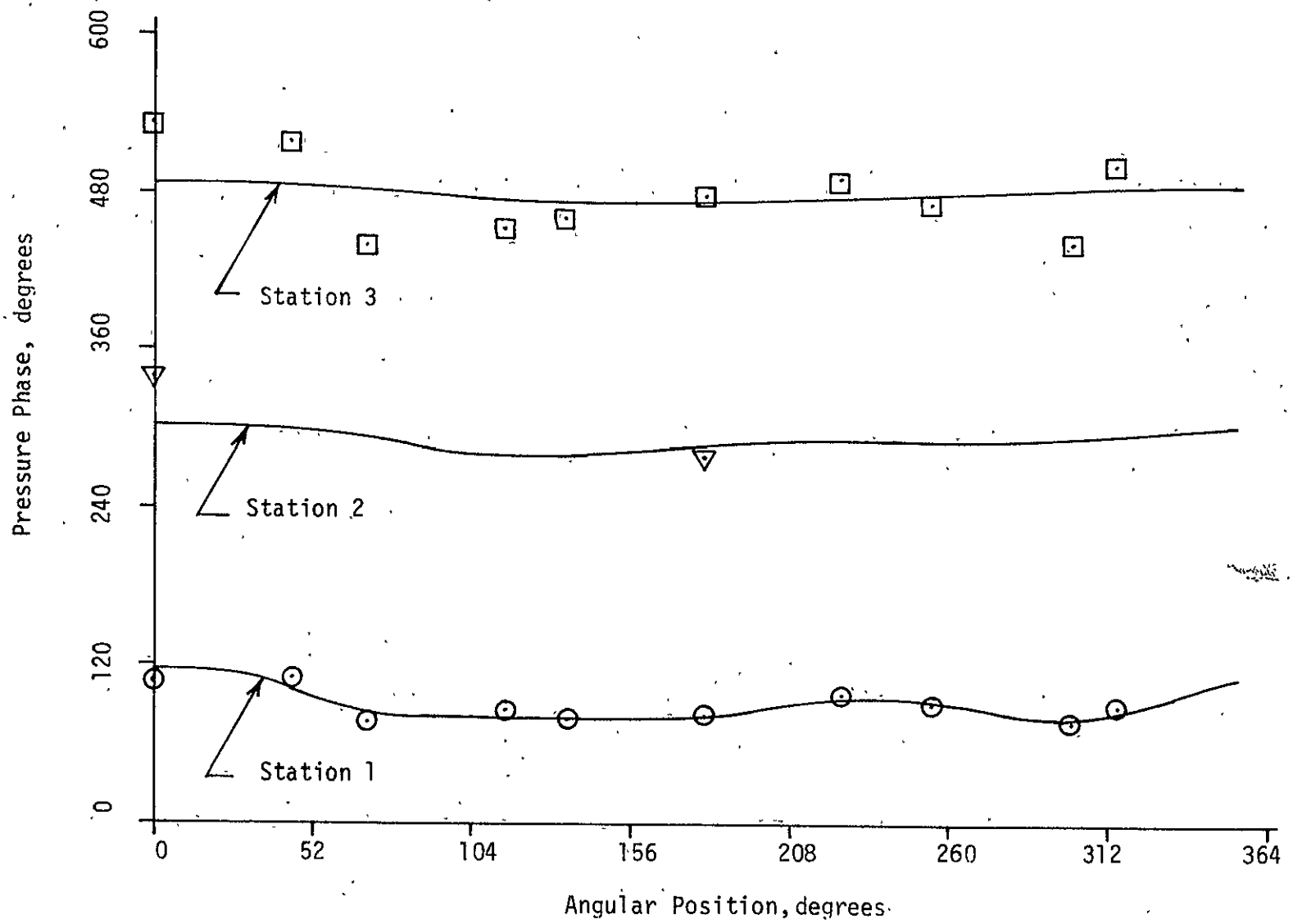

Figure 30b. Comparison of the theoretical and experimental pressure phase with the variable centerbody installed; v = 184ft/sec., f = 3150 Hz, $\beta = .75 + .13i$.

attenuation of the amplitudes is again satisfactorily predicted although the circumferential variation is not. The phase results are quite good although there is a fair amount of scatter in the experimental results.

The general agreement between theory and experiment is considered satisfactory, discounting the difficulties introduced by the liner inhomogeneities. These difficulties also appeared in the constant-area, no-mean flow cases for which the theory is well established and can not be considered as a shortcoming of the non-parallel theory. Indeed, the non-parallel theory has proven to yield better results than a quasi-parallel approximation in those instances in which there was a difference between the two approximations. The agreement for cases with a mean flow that are reported in this section has been shown to be better than that for cases without flow; why this should be so is not clear.

Overall, the comparisons lend support to the validity of the modeling of the effects of the axial variations that occur in the duct. In addition, the need to develop a procedure to calculate the effect of circumferential variations in the duct properties is clearly present.

6. Summary

An experimental facility has been constructed for the study of acoustic wave propagation in annular ducts that carry mean flows with both axial and transverse velocity gradients. The test section can be selected to have either a rigid or lined outer wall; the cross-sectional area can be either constant or variable by selection of either a straight or variable-radius centerbody, which is rigid. The duct liner is point reacting and consists of a Feltmetal facing sheet covering cellular backing cavities that are nominally tuned to a frequency of approximately 3000 Hz.

The design of the duct is such that the mean boundary layer is thin within the test section; ambient noise levels are controlled by means of two line mufflers and an anechoic duct termination so that a good signal to noise ratio is achieved. Four acoustic drivers provide the input signal to be studied, and control of the relative amplitudes and phases of the drivers permits some control of the complexity of the circumferential variation (spinning modal structure) of the acoustic disturbance. The duct has been instrumented to permit acquisition of narrow-band data for determination of the relative amplitudes and phases of the acoustic disturbance along the outer wall of the test section. The test sections are provided with sufficient microphone probe locations to permit resolution of the modal content of the signal up to the third circumferential mode.

Preliminary experimental tests with both lined and hard-walled test sections have established those frequencies at which resonances within the duct occur. The resonant frequencies, which are not suitable for extensive testing for comparison with analytical predictions for propagating waves, are shown to be the hard-wall cut-on frequencies; two additional resonances occur in the signal-insertion section when the lined test section is installed but apparently do not cause problems for study of propagating waves in the lined test section itself. Three frequencies below cut on of the first radial mode were selected for detailed studies of the circumferential and axial variation of the acoustic pressure and phase in variable-area ducts and for comparison with analytic predictions.

Analytical formulas describing the wave propagation in hard-wall and lined annular ducts without a mean flow have been developed, and a previously-developed computer code for prediction of propagation in annular ducts with flow has been modified to carry out the computational studies for this investigation. All analytical methods are based on the method of multiple scales for slowly-varying duct properties. Results from the computer code were used in the preliminary design stage of the experimental facility to determine a suitable range of values for the area variation of the duct and for the liner resistance.

The computer code has also been used to investigate the behavior of the variable-area effects in the presence of an "optimum" liner for a variety of flow conditions. It is

shown that the non-parallel results develop a singularity at a multiple root of the parallel duct eigenequation as a consequence of an improper description of the acoustic-propagation process by the parallel-duct theory.

Comparison of experimental data and theoretical predictions in hard-walled ducts without mean flow yields generally satisfactory results. The phase results at all frequencies are good, and a general intensification of the acoustic amplitude in the variable-area section is predicted. At the two lower frequencies, 840 Hz and 2640 Hz, the circumferential variation of the pressure amplitude is described well by the theoretical predictions, but at the highest frequency, 3150 Hz, this variation is inadequately predicted.

For lined ducts without flow, experimental results for a constant-area duct are used to establish the liner acoustic properties by comparison with well-establised analytical methods for constant-area ducts. The experimental data show an intensification of the m=1 circumferential mode in many instances that is though to occur as a consequence of the liner being inhomogeneous in its acoustic properties. Consequently, the liner properties are determined to be those that give the best average fit of the circumferential variation, and these liner properties are used to establish the ability of the analytic procedures to predict the general effects of the area variations for cases both with and

without a mean flow. Tests with flow in a constant-area duct have shown that the duct liner properties do not change appreciably in the presence of a mean flow.

For cases without flow, the general agreement between theoretical results and experimental data is good at only the 2640 Hz frequency. However, the computer code for cases with flow predicts variable-area effects that are in reasonable agreement with the experimental data. Although the circumferential variations due to the liner inhomogeneities are not predicted, the general effects of the axial variations of the mean flow and cross-sectional area are predicted quite well. The non-parallel theory is shown to yield better results than a quasi-parallel theory in those instances in which they yield different results. Overall the comparisons lend support to the validity of the modeling of the effects of the axial variations that occur within the duct, while pointing to a strong need to develop a procedure to determine the effects of circumferential variations in the duct properties.

References

1. Nayfeh, A. H., Kaiser, J. E., and Telionis, D. P., "Acoustics of Aircraft Engine-Duct Systems", AIAA Journal, Vol. 13, pp. 130-153, 1975.
2. Nayfeh, A. H., "Sound Propagation Through Nonunform Ducts", NASA CP-2001, Vol. 3, pp. 821-833, 1976.
3. Webster, A. G., "Acoustical Impedance and the Theory of Horns and of the Phonograph" Proceedings of the National Academy of Science, Vol. 5, pp. 275-282, 1919.
4. Isakovitch, M. A., "Scattering of Sound Waves on Small Irregularities in a Wave Guide", Akusticheskii Zhurnal, Vol. 3, 1957.
5. Salant, R. F., "Acoustic Propagation in Waveguides with Sinusoidal Walls", The Journal of the Acoustical Society of America, Vol. 53, pp. 504-507, 1973.
6. Nayfeh, A. H., "Sound Waves in Two-Dimensional Ducts with Sinusoidal Walls", Journal of the Acoustical Society of America, Vol. 56, pp. 768-770, 1974.
7. Nayfeh, A. H., "Acoustic Waves in Ducts with Sinusoidally Perturbed Walls and Mean Flow", Journal of the Acoustical Society of America, Vol. 57, pp. 1036-1039, 1975.
8. Nayfeh, A. H. and Kandil, O. A., "Propagation of Waves in Cylindrical Hard-Walled Ducts with General Weak Undulations", AIAA Paper No. 77-1282, 1977.
9. Alfredson, R. J., "The Propagation of Sound in a Circular Duct of Continuously Varying Cross-Sectional Area", Journal of Sound and Vibration, Vol. 23, No. 4, pp. 433-442, 1972.

10. Lansing, D. L. and Zorumski, W. E., "Effects of Wall Admittance Changes on Duct Transmission and Radiation of Sound", Journal of Sound and Vibration, Vol. 27, No. 1, pp. 85-100, 1973.

11. Zorumski, W. E., "Acoustic Theory of Axisymmetric Multisectioned Ducts", NASA TR R-419, May 1974.

12. Nayfeh, A. H. and Telionis, D. P., "Acoustic Propagation in Ducts with Varying Cross-Sections", The Journal of the Acoustical Society of America, Vol. 54, No. 6, pp. 1654-1661, 1973.

13. Beckemeyer, R. J. and Eversman, W., "Computational Method for Studying Acoustic Propagation in Nonuniform Waveguides", AIAA Paper 73-1006, Seattle, Wash. 1973.

14. Eversman, W., Cook, E. L., and Beckemeyer, R. J., "A Method of Weighted Residuals for the Investigation of Sound Transmission in Non-Uniform Ducts Without Flow", Journal of Sound and Vibration, Vol. 38, pp. 105-123, 1975.

15. Quinn, D. W., "An Integral Equation Method for Ducts with Varying Cross Section and Axially Varying Impedance", AIAA Paper No. 76-495, 1976.

16. Kaiser, J. and Nayfeh, A. H., "A Wave-Envelope Technique for Wave Propagation in Nonuniform Ducts" AIAA Journal, Vol. 15, No. 4, pp. 533-537, April 1977.

17. Quinn, D. W., "A Finite Difference Method for Computing Sound Propagation in Nonuniform Ducts", AIAA Paper No. 75-130, 1975.

18. Baumeister, K. J. and Rice, E. J., "A Difference Theory for Noise Propagation in an Acoustically Lined Duct with Mean Flow", AIAA Paper 73-1007, 1973.

19. Baumeister, K. J., "Generalized Wave Envelope Analysis of Sound Propagation in Ducts with Variable Axial Impedance and Stepped Noise Source Profiles", AIAA Paer No. 75-518, 1975.

20. Watson, W. R., "Finite Element Analysis of Sound Propagation in a Rectangular Duct of Finite Length with Peripherally Variable Liners", AIAA Paper No. 77-1300, 1977.

21. Eversman, W. and Astley, R. J., "Transmission in Non-uniform Ducts-A Comparative Evaluation of Finite Element and Weighted Residuals Computational Schemes", AIAA Paper No. 77-1299, 1977.

22. Powell, A., "Theory of Sound Propagation Through Ducts Carrying High-Speed Flows", Journal of the Acoustical Society of America, Vol. 32, pp. 1640-1646, 1960.

23. Eisenberg, N. A. and Kao, T. W., "Propagation of Sound Through a Variable-Area Duct with a Steady Compressible Flow", Journal of the Acoustical Society of America, Vol. 49, pp. 169-175, 1971.

24. Davis, S. S. and Johnson, M. L., "Propagation of Plane Waves in a Variable Area Duct Carrying a Compressible Subsonic Flow", presented at the 87th Meeting of the Acoustical Society of America, New York, 1974.

25. Myers, M. K. and Callegari, A. J., "On the Singular Behavior of Linear Acoustic Theory in Near-Sonic Duct Flows", Journal of Sound and Vibration, Vol. 51, No. 4, pp. 517-531, 1977.

26. Callegari, A. J. and Myers, M. K., "Nonlinear Effects on Sound in Nearly Sonic Duct Flows", AIAA Paper No. 77-1296, 1977.

27. Nayfeh, A. H., Shaker, B. S., and Kaiser, J. E., "Computation of Nonlinear One-Dimensional Waves in Near-Sonic Flows", AIAA Paper No. 77-1297, 1977.

28. Huerre, P. and Karamcheti, K., "Propagation of Sound Through a Fluid Moving in a Duct of Varying Area", in Interagency Symposium of University Research in Transportation Noise, Stanford, Vol. II, pp. 397-413, 1973.

29. Grim, D. W., "Application of Ray Acoustics to the Propagation of Sound in Ducts Containing Sheared Flow", M.S. Thesis, Virginia Polytechnic Institute and State University, 1972.

30. King, L. S. and Karamcheti, L., "Propagation of Plane Waves in the Flow Through a Variable Area Duct", AIAA Paper 73-1009, 1973.

31. Hogge, H. D. and Ritzi, E. W., "Theoretical Studies of Sound Emission from Aircraft Ducts", AIAA Paper 73-1012, 1973.

32. Tam, C. K. W., "Transmission of Spinning Acoustic Modes in a Slightly Nonuniform Duct", Journal of Sound and Vibration, Vol. 18, No. 3, pp. 339-351, 1971.

33. Nayfeh, A. H., Telionis, D. P., and Lekoudis, S. G., "Acoustic Propagation in Ducts with Varying Cross Sections and Mean Flow", In. Aeroacoustics, Vol. 37, Progress in Astronautics and Aeronautics (H. T. Nagamatsu, Ed.), MIT Press, pp. 333-351, 1975.

34. Nayfeh, A. H., Kaiser, J. E., and Telionis, D. P., "Transmission of Sound Through Annular Ducts of Varying Cross Sections", AIAA Journal, Vol. 13, No. 1, pp. 60-65, 1975.

35. Nayfeh, A. H. and Kaiser, J. E., "Effect of Compressible Sheared Mean Flow on Sound Transmission Through Variable-Area Plane Ducts", AIAA Paper 75-128, 1975.

36. Eversman, W., "A Multimodal Solution for the Transmission of Sound in Nonuniform Hard Wall Ducts with High Subsonic Flow", AIAA Paper No. 76-497, 1976.

37. Nayfeh, A. H., Shaker, B. S. and Kaiser, J. E., "Transmission of Sound Through Nonuniform Circular Ducts with Compressible Mean Flows", NASA CR-145126, 1977.

38. Sigman, R. K., Majjigi, R. K. and Zinn, B. J., "Use of Finite Element Techniques in the Determination of the Acoustic Properties of Turbofan Inlets", AIAA Paper No. 77-18, 1977.

39. Abrahamson, A. L., "A Finite Element Model of Sound Propagation in a Non-Uniform Circular Duct Containing Compressible Flow", AIAA Paper No. 77-1301, 1977.

40. Plumblee, H. E., "A Theoretical and Experimental Study of Sound Attenuation in an Annular Duct", AIAA Paper 73-1005, 1973.

41. Plumblee, H. E., Dean, P. D., Wynne, G. A., and Burrin, R. H., "Sound Propagation in and Radiation from Acoustically Lined Flow Ducts; A Comparison of Experiment and Theory", NASA CR-2306, 1973.

42. Nayfeh, A. H., Hurst, C. J., Marshall, R. L., and Shaker, B. S., "Sound Propagation and Attenuation in Ducts with Varying Cross Sections", Proceedings, Third Interagency Symposium on University Research in Transportation Noise, University of Utah, Nov. 1975, pp. 591-600.

43. Benzakein, M. J. and Smith, E. B., "Turbine Noise Generation and Suppression", ASME Paper 73-WA/GT-7, 1973.

44. Anon., "Instructions and Applications; Half-inch Condensor Microphones", B&K Co., p. 36, Sept. 1967.

45. Nayfeh, A. H., PERTURBATION METHODS, Wiley-Interscience, New York, Chapter 6, 1973.

46. Tester, B. J., "The Optimization of Modal Sound Attenuation in Ducts, in the Absence of Mean Flow", Journal of Sound and Vibration, Vol. 27, No. 4, pp. 477-513, 1973.

47. Zorumski, W. E. and Mason, J. P., "Multiple Eigenvalues of Sound Absorbing Circular and Annular Ducts", Journal of the Acoustical Society of America, Vol. 55, No. 6, pp. 1158-1165, 1974.

48. Shauer, J. J. and Hoffman, E. P., "Optimum Duct Wall Impedance Shear Sensitivity", AIAA Paper 75-129, 1975.

49. Rice, E. J., "Spinning Mode Sound Propagation in Ducts with Acoustic Treatment and Sheared Flow", AIAA Paper 75-519, 1975.

50. Nayfeh, A. H., "Nonlinear Propagation of a Wave Packet in a Hard-Walled Circular Duct", Journal of the Acoustical Society of America, Vol. 57, No. 4, pp. 803-809, 1975.

51. Alber, I. E., "An Integral Dissipation Method, PROCEEDINGS, COMPUTATION OF TURBULENT BOUNDARY LAYERS, Vol. I, S. J. Kline et al, eds, Stanford University, California, pp. 126-135, 1968.

DISTRIBUTION LISTS

NASA-Lewis Research Center
Attn: Kenneth J. Baumeister
21000 Brookpark Road
Cleveland, OH 44135

NASA-Lewis Research Center
Attn: Leonard W. Schoopen
2100 Brookpark Road
Cleveland, OH 44135

NASA Scientific and Technical Information Facility
Attn: Accessioning Department
P. O. Box 8757
Balt./Wash. International Airport, Md. 21240

NASA-Lewis Research Center
Attn: Library (M.S. 60-3)
21000 Brookpark Road
Cleveland, OH 44135

NASA Lewis Research Center
Attn: M. F. Heidmann (M.S. 500-208)
21000 Brookpark Road
Cleveland, OH 44135

NASA Lewis Research Center
Attn: L. W. Schopen (M.S. 500-305)
21000 Brookpark Road
Cleveland, OH 44135

NASA Lewis Research Center
Attn: Dr. B. Lubarsky (M.S. 3-3)
21000 Brookpark Road
Cleveland, OH 44135

NASA Lewis Research Center
Attn: W. L. Stewart (M.S. 3-5)
21000 Brookpark Road
Cleveland, OH 44135

NASA Lewis Research Center
Attn: R. W. Schroeder (M.S. 500-207)
21000 Brookpark Road
Cleveland, OH 44135

NASA Lewis Research Center
Attn: C. E. Feiler (M.S. 500-208)
21000 Brookpark Road
Cleveland, OH 44135

NASA Lewis Research Center
Attn: E. J. Rice (M.S. 500-208)
21000 Brookpark Road
Cleveland, OH 44135

NASA Lewis Research Center
Attn: J. F. Groeneweg (M.S. 500-208)
21000 Brookpark Road
Cleveland, OH 44135

NASA Lewis Research Center
Attn: N. T. Musial (M.S. 500-311)
21000 Brookpark Road
Cleveland, OH 44135

NASA Lewis Research Center
Attn: Library (M.S. 60-3)
21000 Brookpark Road
Cleveland, OH 44135

NASA Lewis Research Center
Attn: Report Control Office (M.S. 5-5)
21000 Brookpark Road
Cleveland, OH 44135

NASA Langley Research Center
Attn: Mr. Homer Morgan (M.S. 239)
Hampton, VA 23665

NASA Langley Research Center
Attn: Mr. David Chestnutt (M.S. 239)
Hampton, VA. 23665

NASA Langley Research Center
Attn: Mr. Donald L. Lansing (M.S. 239)
Hampton, VA. 23665

NASA Langley Research Center
Attn: Mr. Joseph Posey (M.S. 239)
Hampton, VA. 23665

Dr. Sanford Davis
NASA Ames Research Center
Mail Stop 227-9
Moffett Field, CA 94035

NASA Headquarters
Attn: Harry W. Johnson (Code RL)
600 Independence Ave., SW
Washington, D. C. 20546

NASA Headquarters
Attn: Gordon Bannerian (Code RLN)
600 Independence Ave., SW
Washington, D. C. 20546

Dr. Alan Hersh
Hersh Acoustical Engineering
9545 Cozycroft Avenue
Chatsworth, CA 91311

Mr. Richard Hayden
Bolt, Beranek & Newman, Inc.
50 Moulton Street
Cambridge, MA 02138

AFAPL, Turbine Engine Division
Attn: Robert McGregor
Wright-Patterson AFB, OH 45433

Dr. Ali H. Nayfeh
Virginia Polytechnic Institute & State University
Dept. of Engineering Science & Mechanics
Blacksburg, VA 24061

Professor John Cole
Tufts University
Dept. of Mechanical Engineering
Medford, MA 02155

General Electric Company
Attn: R. E. Kraft
Aircraft Gas Turbine Division
Evendale, OH 45215

General Electric Company
Attn: Mr. R. Mottsinger
Aircraft Gas Turbine Division
Evendale, OH 45215

Dr. Andrew Bauer
McDonnell-Douglas Aircraft
3855 Lakewood Boulevard
Long Beach, CA 90846

Dr. Ben Zinn
Georgia Institute of Technology
Atlanta, GA 30332

Mr. Harry E. Plumblee, Jr.
Lockheed-Georgia Company
Marietta, GA 30061

Mr. Abbott A. Putnam
Combustion Systems Section
Battelle Columbus Laboratories
505 King Avenue
Columbus, OH 43201

Dr. B. Lakshminarayana
Aerospace Engineering Department
Penn State University
University Park, PA 16802

Professor K. Uno Ingard
Massachusetts Institute of Technology
Dept of Aeronautics & Astronautics
Cambridge, MA 02139

Dr. S. H. Ko
Naval Underwater System Center
Code TD-12
New London, CT 06320

Dr. Ronald L. Panton
University of Texas at Austin
Austin, TX 78712

Department of Transportation
Attn: Charles R. Foster
400 - 7th Street, SW
Washington, D. C. 20590

Mr. Mark Orelup
Detroit Diesel Allison Division
P. O. Box 894
Indianapolis, IN 46206

Dr. John J. Schauer
University of Dayton
School of Engineering
Dept. of Mechanical Engineering
Dayton, OH 45469

Mr. A. Anderson
The Boeing Company
P. O. Box 3707
Seattle, WA 98124

Mr. Les Wirt
Lockheed of California
Burbank, CA 91503

Wyle Laobratories
Huntsville, AL

Dr. R. Mani
General Electric Company
Research & Development Center
P. O. Box 43
Schenectady, NY 12301

Office of Environmental Quality
Attn: John O. Powers
800 Independence Ave., SW
Washington, D. C. 20591

Environmental Protection Agency
Attn: John Schettino
Crystal Mall, Building 2
1921 Jefferson Davis Highway
Arlington, VA 20460

Environmental Protection Agency
Attn: William Sperry
Crystal Mall, Building 2
1921 Jefferson Davis Highway
Arlington, VA 20460

Federal Aviation Administration
Attn: Robert J. Koenig (Code ARD-551)
800 Independence Ave., SW
Washington, D. C. 20591

Federal Aviation Administration
Attn: James F. Woodall (CODE AED-500)
800 Independence Ave., SW
Washington, D. C. 20591

Mr. Marvin Schnee
Grumman Aerospace Corporation
Building 35, Dept. 454
Bethpage, NY 11714

Mr. M. D. Nelson
The Boeing Company
Nacelle and Noise Abatement Group
Wichita Division
Wichita, KS 67210

Mr. R. N. Yurkovich
McDonnell-Douglas Aircraft
St. Louis, MO 63178

Dr. L. W. Dean
Pratt & Whitney Aircraft
400 Main Street
East Hartford, CT 06108